Autonomous Ceiling-Following Using Biomimetic Vibrissal Sensors on a Quadrotor

Thesis Report

Nils de Krom

Delft University of Technology

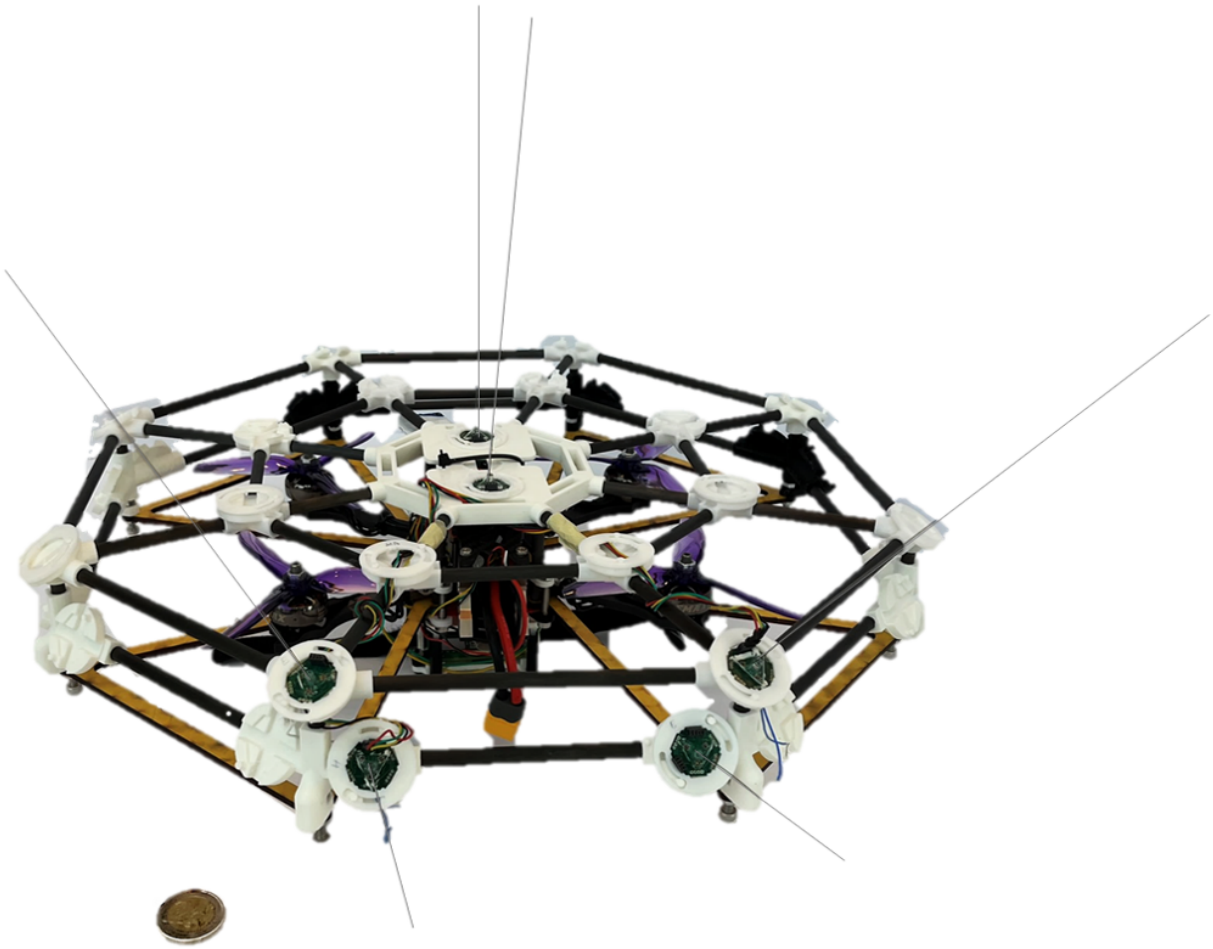

TU Delft

This page is intentionally left blank

Autonomous Ceiling-Following Using Biomimetic Vibrissal Sensors on a Quadrotor

Thesis Report

by

Nils de Krom

Student Number: 4883349

to obtain the degree of Master of Science
at the Delft University of Technology
to be defended publicly on October 24, 2024 at 13:30

Thesis Committee:

Chair:	Dr. Ir. C. de Wagter
Supervisor:	Dr. Ir. S. Hamaza
External Examiner:	Dr. J. Jovanova
Institution:	Delft University of Technology
Place:	Faculty of Aerospace Engineering, Delft
Project Duration:	September 2023 - September 2024

An electronic version of this thesis is available at `https://repository.tudelft.nl/`.

TU Delft

Preface

This report contains the outcome and marks the end of my Master Thesis at the Faculty of Aerospace Engineering at the Delft University of Technology. This master thesis focused on achieving tactile navigation with an aerial platform in hard-to-reach environment with low visibility by mimicking the sensory system of nocturnal animals consisting of vibrissal sensors, whiskers. Nocturnal animals have proven that vibrissal sensors allow for exploration and navigation of environments with low visibility. The goal of my research has been to introduce the world of whisker-based tactile sensing to aerial robotics, by designing and controlling a whiskered drone, with biomimetic vibrissal sensors, for rugged ceiling contour-following tasks.

The journey from the initial concept idea to the final outcome has been challenging with many highs and lows. However, these highs and lows resulted in many teachable moments, which allowed me to learn many new skills. Even tough this journey has been a challenge, seeing my designs and ideas come to life has been incredible.

I would like to express my gratitude to my supervisor Dr. Ir. Salua Hamaza for her support, guidance, and personal and project related advice throughout this thesis. I am incredibly grateful for working together with Mahima Yoganarasimhan during our theses. It has been an amazing adventure, thank you for the interesting discussions, your support, the amazing moments we had, and for being a friend.

Additional I would like to thank everyone at the MavLab for their help, support, and introducing me to the world of micro aerial vehicles.

Lastly, I would like to thank my amazing and loving family for their unwavering support and encouragement.

Nils de Krom
Delft, October 2024

Contents

Part 1
Introduction

A current trend in the field of robotics is to use robots, autonomous vehicles, to perform exploration, localization, and mapping tasks in known and unknown environments. Using robots for these tasks allows for exploring environments that are difficult or dangerous for humans to explore. This trend is also proven by the winners of the DARPA Subterranean Challenge, who have shown that exploration and object localization could be performed with the help of multiple different robotic vehicles. These vehicles were equipped with visual sensors, such as RGB cameras, and laser sensors, such as LIDAR.[5]

These sensor types have their limitations, they often have a high power consumption, are relatively heavy, and they are not always as effective. Their effectiveness heavily decreases in environments with low visibility due to dust, darkness, and smoke, such as natural caves and tunnels. To be able to explore such environments a new sensory system is needed. Luckily, such a sensory system can be observed in nature, a tactile based sensory system that can be used as range sensors. More specifically, the sensory system embedded in the body of nocturnal animals in the form of vibrissal sensors, whiskers. These animals use their vibrissal sensors for tracking, orienting, exploring, and localizing objects in their environment. [4]

As the whisker-based sensory system is proven by nature, current robotic applications already exist that make use of biomimetic vibrissal sensors on moving platforms for exploration and navigation tasks. Examples of such platforms equipped with whiskers are the WhiskerBot [2], the SCRATCHbot [3], and the CrunchBot [1]. However, these current applications are wheeled ground robots, designed to explore environments with smooth floors and unable to operate in hard-to-reach environments with rocky and uneven floors that can be found in cave-like environments.

Using aerial vehicles in combination with biomimetic vibrissal sensors would allow for performing exploration and navigation tasks in such low visibility hard-to-reach environments. Integrating biomimetic vibrissal sensors on aerial platforms is currently not performed in this research area.

Therefore, the aim of this research is obtaining an initial proof of concept of a whisker-based aerial platform, able to trace rugged ceiling contours via non-intrusive tactile sensing in unknown environments. This goal is to be achieved by answering the following research question:

"How can whisker-based tactile sensing be used to perform autonomous contour following navigation tasks in unknown environments, while flying in proximity with rugged ceilings, with a quadrotor?"

This report is structured as follows. First of all, the scientific article containing the research conducted to fulfill the set out goal and to answer the research question is presented in Part 2. Second, Part 3 contains an in-depth literature study, in which the different research fields related to this project are examined. The analyzed research fields are the use of whiskers in nature and robotics, contour-following navigation tasks, and flying in proximity with ceilings.

Part 2

Scientific Article

This page is intentionally left blank

Autonomous Ceiling-Following Using Biomimetic Vibrissal Sensors on a Quadrotor

N.W.M. (Nils) de Krom*
Faculty of Aerospace Engineering Delft University of Technology, Kluyverweg 1, Delft

ABSTRACT

Low visibility in hard-to-reach environments, such as natural caves and tunnels, poses challenges for exploration due to the limited effectiveness of traditional sensors, such as cameras and distance sensors. Nature offers a solution to this problem embedded in the body of nocturnal animals in the form of *vibrissal sensors*, whiskers. In this paper, we take inspiration from this principle and develop artificial biomimetic whiskers to aid quadrotors' navigation. Specifically, we design and control a whiskered drone for ceiling contour-following tasks, enabling tactile tracing of rugged ceilings while mitigating aerodynamic disturbances like the "ceiling effect". The proposed whiskered drone design allows for multiple whiskers in various orientations, providing real-time tactile feedback to guide the ceiling-following controller. Flight experiments validate the system's effectiveness in navigating both smooth and rugged ceilings, demonstrating the potential for whisker-based tactile navigation and future autonomy.

1 INTRODUCTION

The urge to explore is embedded in the nature of mankind. In the early days humans used to explore new and unknown environments by themselves on foot. However, exploring unknown environments, for example caves, could be very difficult, time consuming, and dangerous for a human. Luckily, due to the technological developments in the past decades autonomous vehicles can perform such exploration and mapping tasks.

This is proven by the winners of the DARPA Subterranean Challenge. They showed that by using walking, driving, and flying vehicles exploration and object finding could be performed. These robots made use of laser sensors, such as LIDAR, and visual sensors, such as RGB cameras. [1]

Unfortunately, these sensor types will not be effective in environments with low visibility, due to smoke, darkness, or dust. Hence, a different type of sensor is needed to be able to explore and navigate through these environments. Nature already found a solution to this problem. When looking at the exploratory behavior of nocturnal animals or animals living in poorly-lit environments, it can be observed that these animals make use of tactile sensors. There are many different types of tactile sensors in nature, which are used for many different applications, but they are all directly or indirectly used as range sensors. An example of such tactile sensors are antennae, used by the arthropods family as their most important attribute to obtain tactile stimuli, they are for example used for environmental exploration during the night.[2][3] Besides antennae, another sensor type proven to be very effective are whiskers or vibrissae, often found on mammals. For example, rodents have micro- and macrovibrissae, which in combination with head and body motions are used for localising, orienting, exploring, and tracking the environment.[4]

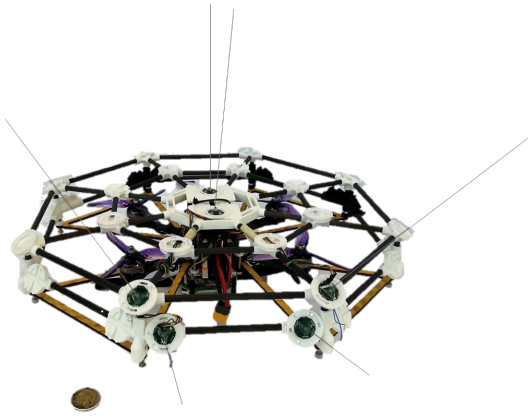

Figure 1: Designed whisker-based aerial platform. Size comparison with a 2 euro coin.

Hence, using whiskers on a robotic platform could lead to exploration and navigation tasks through poorly-lit environments. The use of whiskers in robotic applications is already viable, see Figure 2.

The ones from Figure 2 that do focus on exploration and navigation tasks are the Koala Robot [5], the WhiskerBot [6], Shrewbot [7], the SCRATCHbot [8], and the CrunchBot [9]. All these different robots try to mimic the behavior of a rat, by using the active whisking observed by rats for exploring the environment. This is beneficial, because with active whisking a larger space is sampled which increases the chance of detecting an obstacle, which is preferable when moving in an unknown environment. Furthermore, they also try to mimic the rats sensory surface, i.e. by applying a conical shape to the robots' "head", as can be seen for the WhiskerBot, Shrewbot, and SCRATCHbot, or by using a ratio between whisker lengths similar as the ratio observed for rats.

The known whisker-based robotic applications, shown in

*Email address: N.W.M.deKrom@student.tudelft.nl

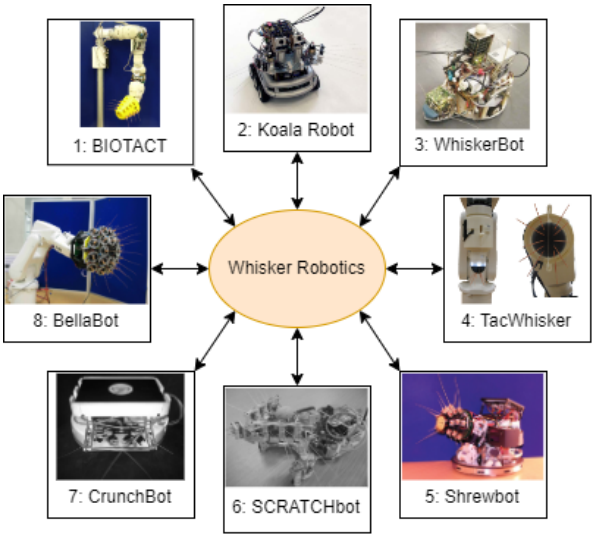

Figure 2: Overview of different whisker applications in robotics. (1: [10], 2: [5], 3: [6], 4: [11], 5: [7], 6: [8], 7: [9], 8: [12].)

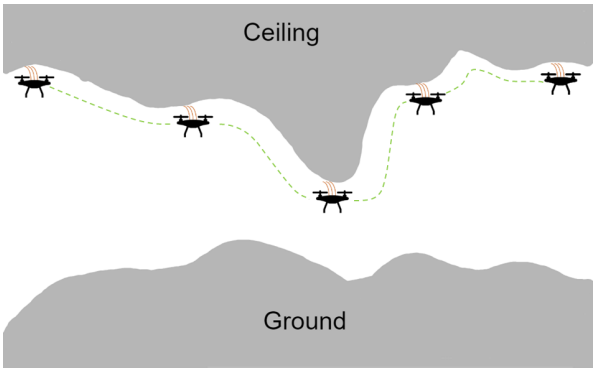

Figure 3: Visualisation of the goal of the research.

Figure 2, are based on ground robots, either wheeled ground robots or robotic arms. These whisker-based robot types could potentially be used to explore low visibility environments. However, the wheeled robots are designed to explore environments with smooth floors, hence they cannot traverse environments with rugged, rocky, and uneven floors, such as caves. For such environments aerial vehicles should be used to fulfill the exploration task. But existing research does not show applications of whiskers on aerial platforms. Which raises the question, is a whisker-based aerial platform achievable and will it be able to perform exploration and navigation tasks. This question leads to the contribution of this work.

The goal of this research is to obtain an initial proof of concept of a whisker-based aerial platform that can trace rugged ceiling contours via non-intrusive tactile sensing, paving the way for future flight autonomy in dark unknown environments, Figure 3.

To obtain this goal, this research will present the mechanical design of a new aerial platform, which allows for the placement of multiple whisker, Figure 1. Furthermore, the used whisker design and how the obtained tactile information is integrated in the system will be explained. Then, the designed tactile contour following controller is presented. Finally, all the components will be combined to demonstrate that whisker-based tactile sensing can be used on a quadrotor to perform a ceiling contour following task.

2 Whiskered Drone

2.1 *Mechanical Design*

To fulfill the goal of performing whisker-based tactile navigation and exploration in unknown environments with rugged ceilings, such as caves, requirements should be set for the mechanical design of the aerial platform. The design shall allow for placing multiple whiskers, allow for different whisker orientations, and it shall be able to withstand bumping and flying into objects.

Related to the first requirement, the design should allow for placing multiple whiskers such that a whisker array can be obtained. This design choice is supported by both [13] and [5]. They state that using an array of whiskers leads to more precise sensory data. Furthermore, nature also shows that animals with whiskers make use of a sensor array.[4] However, there are many different array designs, which leads to two unknowns: how many whiskers should the design accommodate and what should the spacing between the whiskers be.

Existing literature does not provide a clear answer on the amount of whiskers that should be used. However, it shows a certain trend based on the tactile sensing task. For classification tasks, a relatively large amount of whiskers is used to obtain large batches of accurate texture data.[13] In mobile robotics, multiple smaller arrays surround the robot, to increase the chance of obstacle detection. This same trend can be observed for spacing between whiskers. For tasks that require high accuracy, the whiskers are placed relatively close to each other.[14] Tasks that require more global data, such as obstacle detection, have whiskers that are more spread out to increase the chance of detecting obstacles. Based on this observed trend and the goal of the drone, it was decided to use larger spacing between whiskers.

As stated by the third requirement, the design should be able to withstand contact with objects, protecting the drone from impact, and for stability reasons it is preferred that the design is symmetrical. Hence, a cage like structure was designed. In Figure 1, it can be seen that the design consist of three octagons, with each intersection point, the white connectors, being a placement position for a whisker and the inner base allows for placing three whiskers. All the connectors have a simple whisker fastening click-on system, which allows for quickly repositioning the whiskers. Furthermore, the nodes on the outer ring are angled with 30 degrees relative to the horizontal top plane.

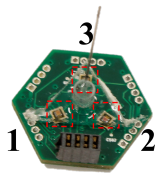

Figure 4: Visualisation of the follicle with numbered barometers.

In Figure 1 it can be seen that there are also placement options on the side of the cage. While these locations are not required for the goal in this research, they are needed for future research in not only following ceilings but also for following walls and in the end flying in caves.

In summary, the cage allows a total of 35 whisker placements, 19 on the top and 16 on the side, it is a modular design which allows for easy replacement of broken parts, and it has a total weight of $346.12[grams]$. More information about the design of the cage and all the individual components can be found in Appendix A.

An important remark is that due to other hardware limitations it was decided to make use of only two whiskers in this research. They are positioned at the top at the center of the cage, seen in Figure 1.

2.2 The Tactile Sensor: Whiskers

The whisker design used in this research are obtained from a previous research, which focused solely on a biomorphic whisker design, [15]. This whisker design consists out of three main components. Firstly, the base component, a hexagon shaped PCB containing three MEMS (microelectromechanical systems) barometers. Secondly, a follicle component containing the three barometers, a plastic tube, the whisker shaft root, and UV resin. Finally, the whisker shaft component, which is made from a nitinol wire with a diameter of $0.4[mm]$. [15]

According to [16] the length of the whisker shaft should be based on its application. It was observed in literature that on "larger" mobile platforms used for exploration and navigation tasks relatively long whiskers were used. Using this observation, it was chosen to use whiskers with a whisker shaft of $20[cm]$. A longer whisker will allow for the earlier detection of changes in the environment. Hence, the increased depth perception allows for maintaining larger distance towards an obstacle.

Deflections of the shaft are measured with the help of the follicle component, Figure 4. When there is contact along the whisker, the follicle will deform, resulting into pressure changes on the barometers that directly feed into the controller design.

An important remark is related to the accuracy and sensitivity of the used whiskers. The process used to fabricate the whiskers is done by hand, [15]. This results into whiskers with differences in sensitivity, accuracy, and behaviour. In this study a slight modification was performed to the fabrication process to try to make the whiskers more similar, the modified fabrication process can be found in Appendix B. However, they remain hand-made, hence the whiskers will have different characteristics.

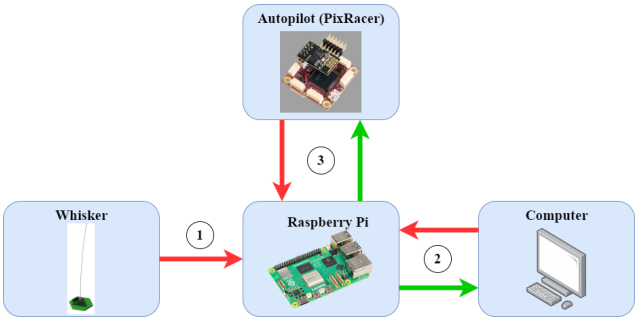

Figure 5: Overview of information flows between the systems.

2.3 System Integration

Multiple components are needed to be able to fly and control the aerial platform and to read the whiskers during flight. First of all, an autopilot module is required, in this research the PixRacer autopilot with PX4 software is used. Second, to be able to read the whiskers on board a Raspberry Pi 5b is implemented on the drone. Lastly, the proposed controller will run on a computer.

The four main components communicate as follows. The whisker sends its readings to the Raspberry Pi, which converts these readings into ROS2 messages which will be send to the computer. The computer uses these readings for the controller and send the required changes in position via a ROS2 message to the Pi. The Pi will then send these changes in position to the PixRacer. Finally, the PixRacer continuously sends the position of the drone to the Pi, which will send it to the computer. It is important to note, that due to the required communication between the different components a system delay is introduced. An overview of the four components and the information flow can be found in Figure 5.

3 Ceiling Following Controller Design

It is very important that the proposed controller is accurate and that it maintains a relatively constant distance towards the ceiling. The main risk is that the controller brings the drone too close to the ceiling, which can result into the ceiling effect playing a role during flight. This effect could influence the behaviour of the drone when flying in close proximity with the ceiling. With the ceiling effect a greater pressure difference across the rotor disks is achieved, due to an increase in the induced velocity from the rotors.[17][18] This causes an increase in thrust, leading to the drone being pulled towards the ceiling. This suction towards the ceiling can re-

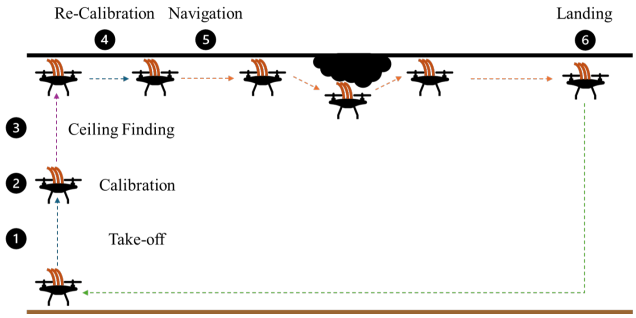

Figure 6: Overview of the 6 main steps in the whiskered drone FSM controller flow.

sult in the drone crashing into the ceiling, but it can also obstruct tracking tasks. Due to differences in desired forces and the actual forces the drone will not be able to follow the target points, leading to target points never being reached.[19] Hence, it is extremely important that the controller makes sure the drone does not get to close to the ceiling, or that it can handle being pulled into the ceiling.

To be able to design the ceiling following controller, first the general behaviour flow, or mission, of the drone was determined, subsection 3.1. Second, a filtering sequence was developed to mitigate the effect of external factors on the sensor readings, subsection 3.2. Both the general behaviour flow and the filtering sequence were used to determine the controller logic, subsection 3.3.

3.1 Behaviour Flow

The general controller behaviour flow is captured with the help of a finite state machine (FSM). Using the goal of this research, stated in section 1, the flow of the FSM can be obtained and is visualised in Figure 6. The first step is the take-off sequence, in which the quadrotor takes off till the whisker calibration height, which is chosen to be $1.2[m]$. When reaching this height with an accuracy of $0.05[m]$, the second step is activated, the whisker calibration sequence. In this step the drone hovers for $25[s]$. This period is used to perform calculations related to filtering, which will be explained in more detail in subsection 3.2. After the calibration sequence, the ceiling finding sequence is performed in step 3. In this sequence the drone gradually starts climbing in a straight line to a preset max height, in this case $1.6[m]$. If before that height a whisker detects a change in pressure, compared to the previous reading, in at least two of the three barometers which is higher than a preset contact threshold, contact with the ceiling is established. The contact threshold is a change in pressure of $> 25[Pa]$. Initial contact with the ceiling could lead to the whiskers orientating themselves opposite to the direction of motion. This could lead to large pressure changes when starting the contour following task due to the whiskers "flipping" their orientation, which could have a dangerous effect on the whisker-based flight controller. I.e. due to the large pressure change the controller could think that it should go up relatively fast, which could result in crashing into the ceiling. To prevent this, step 4 contains the ceiling re-calibration sequence. After initial contact the drone will move $20[cm]$ into the direction of motion, which results into re-orientating the whiskers in the desired orientation. After this movement a $2[s]$ ceiling hover is initialised to let the large changes in pressure dampen out before the contour following task begins, as seen in Figure 7.

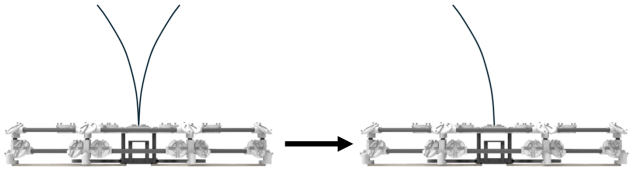

Figure 7: Change in whisker orientation during ceiling calibration sequence.

After the ceiling hover the ceiling contour following navigation sequence, step 5, gets activated. During this stage the quadrotor will try to maintain in contact with the ceiling and follow the shape of the ceiling. When the end of the ceiling is reached, the landing sequence will be initialised and the drone will return back to its home position.

As mentioned in the introduction of this section, there is a risk of getting pulled towards the ceiling during step 5, if the drone gets too close to the ceiling. When this happens the drone will abruptly hit the ceiling, which results in a large change in pressure for the whiskers. This large change in pressure is used in a special sequence to control getting sucked into the ceiling. If the change in pressure is $> 150[Pa]$, step 5 will be put on hold and the drone will go to a hover height $30[cm]$ lower than the previous z-height and $10[cm]$ in y opposite (backwards) to the direction of movement. This is to make sure that the whiskers of length $20[cm]$ are no longer in contact with the ceiling. When this hover height is achieved, step 3 and 4 will be repeated at its current position after a hover of $2[s]$. However, this time the ceiling calibration will have a movement of only $10[cm]$.

3.2 Whisker in-flight Calibration

The used whiskers are very sensitive, which means that unwanted noise can get introduced in the signal by low velocity airflow [16]. Furthermore, the barometers get influenced by the ambient temperature and humidity, which could cause a drift in pressure readings.[15] The same holds for the spring constant of the whiskers, which will also be influenced by the climate of the environment. Not only the climate characteristics can negatively influences the readings, texture of the surface of the environment can also induce excessive unwanted vibrations.[20] The same holds for moving a whisker into an object, which could result into the whisker oscillating in an inconsistent and unpredictable manner.[21] Finally, mo-

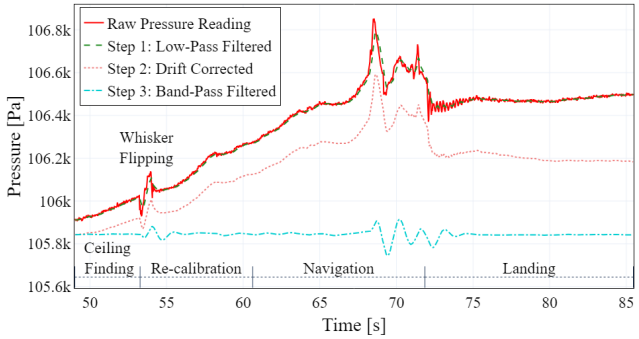

Figure 8: Filtered pressure readings for barometer 2 of the rear whisker after each filtering step, from ceiling finding till landing, during an inclined rugged ceiling flight. Flipping of the whisker can be observed at the start of the re-calibration stage.

tion induced oscillations will occur due to the movement and vibrations of the aerial platform.

A data filtering sequence is required to decrease the effect of all these external factors on the whisker pressure readings. First, to reduce the influence of self induced oscillations a first order Butterworth low-pass IIR filter with a critical frequency of $3[Hz]$ is applied. Second, to account for the temperature drift a temperature correction factor, dT/dt, is determined during the $25[s]$ calibration sequence and subtracted from the data readings. It was observed that with both the low-pass filter and the temperature drift correction not all the noise was filtered out. For that reason a third step was introduced in the filtering sequence. This step applies a first order Butterworth band-pass IIR filter, after the temperature drift correction is applied, with a center frequency of $2[Hz]$, and frequency width of $1[Hz]$. This full data filtering sequence leads to smooth and less noisy readings, that could safely and accurately be used in the proposed controller design. An example of a filtered barometer reading can be found in Figure 8.

3.3 Ceiling-Following Controller

With the help of the filtering sequence, a clean input signal for the controller is obtained. The controller is based on contour following strategies, also known as wall-following strategies. These strategies are in general based on three main parts. The first being, the robot should be able to maintain a desired distance towards the wall. Second, the robot should be able to follow the wall in a parallel manner. Lastly, the robot should be able to detect obstacles and measure distances towards obstacles to be able to account for these.[22][23]

These wall-following strategies are based on robots with distance sensors that return the distance towards the wall and obstacles. The used whiskers only return pressure readings from the three barometers. However, the wall-following strategies are still used but are interpreted slightly differently. The controller aims to maintain a constant pressure value instead of a constant distance, instead of a parallel position towards the wall, the drone will remain in a fixed orientation. Finally, obstacles or changes in the environment will be detected by large changes in the pressure, allowing to account for these obstacles.

For the initial contact detection all three barometers of each whisker are used. However, for the contour following part only the barometer on each whisker that is continuously in compression during the movement in y-direction will be taken into account, which is barometer 2, see Figure 10. This was decided, because in the given use case, the other two barometers do not provide additional information, therefore they can be left out of the equation.

The used controller has three main steps. The first step is for each whisker fitting a curve on a time window of $[t_n - 0.5, t_n][s]$ containing 25 pressure reading data points, where t_n is the timestamp of the latest data point. An advantage of this step is that it filters out some of the remaining unwanted noise. Furthermore, by using the history of the measurements the controller gets a better insight in the flight behaviour of the drone. This allows for determining a more accurate and smoother change in z-position. The curve fitting is performed with an ordinary least squares (OLS) estimator. This requires a regression matrix, containing all the regressor terms used by the OLS estimator. The construction of the regression matrix is shown in Equation 1. In this matrix the amount of rows equals the amount of data points, N, and the number of columns is based on the number of regressor terms, hence the order of the model. Using this matrix the OLS parameter vector for the fitted curve can be obtained with Equation 2.

$$A(x) = \begin{bmatrix} 1 & p_1(x(1)) & \dots & p_M(x(1)) \\ \vdots & \vdots & \vdots & \vdots \\ 1 & p_1(x(N)) & \dots & p_M(x(N)) \end{bmatrix} \tag{1}$$

$$\hat{\theta}_{OLS} = \left(A^T(x) \cdot A(x)\right)^{-1} \cdot A^T(x) \cdot y \tag{2}$$

The equation of the fitted curve can be obtained with the help of Equation 3.

$$p(x) = \hat{y}_{OLS} = A(x) \cdot \hat{\theta}_{OLS} = \theta_0 + \theta_1 \cdot x + \theta_2 \cdot x^2 + \dots \tag{3}$$

In this research it was chosen to use a third order OLS model. It was observed that for higher orders the accuracy of the fit would not increase with a significant amount.

To get a better insight about the change in pressure in the time window the derivative of the fitted curve is calculated. For each point in the time window the value for the derivative is obtained and the average derivative over the entire time window is calculated. This average derivative represents the average slope of the curve, which can be translated to behaviour of the drone. If the drone is getting closer to the ceiling, barometer 2 will be more compressed resulting in an

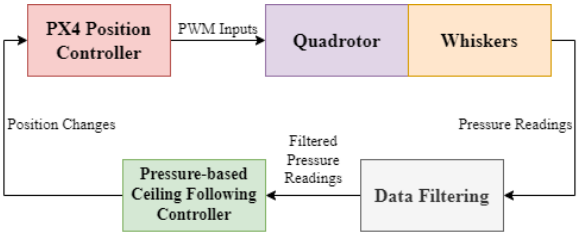

Figure 9: Simplified structure of the used controller logic.

increase in pressure, the slope is positive. The opposite holds for the drone getting further away from the ceiling.

Hence, this average slope for each whisker can be combined to determine the average slope, $\frac{dP}{dt}_a$, over the whiskers and can be used to determine the required change in z-position. To maintain a constant pressure the aerial platform should go down when the slope is positive and up when the slope is negative. This can be translated to a position-based control law, shown in Equation 4. This control law consists out of three parts, set by a lower and upper threshold. A lower threshold, ϵ_{low}, is set to make sure that if there are minimal changes the drone does not change its position, cause these changes could be induced by environmental factors like airflow. Hence, the first part results into a $0.0[m]$ z-change. The lower threshold is set to $2[\frac{Pa}{s}]$. The second part is the main law, if the average slope is between the lower and upper threshold a change in z is calculated. It was determined that the maximum z-change per timestamp is $0.1[m]$. This is to prevent large and sudden changes which could induce vibrations and unwanted behaviour in the whiskers. The upper threshold is dependent on the sensitivity of the used whiskers. The more sensitive they are the higher the threshold will be, for the used whiskers in the final experiments an upper threshold, ϵ_{up}, of $30[\frac{Pa}{s}]$ is set. The final part holds for values of the average slope above the upper threshold, the change in z will be set to the maximum allowed z-change.

$$dz = \begin{cases} 0 & \text{if} \quad \frac{dP}{dt}_a \leq \epsilon_{low} \\ \frac{1}{10 \cdot \epsilon_{up}} \cdot \frac{dP}{dt}_a & \text{if} \quad \epsilon_{low} < \frac{dP}{dt}_a \leq \epsilon_{up} \\ \frac{1}{10} & \text{if} \quad \frac{dP}{dt}_a > \epsilon_{up} \end{cases} \quad [m] \qquad (4)$$

The determined z-changes for each timestamp are sent to the PX4 position controller, this will result into a change in pressure, resulting in a change in z-position. It is expected that the resulting flight behaviour will represent a sine wave, as the pressure will go down when the drone goes down, which results in the controller wanting to go up. The simplified controller loop can be visualised in a flow diagram which is shown in Figure 9.

4 Flight Experiments

The experiments are divided into two main categories, experiments with a straight ceiling, subsection 4.1, and experiments with a slightly inclined ceiling, subsection 4.2. In each main category two different environments will be tested, a ceiling with a smooth surface or a rough surface, which represents a cave like environment. As mentioned in subsection 3.2, the texture of the surface can lead to unwanted vibrations and changes in pressure readings, which could lead to false controller inputs. Therefore, the distinction between smooth and rough surface environments is made to analyse the controllers adaptability to the texture and shape changes of a rough surface. It should also be noted that the controller has no knowledge of the environment beforehand. Furthermore, as mentioned earlier two whiskers are placed on top of the structure of the aerial platform. The used aerial platform configuration together with its direction of movement during the experiments can be seen in Figure 10.

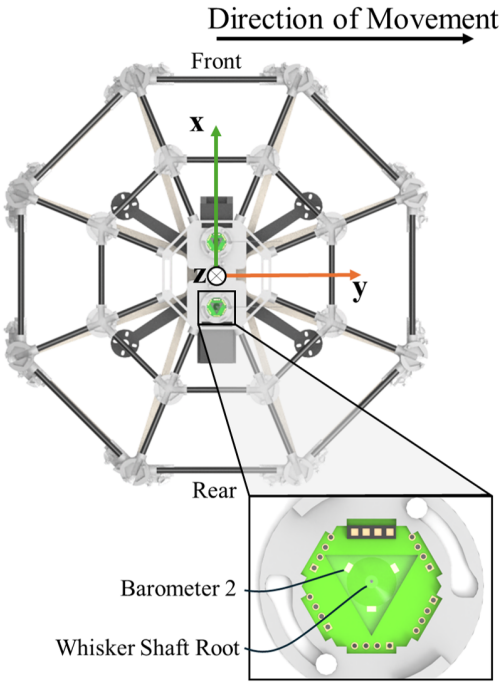

Figure 10: Render of the used aerial platform during the flight experiments. Two whiskers are placed on the top at the centre, one above the centre in the top view, the front whisker, and one below, the rear whisker. Direction of movement during the performed flight experiments is in the y-direction.

4.1 *Straight Ceiling Flight Experiments*

As mentioned earlier, the straight ceiling experiments are done for both a fully smooth and a partially rugged ceiling. To perform these experiments an artificial ceiling is made of $0.75[m]$ by $2.0[m]$ at a height of approximately $1.60[m]$. A visualisation of the used set-up for the smooth ceiling can be found in Figure 11 and the visualisation of the rough ceiling can be found in Figure 12. The rugged ceiling is made with four fake cave parts of $15[cm]$ by $20[cm]$, more detailed images of these cave structures can be found in Appendix C,

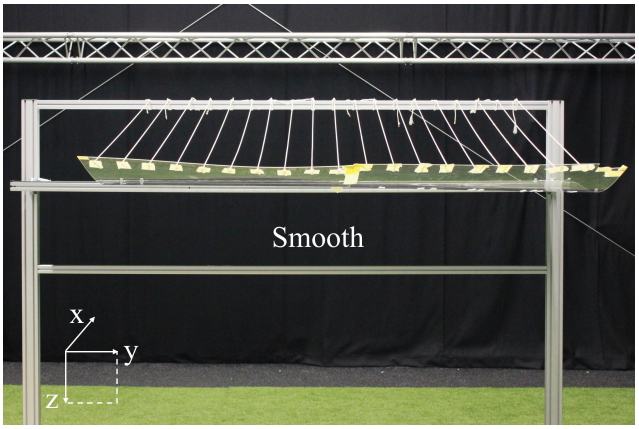

Figure 11: Ceiling set-up used for the straight and smooth ceiling flight experiments.

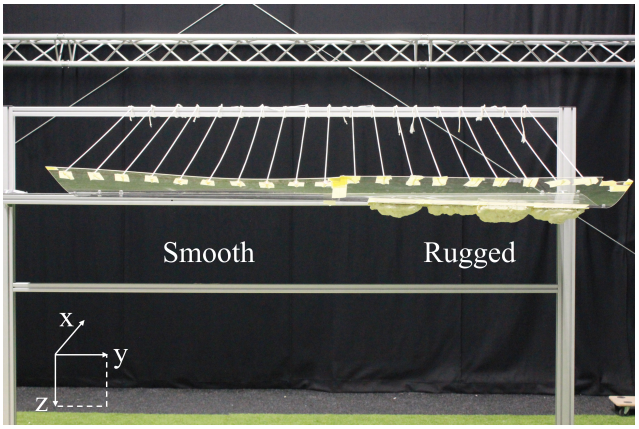

Figure 12: Ceiling set-up used for the straight and rough ceiling flight experiments.

and are placed in the ceiling x center and $8[cm] - 88[cm]$ in y-direction from the right side of the ceiling.

4.1.1 Straight Ceiling: Smooth

For the straight and smooth ceiling experiments tests are performed with an upper threshold, ϵ_{up}, of $15[\frac{Pa}{s}]$ and $30[\frac{Pa}{s}]$. The first experiment for an upper threshold of $15[\frac{Pa}{s}]$ shows that the proposed controller can follow a ceiling, Figure 13. It is also observed that the distance does not become larger than $20[cm]$, meaning the whiskers are always in contact with the ceiling. An interesting observation is that the expected sine-wave behaviour can be clearly seen in the flight pattern in Figure 13.

The previously mentioned sine-pattern can be further explained with the help of the average $\frac{dP}{dt}$-values during flight, shown in Figure 14. Here a clear wave pattern can be observed, which directly results in a similar pattern in z-change commands, Figure 34. The larger the z-changes become the

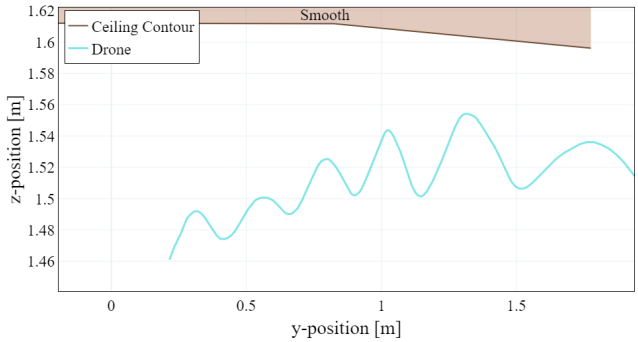

Figure 13: z-position vs. y-position of the drone during the contour following stage for a smooth and straight ceiling, $\frac{dP}{dt} = 15[Pa]$. The drone maintains a mean distance towards the ceiling of $0.102[m]$ with $\sigma = 0.026[m]$.

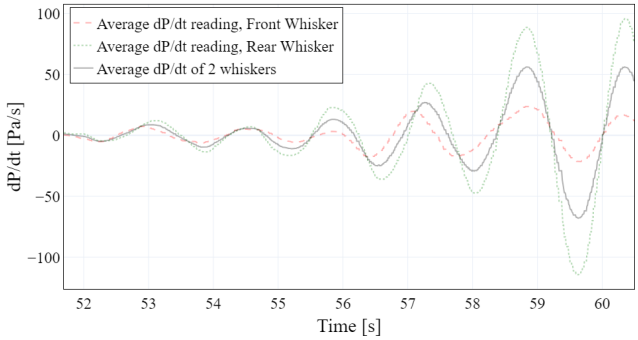

Figure 14: The average values for the slopes of the pressure readings over time during the contour following stage for a smooth and straight ceiling, $\frac{dP}{dt} = 15[\frac{Pa}{s}]$. The figure clearly shows the expected wave patterns in the curves.

larger the amplitudes in the oscillations become in Figure 14. This is expected and can be explained by the fact that large z-changes will lead to fast and more abrupt changes in pressure, leading to larger slopes.

The explanation of larger and more abrupt changes in pressure is supported by the pressure readings of both whiskers during the contour following sequence, Figure 15. However, what can be seen is that the pressure readings are oscillating around the initial starting pressure of the contour following stage, with for both cases only a small decrease in mean pressure. This demonstrates the good performance of the controller in being able to fulfill the aim to maintain a relatively constant pressure value during flight.

As mentioned before, the straight and smooth ceiling experiment is also performed with a upper threshold of $30[\frac{Pa}{s}]$. This was done to see the difference in behaviour based on this threshold. Not all figures for the larger threshold are shown in this section, more results can be found in Appendix D. When comparing Figure 14 with Figure 16 it can be seen

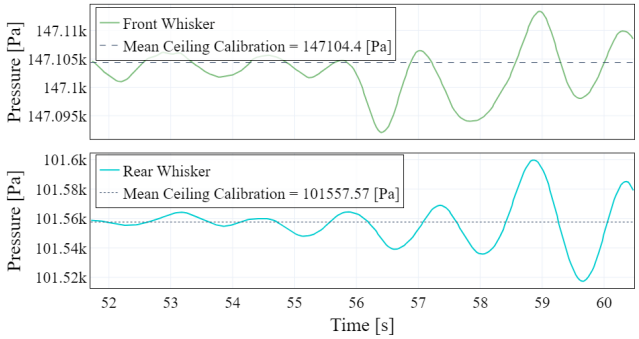

Figure 15: Pressure reading of barometer 2 for the front and rear whisker during the contour following stage for a straight and smooth ceiling, $\frac{dP}{dt} = 15[\frac{Pa}{s}]$. Both reading oscillates around the mean pressure of the ceiling calibration stage, with a small drift resulting in a change in mean pressure for the front whisker of $-1.73[Pa]$ and for the rear whisker of $-0.66[Pa]$.

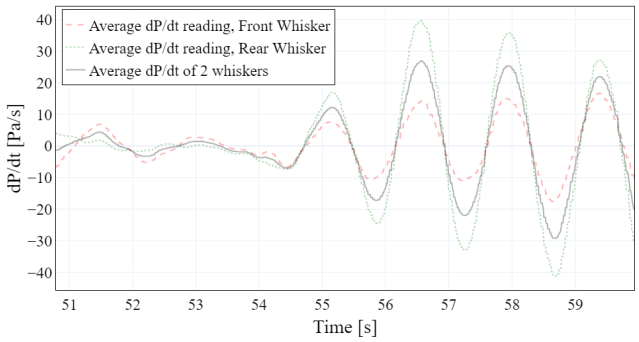

Figure 16: The average values for the slopes of the pressure readings over time during the contour following stage for a smooth and straight ceiling, $\frac{dP}{dt} = 30[\frac{Pa}{s}]$. The figure clearly shows the expected wave patterns in the curves.

that the amplitudes of the waves are smaller for the $30[\frac{Pa}{s}]$ scenario. This was expected, because with a higher threshold the z-changes will less often be set to the maximum value of $0.1[m]$ which results in smaller z-changes during flight resulting in smaller changes in pressure, resulting in smaller slopes. These smaller changes in pressure can also be observed when comparing Figure 15 with Figure 17. Furthermore, it can be concluded that also with a larger upper threshold the controller is able to maintain for both whiskers a relatively constant pressure, by oscillating around the starting pressure. The main difference between the two threshold is that a larger threshold will result into a smoother and less oscillatory flight for a smooth and straight ceiling, because the maximum z-change will be reached less often so the oscillations will be smoother.

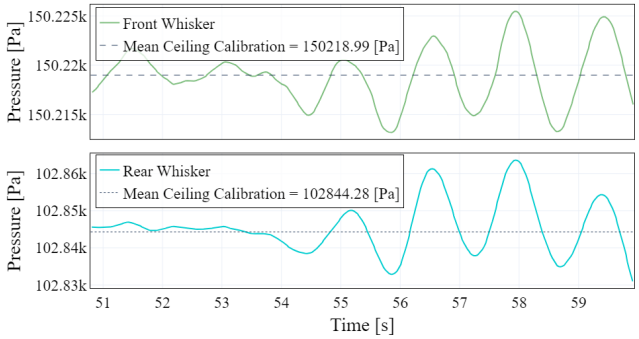

Figure 17: Pressure reading of barometer 2 for the front and rear whisker during the contour following stage for a straight and smooth ceiling, $\frac{dP}{dt} = 30[\frac{Pa}{s}]$. Both reading oscillates around the mean pressure of the ceiling calibration stage, with a small drift resulting in a change in mean pressure for the front whisker of $-0.04[Pa]$ and for the rear whisker of $1.32[Pa]$.

4.1.2 Straight Ceiling: Rough

For the straight and rough ceiling experiments it was chosen to use an upper threshold of $30[\frac{Pa}{s}]$. It was shown previously that a larger threshold leads to less maximum z-changes. Following a rough ceiling will lead to large changes in pressure due to the texture which will influence the behaviour of the whiskers. It should be noted that the cave parts are estimated in the plots as ellipsoids.

There is only a 15 by $80[cm]$ strip of rugged ceiling, therefore it is important to validate the ability of the drone to follow this line and that the whiskers are continuously in contact with that strip. This can be confirmed with the help of Figure 18. This figure shows that from the moment the cave structure starts the whiskers are in the required $x - y$ plane locations.

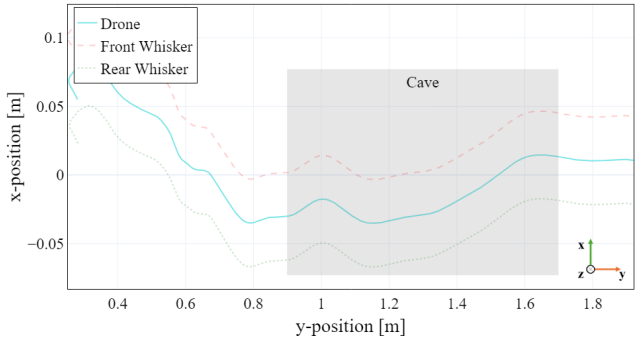

Figure 18: x-position vs. y-position of the drone during the contour following stage for a rough and straight ceiling. Showing a deviation in x during flight, but both whiskers are in contact with the cave parts.

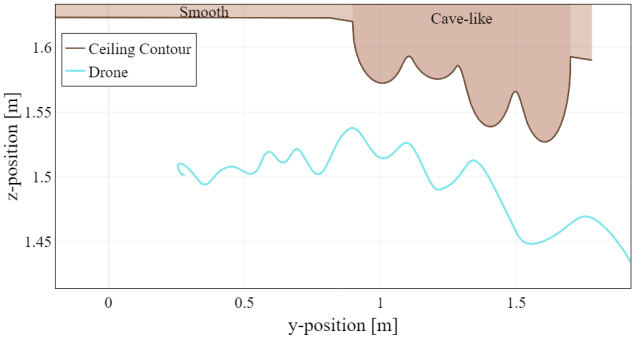

Figure 19: z-position vs. y-position of the drone during the contour following stage for a rough and straight ceiling. The drone maintains a mean distance towards the ceiling of $0.098[m]$ with $\sigma = 0.025[m]$.

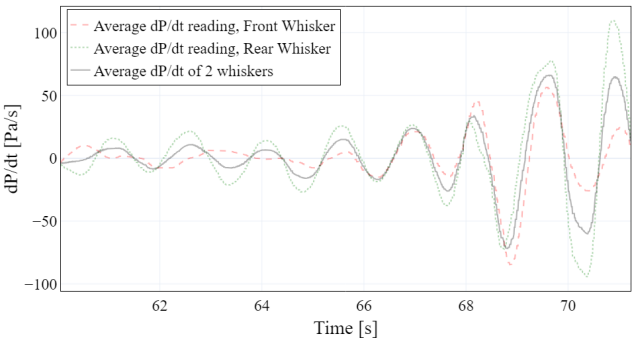

Figure 20: The average values for the slopes of the pressure readings over time during the contour following stage for a rough and straight ceiling.

Figure 19 shows that the proposed controller is also able to accurately follow the cave structure, without getting to close or too far away from it. The maximum distance of $20[cm]$ is not reached, hence the whiskers are continuously in contact. An interesting observation that can be made from Figure 19 is the small delay in following the structure of the cave, but even with this small delay the controller is able to follow the structure.

The moment the drone gets into contact with the cave structure can clearly be observed in Figure 20, where around $67[s]$ the values drastically increase. However, even with this drastic increase, the controller is still able to counter act this and maintain a constant pressure value, which can be seen in Figure 21. It can however be observed that the averages during the ceiling following phase are slightly different from the initial starting averages. This could be caused by the rough texture of the cave parts which causes the large oscillations in the pressure.

In conclusion, this experiment shows that the proposed controller is able to not only follow a smooth surface, but is also able to withstand and control large oscillations caused by rough textures, while maintaining a relatively constant pressure. Hence, it is able to detect obstacles such as the cave structures by large changes in pressure and is able to avoid them.

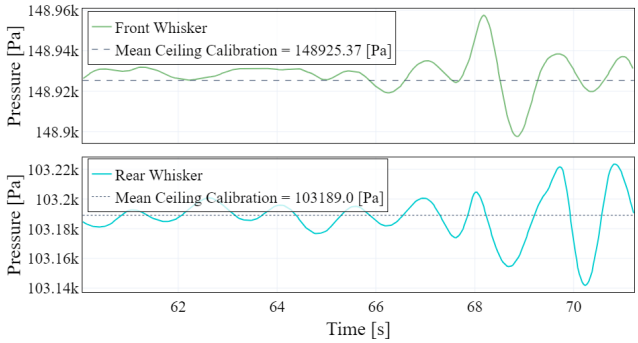

Figure 21: Pressure reading of barometer 2 for the front and rear whisker during the contour following stage for a straight and rough ceiling. Both reading oscillates around the mean pressure of the ceiling calibration stage, with a small drift resulting in a change in mean pressure for the front whisker of $3.30[Pa]$ and for the rear whisker of $-1.12[Pa]$.

4.2 Inclined Ceiling Flight Experiments

Real world environments such as caves do not only consist out of straight ceilings, but there are also inclined surfaces. For that reason it was decided to perform initial experiments with the proposed controller for a slightly inclined ceiling to provide the initial proof-of-concept for such environments. The experimental set-up has a change in height of $10[cm]$ over the ceiling length of $2[m]$, resulting in an angle of $2.86[deg]$. This is a relatively small angle, but it should be noted that the aerial platform only has whiskers on the top and is unable to look ahead. The set-up for the inclined and smooth ceiling is shown in Figure 22 and the inclined rugged ceiling can be found in Figure 23. For the rugged ceiling the same cave parts are used as for the straight rugged ceiling and they are located at the same positions.

4.2.1 Inclined Ceiling: Smooth

Using the observation from the smooth and straight ceiling experiment related to the upper threshold it was once again decided to use an upper threshold of $30[\frac{Pa}{s}]$ for the smooth and inclined ceiling set-up to ensure a smoother flight.

Figure 24 demonstrates the performance of the ceiling following controller in an environment with an inclined ceiling. It can be seen that the controller is able to follow the ceiling, while maintaining contact during the entire ceiling following phase, as the maximum distance towards the ceiling of $20[cm]$ is never reached.

Figure 22: Ceiling set-up used for the inclined and smooth ceiling flight experiments.

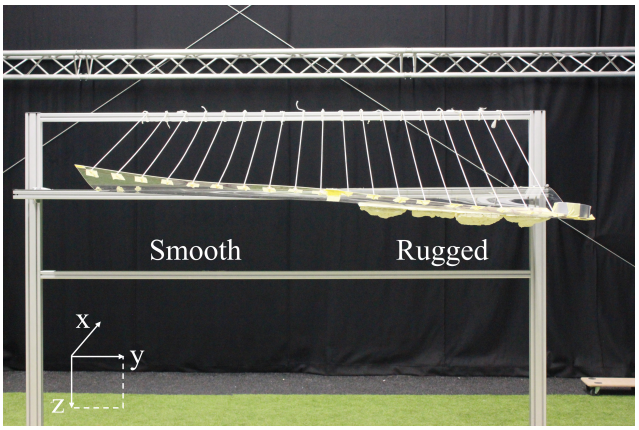

Figure 23: Ceiling set-up used for the inclined and rough ceiling flight experiments.

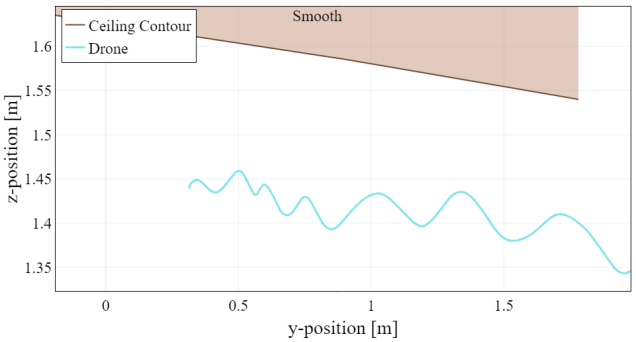

Figure 24: z-position vs. y-position of the drone during the contour following stage for a smooth and inclined ceiling. The drone maintains a mean distance towards the ceiling of $0.163[m]$ with $\sigma = 0.015[m]$.

An interesting observation that can be made is when comparing Figure 25 with Figure 16. It can be seen that for the inclined ceiling the average slope amplitudes are larger and occur sooner. This could be explained by the fact that the ceiling is inclined, meaning that going forward already leads to an increase in pressure by the fact that the ceiling is by itself getting closer. Hence, for same inputs for the inclined scenario bigger changes in pressure will be registered leading to larger slope changes. This will result into maximum z-changes, see Figure 37, leading to bigger wave amplitudes.

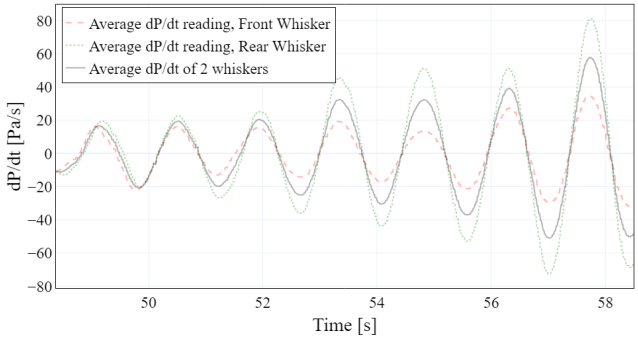

Figure 25: The average values for the slopes of the pressure readings over time during the contour following stage for a smooth and inclined ceiling.

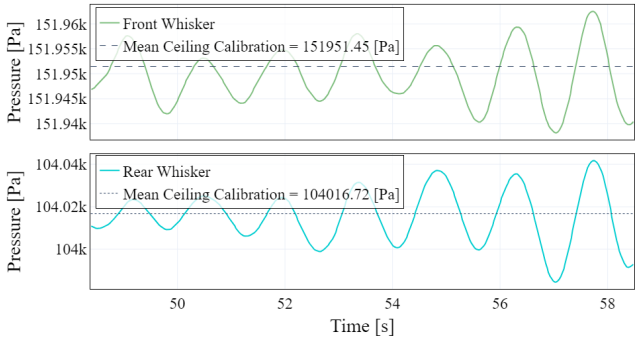

Figure 26: Pressure readings of barometer 2 the front and rear whisker during the contour following stage for an inclined and smooth ceiling. Both readings oscillates around the mean pressure of the ceiling calibration stage, with a small drift resulting in a change in mean pressure for the front whisker of $-1.67[Pa]$ and for the rear whisker of $-1.28[Pa]$.

A more important result is related to the ability of the controller to maintain relatively constant pressure values for both whiskers in this environment. When looking into the pressure readings during the ceiling following, Figure 26, it can be seen that for both whiskers the averages during the ceiling following is lower than the initial start value. However, both graphs show a clear oscillation around the mean value. Hence, the controller is able to aim for a constant pressure reading for both whiskers while following an inclined ceil-

ing. While the controller is able to follow the ceiling in a smooth manner showing an initial proof-of-concept, there are still some important remarks that need to be made related to this environment, which will be done later in this section.

4.2.2 Inclined Ceiling: Rough

For this experiment is was once again chosen to use an upper threshold of $30[\frac{Pa}{s}]$. Also in this case the cave structures are estimated in the plots as ellipsoids. In Figure 27 the location of the cave area is visualised and shows that the whiskers are in the $x-y$ locations of the cave when the cave area starts. Furthermore, the ability to follow the inclined rugged ceiling is shown in Figure 28. Once again the delay in detecting and performing the change in z-position can be clearly seen in this figure. But even with this delay the controller is able to follow the ceiling without bouncing into it or losing contact.

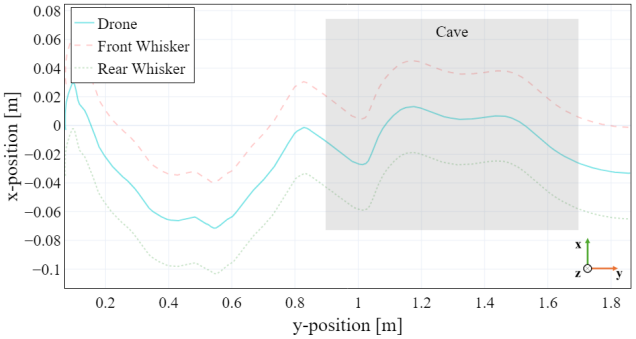

Figure 27: x-position vs. y-position of the drone during the contour following stage for a rugged and inclined ceiling. Showing a deviation in x during flight, but both whiskers are in contact with the cave parts.

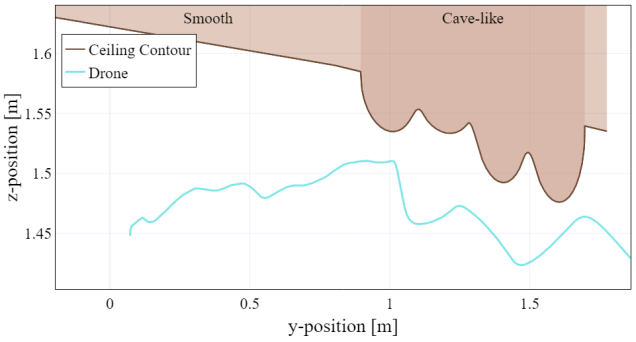

Figure 28: z-position vs. y-position of the drone during the contour following stage for a rugged and inclined ceiling. The drone maintains a mean distance towards the ceiling of $0.103[m]$ with $\sigma = 0.041[m]$.

The initial contact with the cave structure can again be observed in the dP/dt-plot shown in Figure 29. Due to the texture change and the height of the cave elements the pressure of the whiskers increase abruptly, leading to large changes in the slopes of the curve. This can be seen in Figure 30, where around $68[s]$ the pressure readings have a large spike. However, the controller shows good performance by being able to avoid the cave elements and nicely follow them. Giving an initial proof-of-concept for flight in rugged and inclined environments. However, also for this environment there are some important remarks to be made.

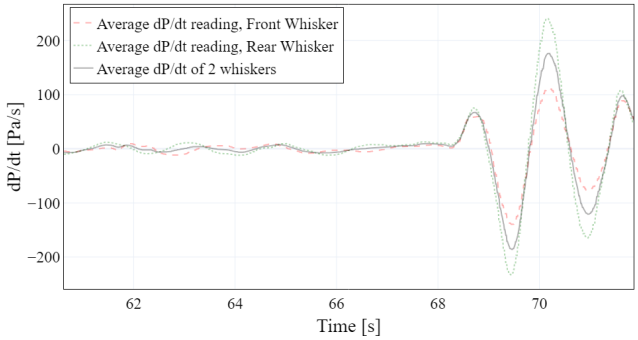

Figure 29: The average values for the slopes of the pressure readings over time during the contour following stage for a rugged and inclined ceiling.

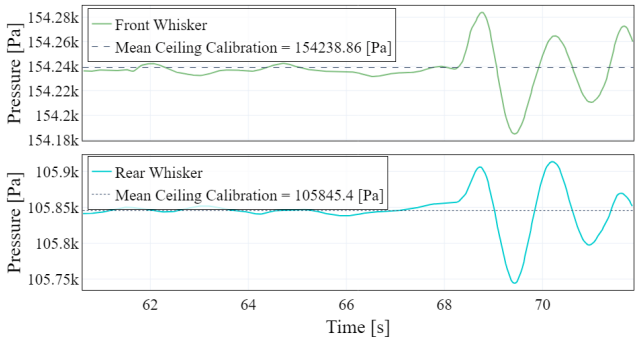

Figure 30: Pressure readings of barometer 2 for the front and rear whisker during the contour following stage for an inclined and rugged ceiling. Both readings oscillate around the mean pressure of the ceiling calibration stage, with a small drift resulting in a change in mean pressure for the front whisker of $-1.41[Pa]$ and for the rear whisker of $0.05[Pa]$.

4.2.3 General Remarks and Observations

During the straight ceiling experiments it was observed that there was often a large deviation in the x-direction during flight. This could be explained by the induced bending moment of the whiskers resulting in an unexpected force in x-direction which the PX4 position controller is unable to eas-

ily cancel out. However, this deviation, together with an additional deviation in y-direction, was also observed in the ceiling finding stage while not being in contact with any objects and without the controller giving position changes in x and y. Hence, the position controller in the autopilot had difficulty with holding a fixed x- and y-position and flying in a straight line. This sometimes lead to failed experiments or missing the cave structures completely during flight.

Furthermore, for the inclined ceiling experiments there are also some general remarks that need to be made. During the experiments it was observed that relatively often after the ceiling calibration stage the platform got too close to the ceiling and got sucked in. This could be explained by the following. It was seen that that during the ceiling hover stage the drone "bounced" back opposite to the future direction of motion due to an induced moment in the whiskers. This phenomena lead to a decrease in pressure, which resulted into the controller wanting to go up with a large amount after the hover stage. Due to the fact that the ceiling is inclined and the delay between getting the change in pressure and performing the required z-change this could result into getting too close to the ceiling.

Moreover, in the inclined scenario the cage of the drone quite often bounced into the ceiling for the smooth scenario and often got stuck on the cave structures in the inclined rugged ceiling scenario. This could be explained by the fact the drone is unable to look ahead. If additional whiskers would be added to the frame that are pointing in a slightly forward direction, it would lower the chances of the frame getting stuck and a more stable flight will be achieved.

5 Conclusion & Recommendations

In this research the design and control of a whisker-based tactile sensing aerial platform was presented which is able to perform ceiling contour following tasks in unknown environments. The proposed modular cage design allowed for placing whiskers on a drone in different orientations. Furthermore, the shown ceiling following controller was developed such that it could maintain a constant pressure and that it could avoid obstacles. Both the modular cage design and the ceiling following controller were validated with the help of flight experiments for both straight and inclined ceilings and smooth and rugged ceilings. These experiments showed that the designed system can properly and accurately follow both smooth and rugged ceilings.

However, there are some recommendations to improve the design for future work. First of all, it is advised to increase the number of whiskers used and to make use of whisker arrays. In the current approach only two whisker are used, which can be translated in analogue to a two pixel camera for environmental observations. Increasing the amount of whiskers will result into knowing more information about the environment, which will make the changes in height more accurate. Knowing more about the environment also means that there is a possibility to perform tactile SLAM (Simultaneous Localization and Mapping).

Second, in this research the whiskers were hand-made, resulting in each whisker having different properties and different sensitivity levels. This means the controller needs to be specifically tuned for each pair of whiskers. A more precise manufacturing method that allows for making whiskers with similar characteristics will most likely improve the flight behaviour. If this is not possible, it is once again advised to make use of more whiskers to better predict the behaviour and to filter out unknowns.

Third, for inclined ceilings flights could be improved by adding whiskers under an angle pointing in the direction of movement to detect changes in environment sooner. Decreasing the chance of the cage bouncing into the ceiling or getting stuck.

Acknowledgements

I would like to thank my supervisor Dr. Ir. S. Hamaza, for her support, the useful discussions, and the personal and project related advice she gave me. Furthermore, I would like to thank PhD candidate Choaxiang Ye for introducing me into the world of whisker-based tactile sensing, the help and insights he provided, and for all the useful discussions we had throughout my thesis.

I am incredibly grateful for working with fellow MSc. student Mahima Yoganarasimhan in the field of whisker-based tactile sensing. Together we had many useful and interesting discussions, educational moments, and achievements. On a daily basis, we laughed a lot, which helped me to keep on going. It has been a wonderful adventure, and I would like to thank her for her support, all the amazing moments we had, and for keeping an eye on me during this thesis.

I am also grateful for meeting fellow MSc. students in the MavLab, Georg Strunck, Rita Santos Raminhos, Giorgia Giacalone, and Michele Bianconi. They were always there for me during all the highs and the lows in this thesis and their support, help, and friendship gave me the motivation and energy to push through.

Lastly, I would like to thank those who are the most important to me. My two amazing brothers, Tom en Bart, and my loving parents who have been by my side every step of the way during this entire thesis, supporting me unconditionally.

References

[1] Marco Tranzatto, Takahiro Miki, Mihir Dharmadhikari, Lukas Bernreiter, Mihir Kulkarni, Frank Mascarich, Olov Andersson, Shehryar Khattak, Marco Hutter, Roland Siegwart, et al. Cerberus in the darpa subterranean challenge. *Science Robotics*, 7(66):eabp9742, 2022.

[2] Volker Dürr. Stick insect antennae. *Scholarpedia*, 9(2):6829, 2014.

[3] Tony J Prescott and Volker Dürr. Introduction: The world of touch. In *Scholarpedia of touch*, pages 1–28. Springer, 2015.

[4] Tony J Prescott, Ben Mitchinson, and Robyn Anne Grant. Vibrissal behavior and function. *Scholarpedia*, 6(10):6642, 2011.

[5] DaeEun Kim and Ralf Möller. Biomimetic whiskers for shape recognition. *Robotics and Autonomous Systems*, 55(3):229–243, 2007.

[6] Charles W Fox, Ben Mitchinson, Martin J Pearson, Anthony G Pipe, and Tony J Prescott. Contact type dependency of texture classification in a whiskered mobile robot. *Autonomous Robots*, 26:223–239, 2009.

[7] Martin J Pearson, Ben Mitchinson, J Charles Sullivan, Anthony G Pipe, and Tony J Prescott. Biomimetic vibrissal sensing for robots. *Philosophical Transactions of the Royal Society B: Biological Sciences*, 366(1581):3085–3096, 2011.

[8] Martin J Pearson, Ben Mitchinson, Jason Welsby, Tony Pipe, and Tony J Prescott. Scratchbot: Active tactile sensing in a whiskered mobile robot. In *From Animals to Animats 11: 11th International Conference on Simulation of Adaptive Behavior, SAB 2010, Paris-Clos Lucé, France, August 25-28, 2010. Proceedings 11*, pages 93–103. Springer, 2010.

[9] Charles Fox, Mat Evans, Martin Pearson, and Tony Prescott. Tactile slam with a biomimetic whiskered robot. In *2012 IEEE International Conference on Robotics and Automation*, pages 4925–4930, 2012.

[10] J. Charles Sullivan, Ben Mitchinson, Martin J. Pearson, Mat Evans, Nathan F. Lepora, Charles W. Fox, Chris Melhuish, and Tony J. Prescott. Tactile discrimination using active whisker sensors. *IEEE Sensors Journal*, 12(2):350–362, 2012.

[11] Nathan F. Lepora, Martin Pearson, and Luke Cramphorn. Tacwhiskers: Biomimetic optical tactile whiskered robots. In *2018 IEEE/RSJ International Conference on Intelligent Robots and Systems (IROS)*, pages 7628–7634, 2018.

[12] Tareq Assaf, Emma D. Wilson, Sean Anderson, Paul Dean, John Porrill, and Martin J. Pearson. Visual-tactile sensory map calibration of a biomimetic whiskered robot. In *2016 IEEE International Conference on Robotics and Automation (ICRA)*, pages 967–972, 2016.

[13] M. Lungarella, V.V. Hafner, R. Pfeifer, and H. Yokoi. An artificial whisker sensor for robotics. In *IEEE/RSJ International Conference on Intelligent Robots and Systems*, volume 3, pages 2931–2936 vol.3, 2002.

[14] Chenxi Xiao, Shujia Xu, Wenzhuo Wu, and Juan Wachs. Active multiobject exploration and recognition via tactile whiskers. *IEEE Transactions on Robotics*, 38(6):3479–3497, 2022.

[15] Chaoxiang Ye, Guido De Croon, and Salua Hamaza. A biomorphic whisker sensor for aerial tactile applications. In *2024 IEEE International Conference on Robotics and Automation (ICRA)*, pages 5257–5263, 2024.

[16] William Deer and Pauline E. I. Pounds. Lightweight whiskers for contact, pre-contact, and fluid velocity sensing. *IEEE Robotics and Automation Letters*, 4(2):1978–1984, 2019.

[17] Stephen A. Conyers, Matthew J. Rutherford, and Kimon P. Valavanis. An empirical evaluation of ceiling effect for small-scale rotorcraft. In *2018 International Conference on Unmanned Aircraft Systems (ICUAS)*, pages 243–249, 2018.

[18] P. J. Sanchez-Cuevas, G. Heredia, and A. Ollero. Multirotor uas for bridge inspection by contact using the ceiling effect. In *2017 International Conference on Unmanned Aircraft Systems (ICUAS)*, pages 767–774, 2017.

[19] Takuzumi Nishio, Moju Zhao, Fan Shi, Tomoki Anzai, Kento Kawaharazuka, Kei Okada, and Masayuki Inaba. Stable control in climbing and descending flight under upper walls using ceiling effect model based on aerodynamics. In *2020 IEEE International Conference on Robotics and Automation (ICRA)*, pages 172–178, 2020.

[20] Prasanna Kumar Routray, Aditya Sanjiv Kanade, Kshitij Tiwari, Pauline Pounds, and Manivannan Muniyandi. Towards multidimensional textural perception and classification through whisker. In *2022 IEEE International Symposium on Robotic and Sensors Environments (ROSE)*, pages 1–7, 2022.

[21] Mathew H Evans, Charles W Fox, Martin J Pearson, and Tony J Prescott. Tactile discrimination using template classifiers: Towards a model of feature extraction in mammalian vibrissal systems. In *From Animals to Animats 11: 11th International Conference on Simulation of Adaptive Behavior, SAB 2010, Paris-Clos Lucé, France, August 25-28, 2010. Proceedings 11*, pages 178–187. Springer, 2010.

[22] Xin Wei, Erbao Dong, Chunshan Liu, Guangming Han, and Jie Yang. A wall-following algorithm based on dynamic virtual walls for mobile robots navigation. In *2017 IEEE International Conference on Real-time Computing and Robotics (RCAR)*, pages 46–51, 2017.

[23] Juan Marcos Toibero, Flavio Roberti, and Ricardo Carelli. Stable contour-following control of wheeled mobile robots. *Robotica*, 27(1):1–12, 2009.

A MECHANICAL DESIGN

In this section more information about the modular cage design will be provided. As stated before, the cage can hold 35 whiskers and has a total weight of $346.12[grams]$. The aerial platform is used for tactile navigation, which has a higher risk of hitting object during flight as distances between objects and the drone are relatively small. Hence, this means there is a higher chance of damaging the cage and breaking components. Therefore, it was chosen to make use of a modular design for easy replacement of broken parts.

Besides the general components, the whiskers could also get damaged during flight. To make sure that the whiskers could also be easily replaced the connector nodes have a special fastening system for easy removal. The system consists out of two main parts. The first part being the connectors that are equipped with two pins. The second part is a disc, which can be put on the pins and fastened by rotating the disc. This design acts as a simple click-on click-off system and is shown in Figure 31.

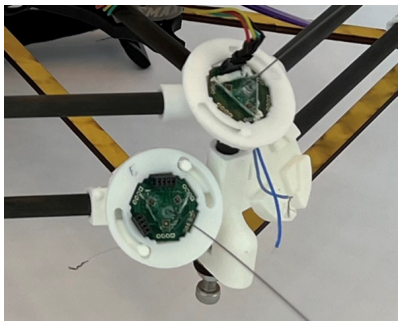

Figure 31: Close-up of the fastening system used to connect whiskers to the connector nodes. Showing the pins on the connectors and the designed fastening disc.

The connectors also contain canals through which the wires of the sensors can flow. This allows for wiring around the cage structure.

An overview of all the main cage components can be found in Table 1. Here, the name of the component, how many times the component is used in the design, and the weight of a single component is given.

Table 1: Overview of the different main cage components

Component	**Amount**	**Weight Single Part**
Inner Connector	8	3.66 [gr]
Outer Connector	8	4.4[gr]
Side Connector	8	10.16[gr]
Base Component	1	28.47[gr]
Whisker Lock Centre	3	0.82[gr]
Whisker Lock	32	0.77[gr]
Pi holder Top	1	11.21[gr]
Pi Holder bottom	1	9.55[gr]
Pi Clamps	4	0.29[gr]
Centre Rod Clamp Bottom	4	1.0[gr]
Centre Rod Clamp Top	4	1.0[gr]
Bottom Frame	2	15.65[gr]
Rod Base to Inner Connector	8	1.32[gr]
Rod Between Inner Connector	8	1.59[gr]
Rod Inner Connector to Outer Connector	8	1.51[gr]
Rod Between Outer Connector	8	2.97[gr]
Rod Base to Bottom	4	1.22[gr]
Rod Outer Connector to Side Connector	4	1.22[gr]
Rod Between Side Connector	8	2.97[gr]

B IMPROVING WHISKER MANUFACTURING

As mentioned in subsection 2.2 the process used to fabricate the whiskers if fully done by hand. This will introduce many inaccuracies and differences in sensitivity and differences in characteristics between whiskers.

One of the steps where inaccuracies are introduced is when the whiskers is placed into the follicle, more precisely the plastic tube, and the UV resin is cured. During this procedure the whisker is being held in place by one hand by the manufacturer and the curing light is being held in the manufacturer's other hand. Because the whisker is held in position by hand, inaccuracies could occur, i.e. the whisker shaft could get slightly angled and it will be cured in that angle. Moreover, if multiple whiskers are made, there is a very small chance that they are positioned exactly in the same way.

To get rid of the inaccuracy of the whisker position during UV curing a special stand was designed during this research. The stand exists out of a base that can hold eight PCBs, a $20[cm]$ rod, and two discs, as can be seen in Figure 32. The two discs each contain eight holes that can be aligned above the center of each PCB position. This allows for placing the whiskers straight into the follicle and the stand also makes the curing process less difficult. It not only increased the accuracy of the procedure it also makes the manufacturing process faster.

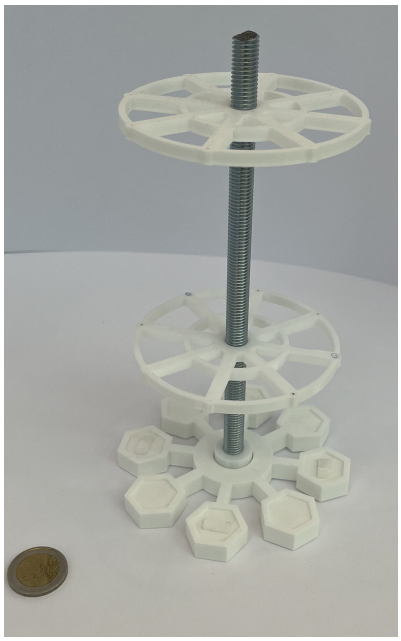

Figure 32: Whisker manufacturing stand with the ability to hold 8 whiskers at once.

Another issue with the current procedure is that the follicles are different for each whisker. Currently for each whisker a triangular mold is made around the three barometers with three pieces of thick tape. This procedure is not very accurate leading to different molds for each whisker, resulting into different follicles for each whisker. It is recommended for future research to design a re-usable mold, which allows for the same follicle design of each whisker. This will improve the similarity between whiskers.

C Cave Structure

In this section photos and additional information of the location and height of the used cave parts will be given.

The cave parts can be seen in Figure 33. The information can be found in Table 2. The cave parts on the experimental set-up are numbered from left to right, starting at 1 ending at 4.

Table 2: Overview of the position in the cave strip and height of the used cave parts.

Cave Part	**Position**	**Height** $[cm]$
1	$0-20[cm]$	4
2	$20-40[cm]$	3
3	$40-60[cm]$	6
4	$60-80[cm]$	6.5

(a) The cave part used on position 1.

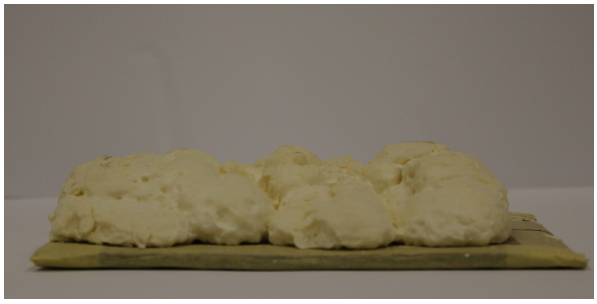

(b) The cave part used on position 2.

(c) The cave part used on position 3.

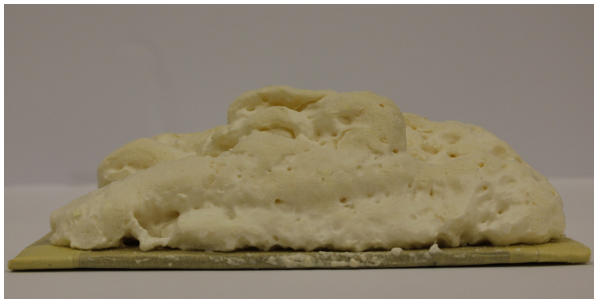

(d) The cave part used on position 4.

Figure 33: Images of the cave structures that were used in the experiments.

D Additional Experimental Results

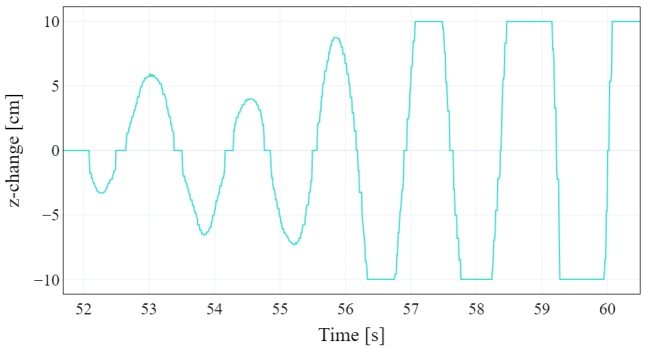

Figure 34: Commanded z-changes during contour following for a smooth and straight ceiling, $\frac{dP}{dt} = 15[Pa/s]$.

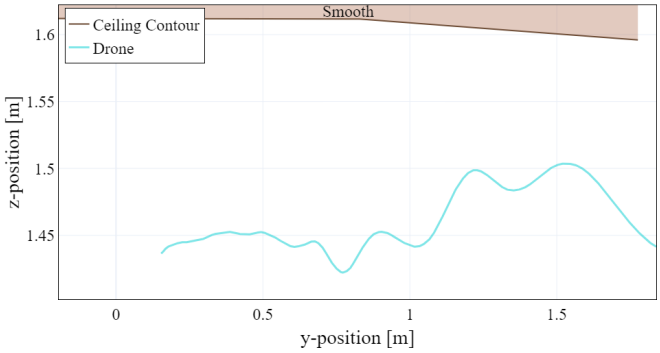

Figure 35: z-position vs. y-position of the drone during the contour following stage for a smooth and straight ceiling, $\frac{dP}{dt} = 30[Pa]$. The drone maintains a mean distance towards the ceiling of $0.153[m]$ with $\sigma = 0.026[m]$.

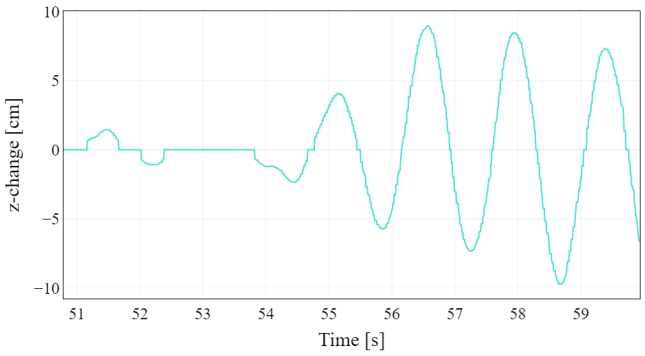

Figure 36: Commanded z-changes during contour following for a smooth and straight ceiling, $\frac{dP}{dt} = 30[Pa]$. A sine wave pattern can be clearly observed in the controller's behavior.

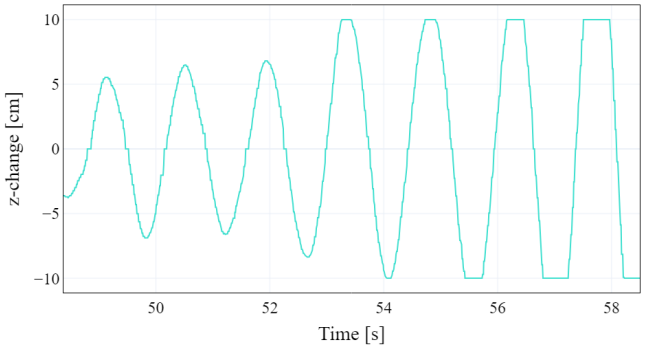

Figure 37: Commanded z-changes during contour following for a smooth and inclined ceiling.

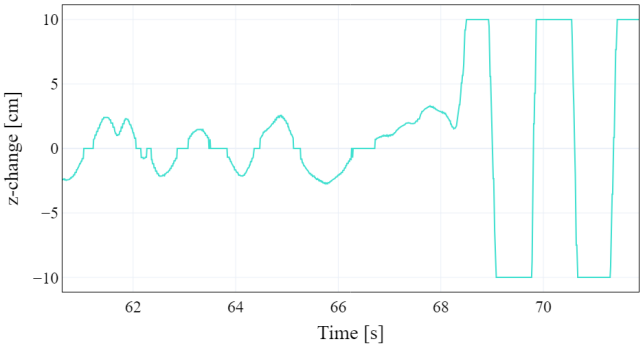

Figure 38: Commanded z-changes during contour following for a rugged and inclined ceiling.

Part 3
Literature Study Report

This part has been graded for the AE4020 Literature Study course

This page is intentionally left blank

Literature Study

Tactile Exploration with Whiskered Drones: An analysis of whiskers and their possible use in aerial tasks

AE4020: Literature Study

Nils de Krom

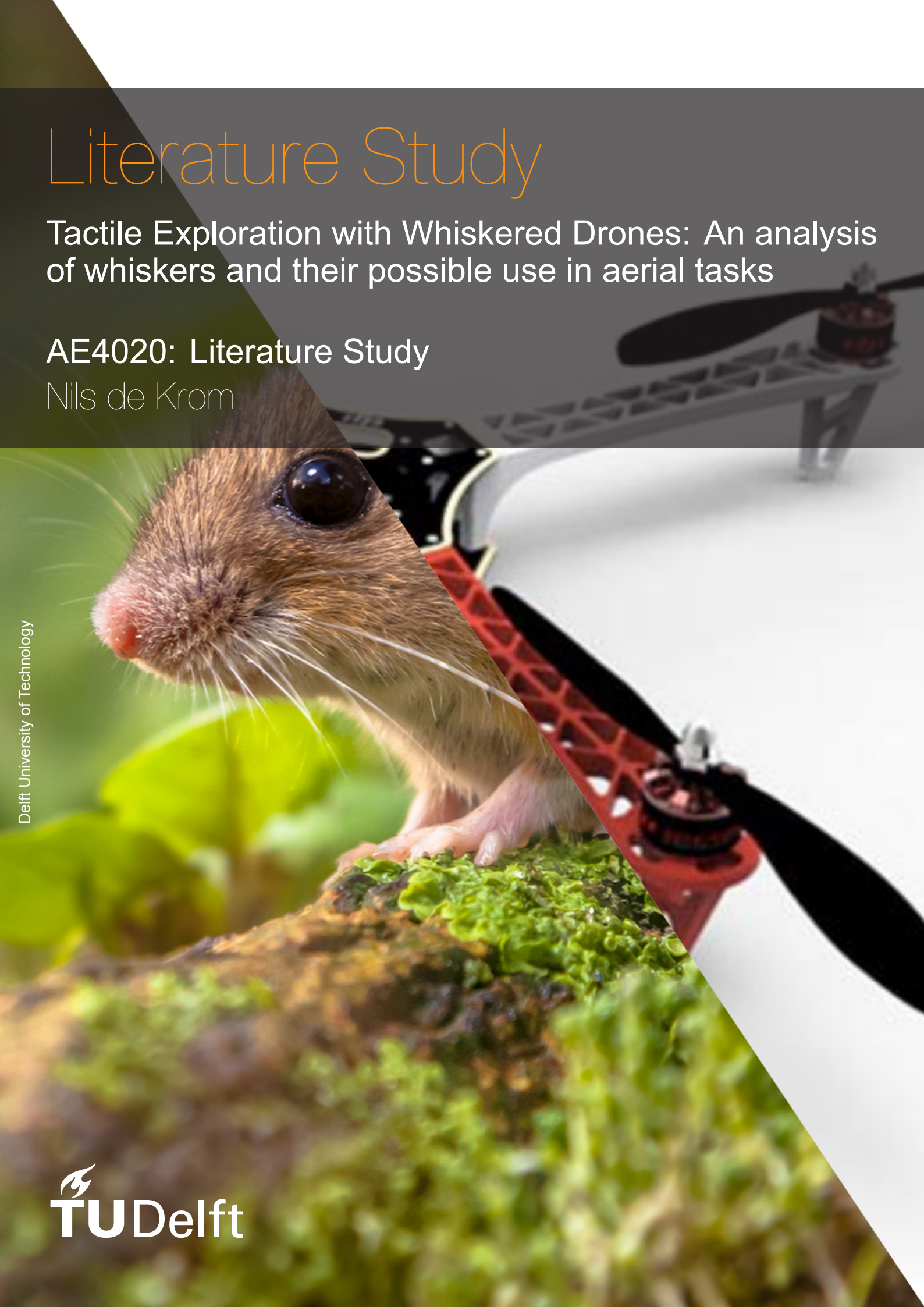

Delft University of Technology

TU Delft

Literature Study

Tactile Exploration with Whiskered Drones: An analysis of whiskers and their possible use in aerial tasks

by

Nils de Krom

Student Number: 4883349

Instructor:	Dr.ir. S. Hamaza
Course:	AE4020: Literature Study
Institution:	Delft University of Technology
Place:	Faculty of Aerospace Engineering, Delft
Project Duration:	May 2023 - August 2023

Cover Image: Combination of image of a male mouse [58] and a drone render [7].

TU Delft

Preface

The report presented in this document is the outcome of the first stage of the MSc. Thesis project about how a contour following navigation task can be performed in an unknown environment, while flying close to the ceiling, with a whisker drone. In this first stage an in-depth literature study has been performed, examining the different research fields related to the project.

By analyzing multiple research papers related to the use of whiskers in nature and in technology, contour following tasks, and flying close to the ceiling a deeper understanding about the topic is obtained. Readers that are interested in the use of tactile sensors in nature can find information about this topic in Chapter 2. Furthermore, for the interested reader, information about artificial whiskers and their existing robotic applications can be found in Chapter 3. Moreover, readers with a specific interest in the effects of flying close to the ceiling can find these in Chapter 4. Finally, information about contour following navigation is provided in Chapter 5.

I would like to express my sincere gratitude to my supervisor Salua Hamaza for all her support, feedback, and guidance during this first stage of my MSc. Thesis.

Nils de Krom
Delft, October 2024

Summary

There are a lot of different environments in the world, such as caves, canyons, and dense forests. Some of these environments can be very difficult and dangerous for humans to explore. For those reasons automated and autonomous systems are used to assist humans in the exploration of these unknown environments. These robotic systems often make use of distal sensors, such as LIDAR, and visual sensors, such as cameras. Unfortunately, there are environments in which these sensors are not efficient or cannot be used. This holds for environments with low visibility, caused by dust, smoker, or darkness. Therefore, to explore these environments different sensor types are needed.

It was concluded from observation in nature that tactile sensors, more specifically whiskers, are used by mammals in nature to perform navigation and exploration tasks. A combination of such whiskers with a robotic system could be the solution for exploring these environments with low visibility. However, environments can not only have low visibility, they can also be hard to access by ground vehicles. For that reason, aerial vehicles such as quadrotors could be used in those environments to solve accessibility problem. Hence, to explore these difficult to access low visibility environments, a combination of whisker-based tactile sensing with a quadrotor could be used.

The above mentioned combination, results in the main goal of the literature study presented in this report. The goal of this report is to find a possible solution for performing an autonomous contour following task in unknown environments, while flying in close proximity with the ceiling, based on whisker-based tactile sensing inputs. The goal is visualised in Figure 1. To find a solution to this problem research was performed in four main fields.

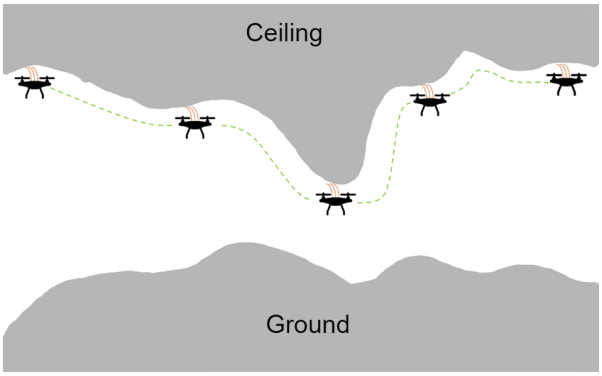

Figure 1: Visualisation of the to be achieved goal of the research.

First of all, the world of tactile sensing was analysed. It was shown that in nature many different types of tactile sensors exist. Arthropods make use of antennae and tactile hairs, fish and amphibians make use of neuromasts, and some aquatic mammals and terrestrial mammals make use of whiskers. An interesting observation was that even tough these are different types of tactile sensors, they are in general used for similar use-cases. They are often used for foraging, hunting, exploration and navigation, and locomotion.

When focusing on the exploratory behavior of animals, based on their tactile sensors, it was observed that they often make use of active sensing strategies to increase the chance of detecting tactile stimuli and that the sensors are used in a closed-loop tactile control system.

Furthermore, there are already some applications of tactile sensing in robotics. These robotic designs are based on observations made in nature. These applications often involve the use of artificial whiskers, which supports the research performed in the second field.

The second research field mainly focuses on whisker-based tactile sensing in robotics. It was found that there are four main design choices for a single artificial whisker, the choice of material, the size of the whisker, the shape of the whisker, and the use of a taper ratio. The type of sensor used to

sense the deflection of the whisker can also vary, it was observed in literature that Hall-effect sensors or barometric pressure sensors are often used.

To design an array of whiskers, multiple design choices also need to be made. The design choices are the number of whiskers used on the array, the use of constant or varying whisker lengths on the array, and the use of a passive or active whisker array.

Furthermore, limitations and drawbacks of the use of whiskers were found. Whiskers are very sensitive, which makes them prone to noise induced vibrations. These vibrations can be caused by the texture of the contact surface or by self-induced motion. Self-induced motion can be caused by using an active whisker array or by applying whiskers on a moving platform. To account for the induced noise, different strategies can be applied. A whisker array can be used in a voting mechanism that cancels out false readings. Moreover, the introduction of adaptive filtering can cancel out self-induced motion in the whisker readings.

The research in this field also covered the current use of whiskers in robotics. It was shown that there are already many applications for texture classification and exploration. However, all these whisker-based robotic applications are either robotic arms on the ground or ground moving robots.

The third topic that was studied, was the ceiling effect topic. The ceiling effect causes an increase in thrust and a decrease in power consumption when flying close to the ceiling. This is caused by a greater pressure difference across the rotor disk.

The research showed that two main methods to approximate the change in thrust and power due to the ceiling exist. The first approach uses thrust and power equations obtained from Momentum Theory and Blade Element Theory and the second approach makes used of variations of the Cheesman-Bennet model. Both approaches are able to properly estimate the change in thrust and power consumption for a quadrotor and there is no clear winner. Literature also showed promising initial results for applications of both methods in controller designs.

The final field included navigation performed by contour following and mapping of an environment with whisker-based tactile sensory data. It showed that contour following is often used in navigation and exploration tasks and that there are many different approaches. A comparison was made between general contour following controllers and intelligent controllers, that use fuzzy logic. It was shown that both controller approaches are able to explore and navigate a mobile robot in an unknown environment.

It was also found that simultaneous localization and mapping (SLAM) can be performed with whisker-based tactile sensors. Three main approaches were found, blob-based mapping, mapping with hierachical priors, and mapping with multi-whisker templates. Furthermore, a special SLAM algorithm called Whikser-RatSLAM exists. This approach is based on the behavior of a rat and it can not only perform mapping but also object recognition and localization.

From the information obtained in the four research field, it was concluded that there are two main gaps in research. The first gap is, that all the current whisker-based robotic applications are performed on ground-based robots. Hence, the application of whiskers on aerial vehicles is not yet researched. Therefore, it is unknown how whiskers will behave on such platforms.

The second gap is related to the ceiling effect. In current studies related to the ceiling effect, the distance towards the ceiling is measured with distance sensors, such as laser sensors, however it is not yet done with tactile sensors, such as whiskers. This means it is not yet known if whisker can actually be used to measure distances towards the ceiling and it is not yet known how the behavior of the whiskers will change when being in close proximity with a ceiling.

Furthermore, the current controller designs based on the ceiling effect are only done for smooth horizontal surfaces. Hence, it is also not yet known if the found ceiling effect estimation will work for asymmetric surfaces.

Contents

Nomenclature

Abbreviations

Abbreviation	Definition
AGDE	Adaptive Group-based Differential Evolution
BET	Blade Element Theory
CIA	Contact-Induced Asymmetry
CNS	Central Nervous System
EGPSO	Evolutionary-Group-based Particle-Swarm Optimization
FC	Fuzzy Controller
FSM	Finite State Machine
MIMC	Minimal Impingement, Maximal Contact
MT	Momentum Theory
SLAM	Simultaneous Localisation And Mapping
tSLAM	Tactile Simultaneous Localisation And Mapping
WF	Wall-Following

Symbols

Symbol	Definition	Unit
A	Area propeller disk	$[m^2]$
c_0	Coefficient related to propeller properties	$[-]$
c_1	Coefficient related to propeller properties	$[-]$
c_2	Coefficient related to propeller properties	$[-]$
c_τ	Torque coefficient	$[N \cdot m \cdot s^2/rad^2]$
c_T	Thrust coefficient	$[N \cdot s^2/rad^2]$
P_a	Aerodynamic power	$[W]$
P_m	Mechanical power	$[W]$
R	Propeller radius	$[m]$
T	Thrust	$[N]$
T_{ICE}	Thrust with influence of the ceiling	$[N]$
T_{OCE}	Thrust without influence of the ceiling	$[N]$
v_i	Induced velocity	$[m/s]$
v_∞	terminal velocity	$[m/s]$
$\dot{z}$	Vertical velocity	$[m/s]$
α	Correction factor	$[-]$
δ	Propeller-to-ceiling-ratio	$[-]$
γ	Ceiling Coefficient	$[-]$
η	Figure of merit	$[-]$
ρ	Density	$[kg/m^3]$
Ω	Rotational velocity	$[rad/s]$

List of Figures

1 Introduction

The urge to explore is embedded in the nature of mankind. In the early days, humans used to explore new and unknown environments by themselves on foot. They would explore caves or map rivers by following this river through the jungle, like Francisco de Orellana did for mapping out the Amazon river.[68] However, exploring unknown environments, for example a cave, could be very difficult, time consuming, and dangerous for a human. Luckily, due to the technological developments in the past decades mankind is now able to use automated and autonomous vehicles to perform exploration and mapping tasks for unknown environments.

The proof of autonomous and automated robots being able to perform exploration and localization tasks in difficult environments was shown by the DARPA Subterranean Challenge. In this challenge the subterranean environment was extremely diverse, containing for example narrow passages and long tunnels. The goal of this challenge was to use automated vehicles to explore this diverse environment and localize object in the environment. The winner showed that by using walking, driving, and flying vehicles exploration and object finding could be performed. These robots made use of laser sensors, such as LIDAR, and visual sensors, such as color cameras. [73]

However, there are environments where these type of sensors are not efficient or cannot be used at all. This would be the case in environments with low visibility, due to smoke, dust, or darkness. To be able to explore and navigate in these environments different type of sensors are needed. Luckily, the solution to this problem can be found in nature. When looking at the exploratory behavior of humans in dark and unknown environment, it can be observed that they use their hand to feel, explore, the environment. Hence, humans make use of tactile sensing. A similar observation can be made in the animal kingdom, specifically for nocturnal animals or animals that live in poorly-lit environment. Rodents also make use of tactile sensing to explore, navigate, and hunt. They have specialised tactile sensors, called whiskers or vibrissae. Whiskers are found on a lot of mammals, and are proven by nature to be very effective tactile sensors. [55]

This could mean that, using the observations from nature about tactile sensors, a robot equipped with whiskers could be able to navigate in environments with poor visibility. However, environments could also be hard to access with ground vehicles, which means aerial vehicles might be needed. It would be interesting to analyse if a combination between an aerial robot and the whisker-based tactile sensor could be achieved to explore such difficult environments.

Such an analysis will be performed in this research. To have a clear image of the main goal of this research, a research objective is derived. The main objective of his study is the following:

Perform an autonomous contour following aerial navigation task in an unknown environment, using a whisker-based tactile sensing approach.

However, this goal is still quite broad and it can be achieved in many different ways. Therefore, this goal should be specified with the help of a research question to obtain a specific approach to fulfill the goal. It was chosen to focus on a ceiling contour following task. The following research question was obtained:

How can whisker-based tactile sensing be used to perform autonomous contour following navigation tasks in unknown environments, while flying in proximity with rugged ceilings, with a quadrotor?

The goal of this research question can be visualised with the help of Figure 1.1. Figure 1.1 shows a quadrotor with whiskers on the top, which follows the contour of the ceiling, while flying very close to the ceiling.

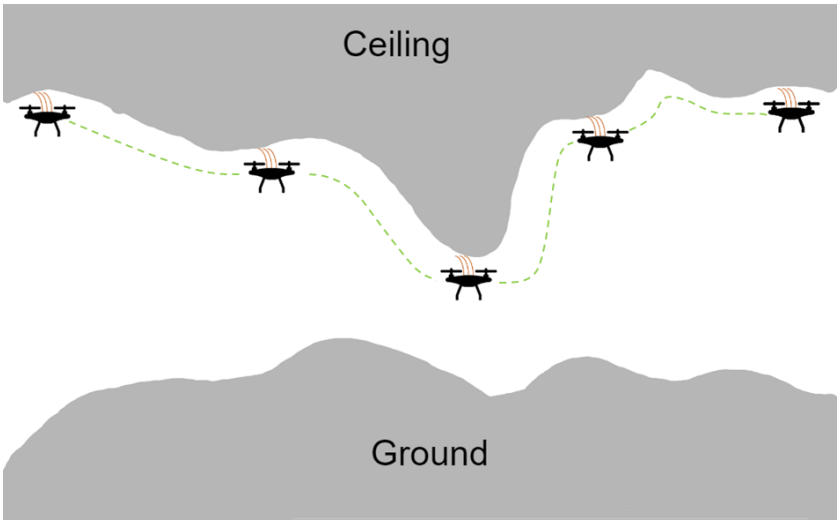

Figure 1.1: Visualisation of the to be achieved goal of the research.

To be able to answer this research question as detailed as possible, six sub-questions are derived from the main research question. Each sub-question will help in finding an answer to a certain part in the research question. The sub-questions are given below.

1. How can whisker-based tactile sensing be used in navigation tasks?
2. How many whiskers does the whisker array have?
3. What is autonomous decision making?
4. What is contour following and how can it be performed by an autonomous system?
5. What are the desired unknown environments?
6. How does flying in proximity with the ceiling, affect the behaviour of the quadrotor?

To provide answers to all the sub-questions, a literature study is performed and the findings are shown in this report. The report is structured as follows. First of all, Chapter 2 gives an introduction to the world of tactile sensing. It will provide information about tactile sensors in nature, their use-cases, and how they are used in exploration tasks. Furthermore, the chapter will show the use of tactile sensors in robotics.

Second of all, Chapter 3 will focus on whisker-based tactile sensing. Different design options for single whiskers and whisker arrays will be discussed. Moreover, limitations and drawbacks of whisker-based tactile sensing will be provided. The chapter will also discuss approaches for filtering the obtained measurement data from the whiskers. Finally, an overview of whisker-based robotics will be given.

Third, the influence of flying close to a ceiling will be explained in Chapter 4. It will describe the ceiling effect principle and multiple different approaches to estimate the influence of the ceiling effect.

Fourth, Chapter 5 focuses on the different approaches that can be used in the design of a contour following controller. Furthermore, it will discuss how whisker sensory data could be used to perform mapping of the environment.

All the key observations from the previous chapters will be concluded in Chapter 6. These key observations will be used to answer the sub-questions, hence the research question. Furthermore, proposals for future projects will be given.

Finally, Chapter 7 will discuss the next steps in this research to obtain the practical solution, together with a global planning.

2
The World of Tactile Sensing

Every living organism is influenced by tactile stimuli. To what degree these tactile stimuli are used and how they are observed depends on the species. The ability to observe tactile inputs is a key characteristic in the world of tactile sensing and therefore an important topic to analyse. Section 2.1 looks into tactile sensing in nature. Focusing on the type of sensors used in nature and their applications.

Tactile sensing is not only important in nature, but it also became an interesting topic in the field of robotics. This research field uses examples from nature to develop tactile sensors that can be used in robotics. Therefore, Section 2.2 introduces the tactile sensors that are currently used and looks into their applications.

An overview of the key findings of this chapter will also be given at the end in Section 2.3.

2.1. Tactile Sensing in Nature

In nature, tactile stimuli are everywhere and therefore there is the need for tactile sensing. It has been found that simple organisms without a Central Nervous System (CNS), such as a single-celled organism, multi-cellular organisms, and plants, are able to perform directional detection of tactile inputs. [55]

For this research, however, looking into organisms with a CNS will suit the desired application more, because the future whiskered drone should be able to respond to the observed touch. Organisms with a CNS can actively sense and respond to touch, and use it to their advantage.[55][56]

In Section 2.1.1 the performed research about tactile sensors in nature is described. Furthermore, Section 2.1.2 describes the exploratory behavior of animals based on their tactile sensors.

2.1.1. Tactile Sensors and their Use-Cases in Nature

There are many different species on Earth. A lot of these species developed specific sensors to sense tactile stimuli, called tactile sensors. While the use-cases for the tactile sensors between species might be the same, different types of tactile sensors are developed. In this section some of these species with their tactile sensors will be discussed.

First of all, the tactile sensors used by the arthropods family are analysed. The arthropods family exists of spiders, Crustaceans, insects and their relatives. The first tactile sensor in this family can be observed when looking into insects and Crustaceans, which is the antenna. The antennae are their most important attributes to obtain tactile information. [21] [55] An example of an insect with antennae can be seen in Figure 2.1, the stick insect. The stick insect uses its antennae as active distance sensors for environmental exploration, for example for obstacle detection and path-finding during the night.

The insect antenna uses multiple mechanosensory submodalities for tactile sensing, such as the campaniform sensilla. Campaniform sensilla are often located at the base of the antenna to be able to sense shear forces induced by the bending of the antenna, they can be seen as strain sensors. Furthermore, the antenna is able to measure vibrations with the help of a chordotonal organ, which can be used to detect postural changes. Besides the campaniform sensilla and the chordotonal organ the antenna also carries thousands of sensory hairs. These hairs are not only used for touch but also for smell, taste, temperature sensing, humidity sensing, and gravity sensing. [21]

Sensory hairs are used in hair fields and as tactile hairs. The hair fields are located near joints of two body segments and allow to measure the joint angle and the deflection, in this case antenna deflection. Hence, they are used for proprioception. The tactile hairs are positioned across the entire antenna and are used for exteroception.

While Crustaceans and insects use a combination of antennea and sensory hairs, spiders only make use of sensory hairs. These hairs are also used as proprioreceptors and exteroreceptors and are located at areas on the body where contact with the environment is most likely to occur. Furthermore, the hairs can differ in length and serve as event detectors and texture classification sensors. They can be deflected by direct contact or via pre-contact, friction forces induced due to airflow.[6] [55] An example of a spider with tactile hairs can be seen in Figure 2.2.

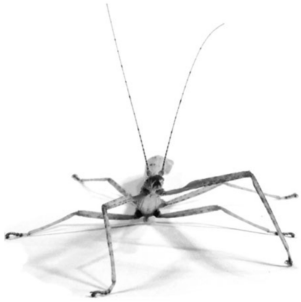

Figure 2.1: Stick insect with two long antennas, used for touch and smell.[21]

Figure 2.2: Honduran Curly Hair Tarantula with tactile hairs. [49]

Aquatic animals, such as fish and aquatic mammals, also use sensors with characteristics similar to tactile hairs. Fish and amphibians make use of neuromasts, which are mechanoreceptor organs. For many fish species these neuromasts are often positioned in a line structure in a canal, called the lateral line system, see Figure 2.3. [9] Fish species use their lateral line system, which provides a version of remote distal touch, for prey localization, obstacle detection, predator evasion, and locomotion.

As can be seen in Figure 2.3 the lateral line system has neuromasts on the outside, called superficial neuromasts, and neuromasts inside the canal, called canal neuromasts. The most important part of a neuromast is its hair bundle, which contains the molecular machinery for mechanotransduction. The hair bundles are influenced by hydrodynamic stimuli, induced by changes in water flow or changes in pressure difference. While superficial neuromasts are directly influenced by the flow, the canal neuromasts are only influenced when there is a pressure difference at the pores that open the canals to the neuromasts. [55][45]

Furthermore, aquatic mammals, for example pinnipeds and manatees, make use of their sensitive vibrissal sensory systems to obtain tactile stimuli. They have long facial whiskers (vibrissae) located on their snout, which form a passive tactile sensory array around the head, see Figure 2.4. [29] Each whisker comes out of a vibrissal follicle-sinus complex, which constitute complex and richly innervated sensory organs that allow for detecting tactile stimuli. The whiskers are used for direct contact sensing, touching objects, and pre-contact sensing, obtaining and analyzing water movements. This means that the whiskers can assist in prey capturing, foraging, locomotion, but also in social interaction.[29] [60][59]

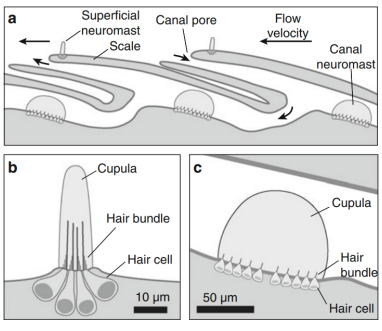

Figure 2.3: Schematic visualisation of the lateral line of a fish. **a** shows the positioning of the superficial neuromasts **b** and the canal neuromasts **c**.[45]

Figure 2.4: A bearded seal, its beard consists out of tactile sensors, whiskers. [61]

Besides aquatic mammals, most terrestrial mammals also have vibrissae, particular the ones that inhabit poorly-lit spaces and are nocturnal. The main focus will be on terrestrial rodents and their whiskers,

for example a rat, see Figure 2.5. Rodents have macrovibrissae and microvibrissae. The macrovibrissae can be actuated to perform active whisking to explore the environment, while microvibrissae are non-actuated and used to investigate the stimuli found in the environment via the active whisking. [56] The use of active whisking, moving the whiskers in an active sweeping motion, together with head an body motions are used for localising, orienting, exploring, and tracking the environment, and for tactile discrimination, locomotion, social interaction, and prey capturing. For example, the hunting behavior of the Etruscan shrew is purely based on tactile cues. They use tactile contact information from a body part of their prey, crickets, to guide their attacks towards their preferred attacking location on the preys body. [62]

Finally, humans also detect tactile stimuli with their tactile sensors. Humans already perform active tactile sensing before they are born and continue to do so for the rest of their lives. While in the early stages of life the mouth and lips are the primary haptic sensors, the hands take over this role in a later stage due to high concentration of tactile sensory afferents in the human hand, Figure 2.6. [55] Humans use their tactile sensors for social touch, environment exploration, and haptic exploration tasks. Such haptic exploration tasks are texture and hardness classification and shape estimations. [39]

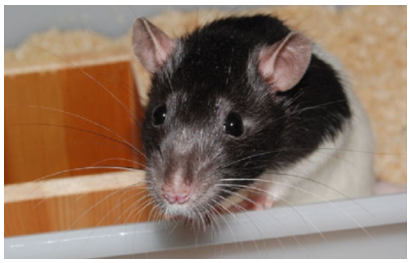

Figure 2.5: A rodent, rat, with whiskers. [56]

Figure 2.6: The main body part with the highest concentration of tactile sensory afferents for humans, the hand.[37]

2.1.2. Exploration Behavior in Nature with Tactile Sensors

Based on their tactile sensors, animals will show certain exploratory behavior. For some of the organism mentioned in Section 2.1.1, the exploratory behavior will be discussed. The main focus will be on whisker-based tactile exploration.

When looking into the exploratory behavior of the stick insect, it can be concluded that it uses an active searching behavior. During locomotion the stick insect keeps moving its antennae in a rhythmic fashion in the direction of walking. This increases the chance of detecting obstacles in its environment. When an obstacle is detected the stick insect will adapt its stepping pattern and leg movements in a context-dependent matter [20], meaning it makes use of a closed-loop tactile system. [21]

According to [28] rodents have a specific exploration pattern when they are places into a dark and unknown environment. They use their whiskers to first explore the entrance to this new environment, then they will perform a wall-following strategy, and finally they will explore the open space in the environment.

Furthermore, when rodents are performing exploratory behavior they use head and body movements together with active whisking in a non-contact and contact scenario. For non-contact whisking the rodent will be whisking in free air without encountering any obstacles. In the case of contact whisking, the rodent has detected an obstacle and uses whisker tapping and brushing behavior to obtain more information about the encountered obstacle. [30] The range of the whisking motion will be selected by the animal in such a way that it optimizes the collection of information during a certain task.[2]

When the whiskers encounter an object the whisking pattern will change. First of all, on the side the contact was made the protraction of the whiskers get suppressed, while on the other side the protraction of the whiskers will be increased, see Figure 2.7. This behavior is called Contact-Induced Asymmetry (CIA) [47][48][19] or Minimal Impingement, Maximal Contact (MIMC) control policy [52]. The goal of this behavior is to increase the amount of whisker contacts. Second, the spread between whisker columns, the protraction angles, is reduced. This is consistent with the MIMC control policy, because rearward,

non-contacting, whiskers will be pointed to the front towards the encountered obstacle. [47][52] From the CIA and MIMC control policies it can be deduced that the there is a closed-loop architecture in the vibrissal system of rodents, which allows efficient adaptive control of the whiskers. [1]

Figure 2.7: Image of a rat showing the MIMC behavior, the whiskers not in contact with the object are fully protracted.[52]

Humans also have a closed-loop tactile system, because they use tactile feedback in their exploratory behavior. In haptic exploration, humans make use of exploratory procedures that allow for an optimized gathering of data for a specific task. Examples of exploratory procedures are lateral motion, pressure, and contour following. With lateral motion the skin is moved across a surface which is used for texture classification. Exploration procedures can also provide multiple data entries. Contour following allows to obtain the shape of an object, but it will also provide information about the textural classification of the object. [39] [40]

During these exploratory procedures, humans make use of tactile suppression. [13] states that the function of tactile suppression is to use motor command feedback to predict and suppress redundant movement-related tactile observations such that the perception of unexpected or novel inputs is enhanced. During movement tactile stimuli that are below a certain threshold will not be detected. [12] This threshold depends on the speed of the movement [17] and the physical relation between movement and stimulus [78].

2.2. Tactile Sensing in Robotics

Many tactile sensor designs in robotics are based on observations about touch in nature, biomimetics. Robotics for example looked into the human hand and skin, to be able to mimic its behavior for an artificial fingertip, see Figure 2.8. The focus has not only been on humans but also on other tactile sensors in the animal kingdom, such as antennae and whiskers. As mentioned in Section 2.1.1 whiskers are used in nature for texture classification and exploration, which make them interesting for the field of robotics. An application of whiskers on a moving robotic platform, the SCRATCHbot [52], can be seen in Figure 2.9. [55][44]

Figure 2.8: Application of artificial fingertip sensors.[44]

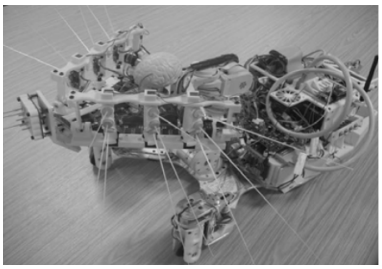

Figure 2.9: Application of whiskers in robotics, the SCRATCHbot.[52]

The examples shown, use different tactile sensors to be able to perform their required tasks. In robotics, tactile sensors are divided in groups based on the transduction methods they use to convert tactile stimuli into a usable form for a robotic system. Tactile sensors used in robotics are: capacitive sensors, piezoresistive sensors, optical sensors, magnetic sensors, binary sensors, piezoelectric sen-

sors, and hydraulic sensors. Where magnetic hall sensors are often used in combination with artificial whiskers.[44]

2.3. Key Findings from the World of Tactile Sensing

In Section 2.1.1 it was shown that there are a lot of different tactile sensors in nature, insect antennae, tactile hairs, lateral line systems, and whiskers. These sensors are used in many different applications of which a summary is shown in Figure 2.10. A key observation about the tactile sensors in nature is that they are directly or indirectly used as range sensors. Therefore, they can be used as main sensor components in exploration. Furthermore, most of the tactile sensors are used by organisms that inhabit poorly lit spaces, meaning tactile sensing is a valid option to replace vision in these scenarios.

In Section 2.1.2 it was explained that organisms use specific tactile exploration strategies, based on the task at hand. Most of these strategies are active sensing strategies in which the tactile sensors are constantly being moved to increase the chance of detecting tactile stimuli. An important observation is that the sensors used in the exploration strategies are implemented in a closed-loop system, meaning that the obtained tactile information is used to correct for example locomotion. Hence, nature makes use of closed-loop tactile control systems. Another interesting observation is the use of tactile suppression, which prevents false reading by damping out motion induced tactile stimuli.

Finally, Section 2.2 showed that tactile sensing applications in robotics exist, which are based on the sensors and applications observed in nature. An important observation is the use of whiskers in robotics on mobile platforms. This is initial proof that whiskers can be used in robotic applications, which represents the foundation of this research.

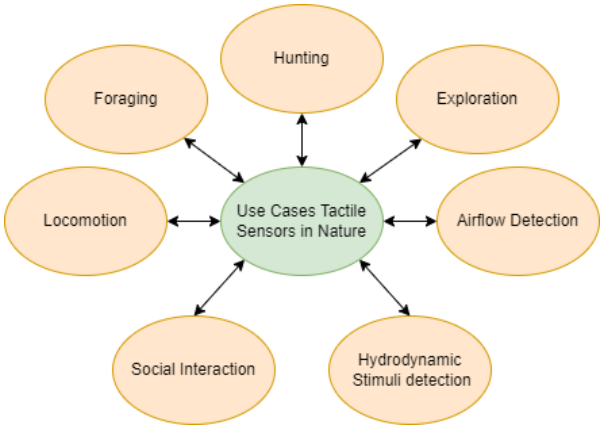

Figure 2.10: Summarizing overview use-cases tactile sensors in nature.

3
Whisker-Based Tactile Sensing

In Chapter 2 the use of whiskers in nature was discussed. It was found that in nature whiskers are used in many different tasks such as exploration, locomotion, and texture discrimination. Chapter 2 also briefly mentioned the use of whiskers in the field of robotics. This chapter will delve more into the design of artificial whiskers and their applications in this sector.

First of all, Section 3.1 will discuss the current applications of tactile sensing in robotics. Second, design options for whiskers will be highlighted in Section 3.2. Third, Section 3.3 explains different options for whisker array design. Fourth, limitations and drawbacks of the use of whisker-based tactile sensing will be mentioned in Section 3.4. Fifth, options for filtering of the obtained data via whiskers are discussed in Section 3.5. Finally, some current whisker applications in robotics will be shown in Section 3.6. Moreover, a summary of all the key findings of the chapter will be provided inSection 3.7.

3.1. Tactile Sensing Applications

As briefly mentioned in Section 2.2 a lot of the tactile sensing designs in robotics are based on ideas derived from observations made in nature. The same holds for the applications of these designs. [23] for example uses a bio-inspired artificial whisker for fluid motion, hydrodynamic stimuli, sensing and [43] uses a hand like structure to grasp objects.

Many studies have also been done in using tactile sensors for texture classifications, examples can be found in [63], [69], and [24]. It is not only valuable to obtain the texture of an object but also to recognize and localize it. Object recognition and localization using tactile sensing is done in [79] and [67].

A relatively new research area is the use of tactile sensors for exploration and navigation. Examples of studies related to this area can be found in [10], which uses a contour-following approach, and [52] which uses active sensing.

A general overview of some of the tactile sensing applications in technological research fields can be found in Figure 3.1.

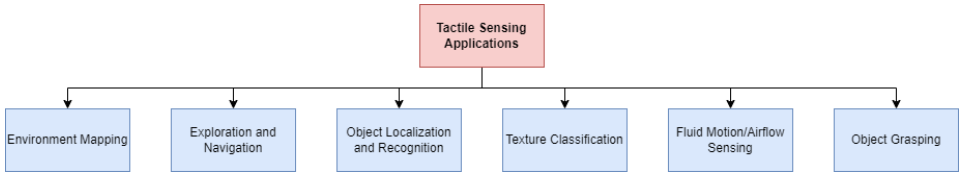

Figure 3.1: Overview of different applications in which tactile sensing could be used.

3.2. Whisker Design Options

When looking at whiskers in nature, there are many different designs. This can be confirmed by comparing the whiskers of the rat shown in Figure 2.5 with the whiskers of the bearded seal in Figure 2.4. The bearded seal has much longer and more curved whiskers than the rat. Furthermore, between species, the shape of the whiskers differs as well. Terrestrial mammals have more tapered whiskers with a round cross-section, while eared seals and walruses typically have non-tapered and oval whiskers. [55]

These different designs in nature might all be applied to artificial whiskers. Therefore, it is important to be familiar with the artificial whisker designs that are currently used, which will be covered Section 3.2.1. Furthermore, sensors are needed to measure the observed tactile stimuli by the artificial whiskers. Different type of sensors that are used in literature will be shown in Section 3.2.2.

3.2.1. Whisker Material, Shape and Dimensions

There are four main design choices for artificial whiskers, which are related to material choice, whisker size, whisker shape, and the use of a taper ratio.

The choice of material is very important since material properties greatly affect the sensory signal's qualities. For example, one of the main material properties is stiffness, because the stiffness of the material influences the frequency properties. Therefore, incorrect material selection could result in significant and persistent oscillations in whiskers, which could result in inaccurate sensor readings.[42]

In literature, different material types are used, varying from thin steel beams [38] and carbon fibre whiskers [63] to glass-fibre composite whiskers.[27] However, the reoccurring material type is the use of plastics. [52][79] Most authors make use of ABS [18] or NanoCure-25. [69], [41], [25], and [51] are studies which include NanoCure-25.

The usage of plastics can be justified relatively easily. Plastics provide specialized production techniques like extrusion and 3D printing, which make it simpler to produce whiskers with variable lengths and unique geometric properties, such as a taper ratio. An example of extruded whisker fibres of different lengths can be seen in Figure 3.2.

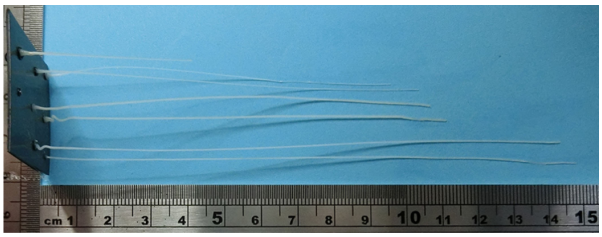

Figure 3.2: Example of extruded whisker fibres with different lengths.[18]

When examining the length and shape of artificial whiskers, it was found in the literature that straight whiskers were typically used. [53] was the only paper found that mimicked the curvature observed at a whisker of a rat. There is no clear reason found in literature why the main design choice is to use straight whiskers. It could be the case that for straight whiskers it is easier to estimate the displacement of the whisker and the induced forces. However this is a speculation and not supported by literature.

The chosen whisker lengths in literature varied between short whiskers between $4 - 8[cm]$ in [18], [79], and [41] and longer whisker with length larger than $14[cm]$ in [27], [25], [52]. [18] states that the chosen whisker length should be based on its application. Long whiskers should be used when the whisker is used in low speed fluid velocity settings, while short whiskers should be used when the whisker is used in high speed fluid velocity sensing. Furthermore, as mentioned in Section 2.1.1 rats use their macrovibrissae for obstacle detection and their microvibrissae for closer inspection of the stimuli to derive for example texture cues.

Using the observation from literature and the observation from nature, the differences in the used artificial whisker lengths in literature could be explained. The whiskers used on "large" mobile platforms are longer whiskers which move at low speeds through the air, hence low fluid velocities. The shorter whiskers are often used in very detailed texture classification tasks, which mimics the use-case of short whiskers in nature.

The final design choice is about the use of a tapered whisker. There are three advantages when using a tapered whisker. First, a small whisker tip will improve the resolution of fine surface features. Second, in case of tip breakage there will be a smaller impact on the natural frequencies of vibration. Finally, it has a large effect on models of static sensing.[77][8] For these reasons, a lot of examples in literature make use of a tapered whisker. The taper ratio used in literature is often $\approx 5:1$, meaning that the diameter at the base is five times larger than the diameter at the tip. This taper ratio is used because it mimics the properties of rodent whiskers. [25]

3.2.2. Sensors for Whisker Deflection Measurements

Many different sensors have been used in robotic whisker implementations over the years to obtain measurement data from the artificial whiskers. For example the electret microphones were used in [42] and strain gauges were used in [27]. However, there is one sensor that is most often used in literature, which is the Hall-effect deflection sensor.

A Hall-effect sensor measures the deflection of a magnet. If such a magnet is placed on the base of a whisker shaft the sensor can be used to measure the deflection of the whisker by measuring the deflection of the magnet with respect to its calibrated origin using the change in magnetic flux. An example of a Hall-effect sensor in combination with a whisker is shown in Figure 3.3. To be able to measure deflections in two directions a tri-axis Hall-effect sensor should be used. [69], [24], [25], [52], and [38] represent research papers that present examples of applications of the Hall-effect sensors for measuring whisker deflections.

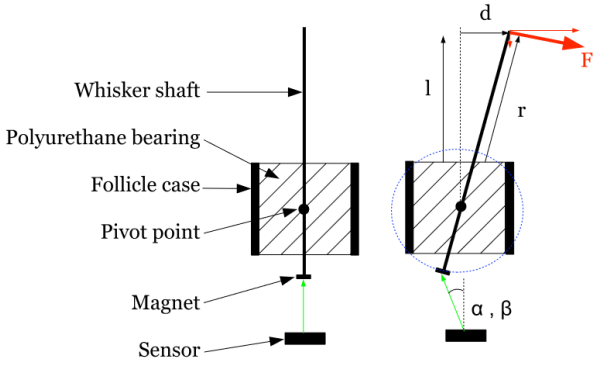

Figure 3.3: Visualisation of the use of a Hall-effect sensor in combination with a whisker.[24]

An new sensor has recently entered the artificial whisker field, the barometric pressure sensor. These sensors are capable of detecting microforces, such as the velocity of the surrounding air, and have a low power consumption. When used in combination with a whisker the sensors use changes in pressure to measure the direction and magnitude of the force applied to the whisker.[70] [79] Examples of the use of the barometric pressure sensor can be found in [18], [63], and [79].

3.3. Whisker Array Design

When looking into the different whisker-based robotics applications, it can be concluded that all these applications use an array of whiskers. This design choice is supported by [42], which states that using an array of whiskers will lead to better and more accurate sensory data. This is confirmed by [38], which states that an array of whiskers can provide more precise information about the shape of an encountered object and the contact distance towards that object rather than a single whisker. Furthermore, the use of a whisker array is also supported when observing vibrissal sensory systems in nature, because these systems are also based on whisker arrays, as shown in Section 2.1.1.

Same as for a single whisker, there are different design options for a whisker array. The whisker array design options are the number of whiskers on the array, using constant or varying whisker lengths, and having an active or passive array.

Number of Whiskers on Array

There are many different array sizes used in literature. Varying from relatively small arrays with five whiskers [79] to large arrays with twenty whiskers [4]. However, there is no clear reasoning in literature why certain array sizes are used. There are reasons for using multiple smaller or larger arrays, hence varying of the total number of whiskers. It was observed in [69] that for applications related to texture classification multiple smaller arrays of four whiskers were used to obtain a set-up with twenty four whiskers. To be able to perform proper classification, large batches of accurate texture data is needed, which can be obtained with a larger total number of whiskers. This is supported by [42]. Furthermore, for mobile robotics it can be seen that multiple smaller arrays are used surrounding the robot to be able to increase the chance of detecting obstacles, an example can be seen in Figure 3.4 which shows the Koala Robot.

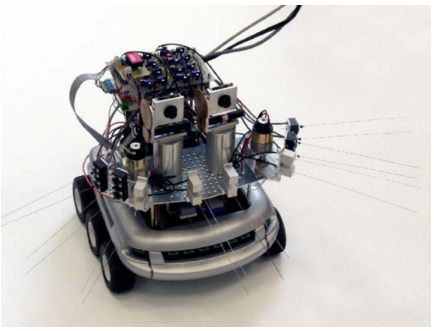

Figure 3.4: An example of the use of multiple arrays on the Koala Robot. [38]

Figure 3.5: An example of a whisker array with little spacing between whiskers. [79]

It is also interesting to look into the spacing between the whiskers on the array. A general observation could be made from the read literature. When the whisker arrays are used for tasks where very accurate and detailed data is required, i.e. for texture classification and object recognition, the whiskers are placed relatively close too each other on the array. An example of such an array can be seen in Figure 3.5, which is used in multiobject exploration and recognition [79]. Similar examples can be found in [69], [41], and [65].

For less accurate tasks, such as global shape recognition, obstacle detection, and tactile stimuli detection, more global data about the environment is needed. Therefore, the whiskers on the arrays are spread out more to increase the chance of detecting i.e. obstacles. This can be seen in Figure 3.4 for the Koala Robot, the whiskers are spread out more to increase the search area. Similar examples can be found in [52] and [25].

Constant or Varying Whisker Lengths

As mentioned in Section 2.1.1, rats have macro- and microvibrissae. This means rats and rodents, have varying whisker lengths in their whisker arrays. A lot of the studies done in the field of artificial whiskers focus on biomimetics, which resulted, in some cases, in artificial whisker arrays with varying whisker lengths.

It was observed that whiskers in each row of the mystacial pad of whisking mammals exponentially increase in length from the front to the rear, with a ratio between the adjacent whiskers, depending on species and the whisker row, between $1.2 - 1.6$.[11] For this reason, [69] uses a ratio of 1.4 for its cone shaped whisker array, allowing all the whiskers to be in contact with a plane surface orthogonal to the axis of the cone. This principle is also used in [51] and [65].

[52] also mimics the rats mystacial pad by having two $3x3$ arrays with whisker lengths, from front to back, varying between $160 - 220[mm]$. However, this whisker-based robotic platform also has an additional array with even shorter whiskers of $80[mm]$ to mimic a rats microvibrissea. Whereas in rats, the shorter whiskers are used similarly, for a closer examination of the tactile stimuli. This shows that based on the tasks of the robotic platform there are different approaches for varying whisker lengths on the platform, varying whisker lengths on the same array, or varying whisker lengths between arrays.

When revisiting the statement from [18], about whisker lengths being dependent on their applications, it can be concluded that if varying whisker lengths are used in the same array, a multi-functional array can be obtained. This could be a very interesting application for a mobile robotic platform, because with the same array it could for example measure airflow disturbance velocities with shorter whiskers, which can then be used to correct readings for the longer whiskers in the same array, that are for example used for obstacle detection.

Active or Passive Whisker Arrays

In nature, many rodents perform active whisking with their macrovibrissae. This has the advantage of sampling a larger space in the environment surrounding their heads and they will be able to point their whiskers to nearby tactile stimuli. [57] Besides the whisking, rodents also perform a tapping behavior with their whiskers to obtain more information about the encountered obstacle.[30] As mentioned in Section 2.1.1 rodents also have passive microvibrissae, which are used to investigate the stimuli found in the environment.

In whisker-based application, active and passive whisker arrays are also used. The active whisker array movement is divided in active whisking, for exploring the environment and for obtaining texture roughness, and whisker dabbing, which is used for material hardness analysis. [63]

The general trend in literature is to mainly use active whisker arrays and it has been proven to be beneficial. [69] and [27] show that active whisking can successfully be used in texture classification. Furthermore, in most of the mobile robotic platforms active whisking by actuated whisker arrays is used. This is beneficial, because it is preferable to detect an obstacle as soon as possible when moving in an unknown environment and with active whisking a larger space is sampled which increases the chance of detecting an obstacle. This principle can be seen for the Koala Robot [38], the WhiskerBot [53], the SCRATCHbot [52], and the Shrewbot [51].

Active whisking does not only increase the chance of detecting an obstacle but it also allows for a more accurate localization of the obstacle. [41] performed a localization experiment with both a static, Figure 3.6 and a dynamic array, Figure 3.7. The dynamic array can actively protract the whiskers and passively retract the whiskers, which allows for a whisking motion. During the experiment a rod had to be localized. The static whisker array was moved in a horizontal dabbing motion across the rod and a similar experiment was repeated using the dynamic array which used whisking to localize the rod. From this experiment it was concluded that the static whisker array resulted in inaccurate and variable readings with $IQR \approx 10[mm]$. The dynamic array resulted in accurate and reliable localization of the rod with $IQR \approx 1.5[mm]$. Hence, the dynamic array is able to perform an active localization task.

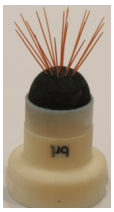

Figure 3.6: The static array used by [41].

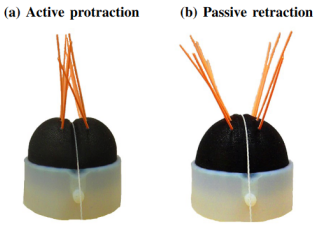

Figure 3.7: The dynamic array used by [41]. Protraction is realised by pulling on the tendon and retraction is done by releasing the tendon.

While most studies use active whisker arrays, [79] proves that a combination of a passive whisker array on a moving platform can perform multiobject exploration and recognition. This means that even tough a passive whisker array is used, active sensing could indirectly be performed by having a moving robotic platform.

3.4. Limitations and Drawbacks of Whisker-Based Tactile Sensing

While whisker-based tactile sensing is a very promising application, it unfortunately has some limitations and drawbacks. In comparison with active sensing systems, such as LIDAR and laser range finders which can obtain long range measurements, whiskers can only obtain measurements from the root to the tip of the whisker. Hence, whisker-based tactile sensing can only obtain short range measurements. This means if whiskers are used on a mobile platform as obstacle detection sensors, the obstacles are only encountered when they are already relatively close to the platform. This is the reason for the second limitation, to prevent crashing into an obstacle the platform must travel at relatively low speeds to be able to account for the nearby obstacles that are detected by the whiskers.

However, the main drawback of the use of whiskers is the danger of noise that induces unwanted vibrations. Whisker-based tactile sensors are in general very sensitive to low forces, which is an advantages in texture classification. This high sensitivity also means that a low velocity airflow could cause the whisker-sensor to sense a deflection [18], which could make a system think it is in contact with an obstacle. Hence, the high sensitivity of whiskers could lead to false measurements.

Unwanted vibrations can also be caused by the texture of the surface. According to [63] abrupt changes in the surface texture could lead to excessive induced vibrations in the whiskers, which negatively influences the measurement data. Furthermore, in the case of rough surface textures the whiskers could get stuck, which will influence the measurements, and when they slip off, the whiskers start resonating at their natural frequency, which also influences the measurements.[27] Hence, rough surfaces could induce unwanted vibrations in whiskers.

Moreover, moving a whisker into an object will cause a whisker to start oscillating in unpredictable manner. This will negatively influence the measurements and could lead to false readings. [24]

Section 3.3 mentioned that active whisking is often used in literature. However, it has one large disadvantage. The sensor output is dominated by the self-motion induced by the active whisking. [41] This self-motion could cause for example false positives in texture classification. [69] However, self-motion is not only created by active whisking but also by the movement of a mobile platform. It is stated in [52] that the head movements of the SCRATCHbot also generated self-motion noise, which can cause the robot to follow objects that are not there.

3.5. Whisker Sensor Data Filtering

As explained in Section 3.4, unwanted vibrations of the whiskers negatively influence the obtained sensor data. To use the sensor data containing these unwanted vibrations, the data must be filtered. Depending on the cause of the unwanted vibration different methods can be used to filter the data.

First of all, the vibrations cause by abrupt changes in texture and by rough surfaces can be removed by using a whisker array. [63] mainly focuses on removing noise in sensor data for texture classification but the method described to account for this noise can be used more generally. The method described to solve the problem, is based on having multiple whiskers with different specifications. The measurement data of all the whiskers and their classification results are implemented in a voting system to decide the correct texture of the encountered surface. Such a voting system can also be used for an array that performs distance measurements. The voting system can rectify an inaccurate distance measurement by one whisker on the array, as a result of unwanted vibrations, if all the other whiskers on the array have accurate distance measurements.

Second, for self-induced deflection of the whiskers by active whisking an approach known from nature can be used. By subtracting a reference signal, which represents the whisker movement due to whisking, the self-induced motion can be partially removed.[41] The same type of approach is used in [52]. It uses cerebellar-inspired algorithms that learn the dynamics of each moving whisker which can then be used to remove the induced noise by the self-motion. The used adaptive self-generated noise cancellation algorithm is explained in [3]. An adaptive noise cancellation filter is used because the parameters used in the filter are task specific. This means that the filter should be able to react to changes in the robot's environment, its dynamics, or the task description as they occur during the robot's mission to ensure that the right amount of noise is filtered out. It was shown by [3] that the adaptive noise cancellation algorithm improved contact detection in the recorded data and it heavily reduced the amount of false positive recorded by the system. A visualisation of the general working principle of adaptive noise cancellation can be seen in Figure 3.8a and the visualisation of the working principle of adaptive noise cancellation of self-induced sensory signals can be seen in Figure 3.8b.

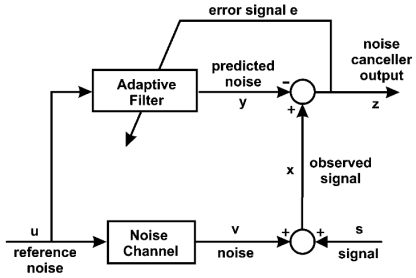

(a) Visualisation of the general adaptive noise cancellation scheme.

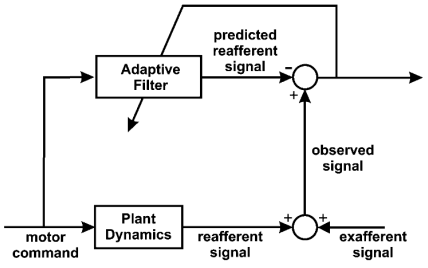

(b) Visualisation of the use of the adaptive noise cancellation scheme in the self-induced sensory signals cancellation frame.

Figure 3.8: Visualisation of the link between general adaptive noise cancellation (a) and the cancellation of self-induced sensory signals due to the plant dynamics (b).[3]

3.6. Whisker-Based Robotics

Numerous references to current whisker-based robotic applications have been provided in this chapter. In this section an overview of the moving robotic platforms found in literature are given, together with their main applications. A visual overview can be found in Figure 3.9.

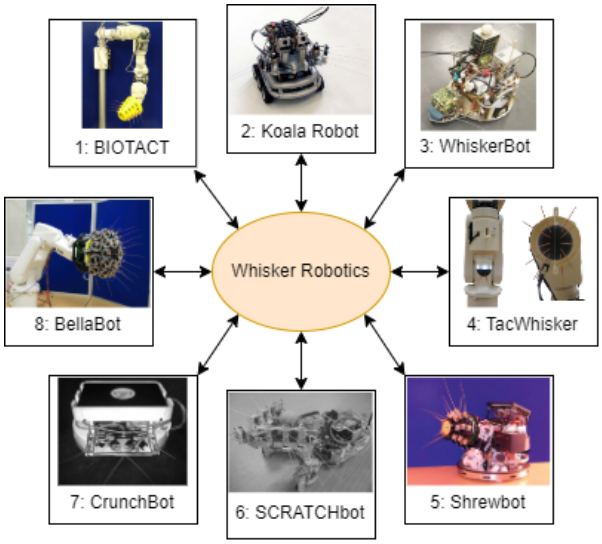

Figure 3.9: Overview of different whisker applications in robotics. (1: [69], 2: [38], 3: [27], 4: [41], 5: [51], 6: [52], 7: [25], 8: [4].)

The first robotic application is the BIOTACT sensor designed in [69]. This application tried to mimic the rats vibrissal system by using a conical shaped head, which mimics the snout of a rat, active whiskers for active whisking, and varying whisker lengths. The main goal of the BIOTACT sensor was to perform tactile classification.

The second robot is the Koala Robot, which is a moving ground robot built by [38]. This robot mimicked the active whisking behavior of a rat to perform localization procedures in unknown environments. During this localization procedure the shape of the localized object was determined using the whiskers.

The third image in Figure 3.9 represents another moving ground robot, the WhiskerBot by [53]. Once again a biomimetic approach was used. The used whiskers were tapered and curved to approximate a nominal rat whisker. The WhiskerBot made use of active whisking with a feedback control system. This feedback control system was based on the contact mediation approach of rats. This robot was used in [27] to perform texture classification while moving.

The TacWhisker design by [41] is shown in image number four. The TacWhisker is a whisker array mounted on a robotic arm. It uses an active whisking design which can compensate for self-induced sensory signals. The TacWhisker can be used to perform tactile stimuli localization tasks.

The fifth robotic application is the Shrewbot by [51]. The sensory design used for Shrewbot tried to mimic the radial characteristic of the rat's sensory surface generated by the whisker tips during exploration. Furthermore, different whisker lengths were used for each row in the array. The goal of the Shrewbot study was to analyze the effect of contact-driven feedback control of whisking on the quantity and quality of vibrissal sensory information.

The sixth images shows the SCRATCHbot [52]. The goal of this design was to completely mimic the vibrissal system of a rat. It has varying whisker length across the whisker arrays, it has microvibrissae on the tip of the robots head, it can change the whisker spread, and it can perform the CIA behavior of a rat. The robot was able to localize and orient itself towards tactile stimuli in the environment. The goal of this design was to obtain better insight on the effect of active sensing control on the obtained signals by the whisker-based sensing system.

The seventh image is a mobile ground robot application which is to be able to perform simultaneous localisation and mapping (SLAM) of the environment based on tactile sensor inputs. [25] The robot makes use of four tapered whiskers and a finite state machine (FSM) model to perform mapping of the environment.

The last shown robotic application is the BellaBot designed by [4]. The robotic arm has a sensor array with twenty whiskers attached to it. This robot was used in research to improve the accuracy of directed motor commands toward tactile stimuli in the environment.

Finally, an interesting observation can be made when looking at the overview shown in Figure 3.9. All the whisker-based robotic applications are either robotic arms on the ground or moving ground robots. This means that the use of whisker-based tactile sensing is so far only proven to work on

ground robots and not on aerial robots. It is therefore not known if all the obtained conclusions and observations mentioned in the papers of these applications will work on aerial robots.

3.7. Key Findings: Whisker-Based Tactile Sensing

In Section 3.1 it was shown that tactile sensing can be used in many different domains. The most important observation was that tactile sensing can be used for exploration and navigation tasks which is key for the main research goal mentioned in Chapter 1.

From Section 3.2 it can be concluded that whisker designs are heavily dependent on the use-case and that the used designs in literature all strongly focus on the whisker designs seen in nature. For the four main design choices shown the following conclusions can be made. Plastics are the main material type used in whisker design, due to their flexibility in design choices. Furthermore, it was derived from literature that the common design choice was the use straight whiskers. Moreover, the length of the whisker is mainly dependent on it applications. Finally, the use of taper ratios in whisker design is justified by the benefits it has and by the use of taper ratios by rodents.

For the array designs no clear rules for the number of whiskers that should be used on an array were found. However, there was a relation observed between the array application and the spacing between the whiskers on the array. For arrays that were used in tasks that required very precise data the spacing between the whiskers was small. Larger spacing between whiskers on the array were used for tasks that needed more global data.

The choice about the use of constant or varying whisker lengths was mainly based on the observations made in nature. Rodents have varying whisker lengths in their vibrissal system and therefore many designs in literature followed this path. Variations in whisker lengths on an array could have very interesting applications, because depending on the length of a whisker it can be used for different applications. Hence, a whisker array can be designed that can fulfill multiple functions.

The main flow seen in literature was the use of dynamic whisking. However, it was also shown that a combination of a static whisker array and a moving platform could perform exploration and navigation task. While dynamic whisker arrays have many advantages, it also has the large disadvantage of causing self-induced motion noise in the sensor readings.

This self-induced motion noise should be removed from the sensing data to be to use the data properly. This can be done with the help of an adaptive noise cancellation filter, which learns the self-induced motion based on the dynamics of the system. Noise can also be caused due to unwanted vibrations induced by rough surfaces and changes in surface texture. However, by using the sensor data from all the whiskers on the array this noise can be filtered out with the help of a voting system.

Another key observation is the following. Section 3.6 showed many different whisker-based robotic applications, but all these whisker-based robotic applications are robots located on the ground. Hence, no proof exists for the use of whiskers in aerial applications.

4

The Influence of Ceiling Effects on Micro Aerial Vehicles

When an aerial vehicle is flying close to the ground, it will experience certain influences due to the ground, this well-known phenomenon is called the ground effect. A little less-known is the phenomenon that describes the effect of flying in proximity with a ceiling, the ceiling effect. This chapter delves into the influence of the ceiling effect on quadrotor vehicles.

The principle and problem of the ceiling effect will be explained in Section 4.1. Further, Section 4.2 will describe different approaches, that use the ceiling effect to their advantage by flying close to the ceiling. Finally, Section 4.3 will summarize the key findings of the chapter.

4.1. The Ceiling Effect Principle

Flying in close proximity with obstacles, influences the behavior of the rotor wake of a rotorcraft. For example, the ground effect results in an increase of lift experienced by the aircraft when flying close to the ground. It is caused by a reduction in the induced velocity from the rotor, which creates a larger pressure difference across the rotor disk, when in proximity with the ground. [15]

A similar observation can be made for the ceiling effect. When flying close to a ceiling the induced velocity from the rotors is also reduced, which causes a greater pressure difference across the rotor disk.[16][66] This causes an increase in thrust, leading to the rotorcraft being pulled towards the ceiling. Furthermore, the resulting suction lowers the air pressure around the propellers, which leads to a decrease in drag and an increase in rotor velocities. [34]

This suction towards the ceiling can be very dangerous when not properly accounted for, it can cause the rotorcraft to crash into the ceiling. It can also obstruct a multirotors' tracking task, because it will not be able to follow the target states and points due to the differences in the desired forces and the actual forces generated due to the suction of the ceiling. The obstruction of the tracking task will lead to the target never being reached or the crashing of the drone into the ceiling. [50]

To be able to perform tasks in proximity with the ceiling, methods are needed to estimate the ceiling effect. These estimation methods can then be used in controller designs to be able to perform flight in proximity with the ceiling. Methods for estimating the ceiling effects will be the main focus of the next section, Section 4.2.

4.2. Approaches for Flying in Close Proximity with a Ceiling

In literature there are two main approaches used to determine the influence of the ceiling on the produced thrust and the power consumption. The first approach focuses purely on Momentum Theory and Blade Element Theory, which will be explained in Section 4.2.1. The second approach will be discussed in Section 4.2.2 and is based on the Cheeseman-Bennet model, which indirectly uses Blade Element Theory [14].

4.2.1. Momentum Theory and Blade Element Theory Approach

In this section the application of the Momentum Theory (MT) and the Blade Element Theory (BET) for the ceiling effect estimates will first be discussed for a single rotor case. Then a multirotor scenario will be discussed. Lastly, the unsteady state scenario for a multirotor will be described.

Single Rotor Ceiling Effect Estimation

To describe the MT for a single rotor the illustration in Figure 4.1 is used. Here, R is the radius of the rotor and D is the distance from the rotor to the ceiling. Furthermore, when using MT it is required to use standard assumptions. Such as, assuming steady, incompressible, one-dimensional, and axisymmetric flow and modeling the rotor as an infinitely thin disc. [32][31]

As can be seen in Figure 4.1 the rotating propellor will generate a constant airflow with induced velocity, v_i, along the rotating axis. The difference in pressure along the propellor disk results in thrust. In traditional MT the generated thrust is equal to the difference between the vertical momentum of the incoming and outgoing airflow. This changes when the rotor is in proximity with a ceiling, because the ceiling influences the vertical movement of the airflow. [32][31]

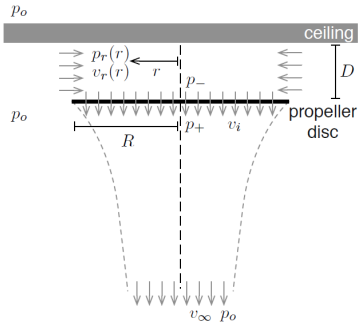

Figure 4.1: Illustration of an axisymmetric propeller below a ceiling, showing the pressure and flow speed at different parts of the system. [32]

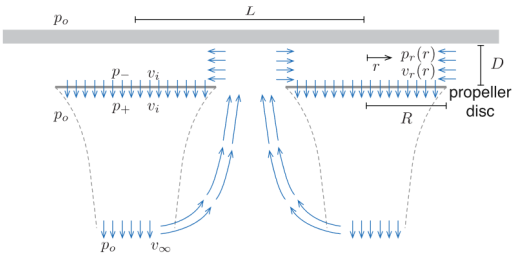

Figure 4.2: Illustration of multiple axisymmetric propellers below a ceiling, showing the pressure and flow speed at different parts of the system. [31]

[32] shows that when taking into account the influence of the ceiling a new relation for v_i based on the distance to the ceiling can be obtained, which is Equation 4.1. The difference with the regular relation, $v_i = \frac{1}{2}v_\infty$ [5], is the ceiling coefficient γ, which depends on the propeller-to-ceiling-ratio, δ. If δ approaches 0, meaning the ceiling is very far away, γ becomes 1 resulting in the regular v_i relation.

To account for some of the made assumptions, [32] introduces the correction factor α to the ceiling effect coefficient which results into Equation 4.2.

$$v_i = \frac{2}{1+\sqrt{1+\frac{1}{8}\delta^2}}\frac{1}{2}v_\infty = \frac{1}{2}\gamma^{-1}v_\infty \quad (4.1) \qquad \gamma(\delta,\alpha) = \frac{1}{2}+\frac{1}{2}\sqrt{1+\frac{\alpha}{8}\delta^2} \quad (4.2)$$

Using Equation 4.1, a new equation for the thrust can be obtained, Equation 4.3. Furthermore, a new equation for the aerodynamic power can be obtained with Equation 4.3, which is shown in Equation 4.4. From this equation is can be concluded that if the ceiling coefficient increase, the rotor is closer to the ceiling, the aerodynamic power to generate the same thrust decreases. [32]

$$T = \frac{1}{2}\rho A v_\infty^2 = 2\rho A\gamma^2 v_i^2 \quad (4.3) \qquad P_a = Tv_i = \gamma^{-1}\cdot T\sqrt{\frac{T}{2\rho A}} \quad (4.4)$$

While the MT derived a model for the thrust and aerodynamic power, the BET will be used to obtain relationships between the rotor velocity and the resulting thrust and aerodynamic power. In these relationships, BET takes the propellers geometry into account. [32] uses the BET results in [5] and Equation 4.3 to derive a new thrust equation depending on the distance to the ceiling and the rotational velocity, Equation 4.5. Where the thrust coefficient, c_T, depends on the dimensionless coefficients c_1 and c_2 which relate to the geometric properties of the propeller.

$$T = 2\rho A\left(\frac{2c_1R\gamma}{1+\sqrt{1+16c_2\gamma^2}}\right)^2\Omega^2 = c_T\Omega^2 \quad (4.5)$$

Furthermore, the torque coefficient c_τ can be derived from Equation 4.6 which uses the fact that $P_m = c_\tau\Omega^3$ and that $P_a = \eta P_m$.

$$P_a = 2\rho A\left(\frac{2c_1R\gamma^{\frac{2}{3}}}{1+\sqrt{1+16c_2\gamma^2}}\right)^3\Omega^3 = \eta P_m \quad (4.6)$$

The resulting equation for c_τ can be found in Equation 4.7. It can be seen that c_τ only depends on the ceiling coefficient.

$$c_\tau = \frac{P_a}{\eta\Omega^3} = \frac{2\rho A}{\eta}\left(\frac{2c_1 R\gamma^{\frac{2}{3}}}{1+\sqrt{1+16c_2\gamma^2}}\right)^3 \tag{4.7}$$

To be able to verify the found equations, [32] used an experimental set-up which could measure the thrust force, current, and angular velocities at different distances from the ceiling. For details about the set-up see [32]. From these measurements values for the unknown coefficients, η, α, c_1, and c_2 were obtained. They also concluded that the thrust would increase by a factor of 1.6 —2.3 for the same power consumption when in proximity with the ceiling. Hence, the input power reduces by a factor of 2.0 —3.5 for the same amount of thrust. Finally, the experiments proved the derived analytical models, meaning they can be used to approximate the ceiling effect. These models can thus be used in controller designs.

Multirotor Ceiling Effect Estimation

The models discussed in [32] are only valid for a single rotor condition. This means that they might not be valid for a quadrotor configuration. Therefore, it is required to analyse such a configuration, which is done by [31].

While the used approach for MT and BET is the same as for the single rotor scenario, there is one big difference for the multirotor case. Multirotor configurations cause flow asymmetry and flow re-circulation, which will influence the ceiling coefficient. A visualisation of this scenario can be seen in Figure 4.2. The propellers obstruct the airflow from entering the streamtubes above the rotors, which leads to re-circulation of the wake causing a reduction in flow momentum. [31].

To account for this re-circulation of the wake, Equation 4.2 needs to be adapted. The new ceiling coefficient equation is shown in Equation 4.8. Here the $1-\alpha_1\delta^2$-term represents the decrease in vertical flow momentum, with α_1 representing the interaction between the the propellers when in proximity with the ceiling, and α_0 has the same function as α in Equation 4.2. Hence, the re-circulation will negatively influence γ.

$$\gamma(\delta,\alpha_0,\alpha_1) = \frac{1}{2}(1-\alpha_1\delta^2) + \frac{1}{2}\sqrt{(1-\alpha_1\delta^2)^2 + \frac{\alpha_0}{8}\delta^2} \tag{4.8}$$

Using this adapted equation for γ, [31] obtains a new equation for c_T shown in Equation 4.9 and a new equation for c_τ, Equation 4.10. In Equation 4.9, c_0, c_1, and c_2 are coefficients related to the blade profile.

$$c_T = 2\rho A\left(\frac{2c_0 R\gamma}{(c_1-c_2\delta)+\sqrt{(c_1-c_2\delta)^2+16c_0\gamma^2}}\right)^2 \tag{4.9}$$

$$c_\tau = \frac{1}{\eta\sqrt{2\rho A}}c_T^{\frac{3}{2}} \tag{4.10}$$

To verify the obtained equations, [31] used benchtop experiments using propellers with a radius of 23-mm and 50-mm. The distance between the rotors and the distance towards the ceiling could be changed in their set-up. They concluded that the presence of a ceiling indeed reduces the power consumption and increases the thrust, and that these changes can be properly estimated by the derived equations. A limitation of the performed study is that it only focused on flat, rigid, and horizontal ceilings.

[31] also concludes that the obtained models could be used in surface locomotion controllers. However, the controller should apply strategies to prevent crashing into the ceiling by maintaining a certain propeller-to-ceiling ratio and the controller should be able to regulate the thrust based on this ratio.

Unsteady State Multirotor Ceiling Effect Estimation

In the previous sections it was assumed that the rotors are in a steady state, hovering below the ceiling. However, in a real scenario, a rotor aircraft will not always be in steady state below a ceiling. It is important to account for changes in vertical velocities when approaching and flying underneath a ceiling.

To analyse the effect of changes in vertical velocities the airflow model in Figure 4.3 is considered. It can be seen that the flow velocity $v(r)$ is now not only influenced by the induced velocity v_i, but also the vertical velocity rate of the quadrotor, $\dot{z}$. [50]

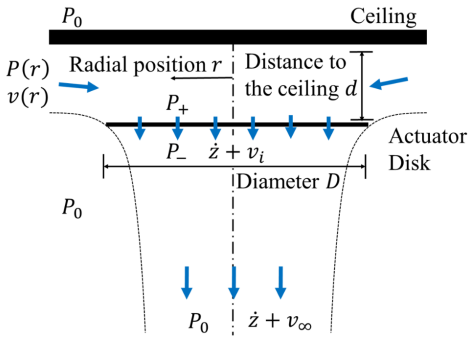

Figure 4.3: Illustration of an axisymmetric propeller below a ceiling, showing the pressure and flow speed at different parts of the system in unsteady state. [50]

The thrust equation, when in proximity with a ceiling, is derived in the same way as conventional MT, however [50] takes $\dot{z}$ into account leading to Equation 4.11. In Equation 4.11 the definition of γ in Equation 4.2 is used.

$$T = \frac{1}{2}\rho A v_\infty (v_\infty + 2\dot{z}) = 2\rho\gamma v_i(\gamma v_i + \dot{z})A \tag{4.11}$$

It is assumed from MT that the thrust equation equals $T_{OCE} = 2\rho A v_i^2$, when being far away from the ceiling. Now the thrust ratio, k_T, between the thrust effected by the ceiling effect, T_{ICE}, and the thrust not effected by the ceiling, T_{OCE}, can be obtained and is represented by Equation 4.12.

$$k_T = \frac{T_{ICE}(\delta, \dot{z})}{T_{OCE}} = \gamma^2(1 + \gamma^{-1}\frac{\dot{z}}{v_i}) \tag{4.12}$$

The unsteady state thrust model is verified in experiments and compared to the steady state model, derived in [32]. It was concluded that in a steady state case, with $\dot{z} = 0.0$, the conventional model represented the steady state better. However, for an unsteady state it was concluded that the model follows the experimental data better than the conventional model.

[50] uses Equation 4.12 in a controller design to analyze the stability of the derived model when performing vertical flight underneath a ceiling. A motor-mapping approach, which used Equation 4.12, was designed. When the ceiling comes closer or when the vertical rate increases the motor-mapping will reduce the rotor inputs. The other way around, the rotor inputs will increase when the ceiling is further away or when the vertical rate decreases. Furthermore, the system estimates self-states and the distance to the ceiling with onboard sensors.

This controller was verified by comparing four different controllers in a vertical climb and descent scenario. The first controller did not use a ceiling effect model, the second controller used the conventional mode, the third controller uses the unsteady state model for $\dot{z} = 0.0$, and the fourth controller uses the unsteady state model considering vertical rates. The experiment was carried out based on changing the altitude and the vertical rates with the Sine Curve Case.

The first conclusion from this experiment was, that the controllers using ceiling effect models were able to follow the target. The controller which not included the ceiling effect crashed into the ceiling. Furthermore, it was shown that the fourth controller outperformed all the other controllers. Meaning the proposed unsteady state controller design can be used to improve the performance of target tracking, when influence by the ceiling effect. [50]

4.2.2. Cheeseman-Bennet Based Approach

Cheeseman and Bennett obtained a mathematical model to describe the ground effect experienced by a helicopter. This model is described with Equation 4.13, which shows the ratio between generated thrust without the ground effect, T_{OGE}, and the thrust experienced when influenced by the ground effect, T_{IGE}. This ratio only depends on the radius R of the rotor and the distance from the ground Z. It is important to state that the model assumes a single rotor, spinning at a constant speed with constant engine power.[14]

Due to the fact that the ground effect and the ceiling effect arise from the same physical phenomena the Cheeseman-Bennet model, Equation 4.13, can also be used for estimating the ceiling effect in a single rotor case.[16]

$$\frac{T_{IGE}}{T_{OGE}} = \frac{T_{ICE}}{T_{OCE}} = \frac{1}{1 - \left(\frac{R}{4Z}\right)^2} \tag{4.13}$$

As mentioned in Section 4.1, flying in proximity with a ceiling increases the rotor velocities. To be able to use Equation 4.13 a constant rotor speed is needed and therefore [16] states that a closed-loop speed controller should be used. Using this approach in experiments with a fixed experimental set-up, [16] validated the use of Equation 4.13 in both a single rotor and multirotor configuration.

According to [16], not using a closed-loop speed controller will break the assumption for Equation 4.13, which mean correction factors are needed to account for that. Both [66] and [34] use an adapted version of Equation 4.13, shown in Equation 4.14. Here K_1 and K_2 are coefficients that are obtained experimentally. In the case of [66] this is done via real life experiments and [34] used CFD simulations.

$$\frac{T_{ICE}}{T_{OCE}} = \frac{1}{1 - \frac{1}{K_1}\left(\frac{R}{Z+K_2}\right)^2} \tag{4.14}$$

While in [66] the coefficients are used in a single rotor case to account for the open-loop speed controller, in [34] they are used to account for the use of a multirotor and the specific design of the used multirotor. Using these coefficients allow for more accurate matching of the experimental and model data. Furthermore, both papers conclude that for a multirotor the ceiling effect becomes already significant at larger propellor-to-ceiling ratios, compared to a single rotor scenario. This conclusion is also supported by [75].

[66] validates their model in a controller design by performing experiments, bridge inspections, with the quadrotor underneath a bridge. Only vertical motion was performed and the distance to the ceiling was measured with optical flow and visual odometry. From these experiments it was concluded that the found model could be successfully used in controller design and that the maximum flight time of the quadrotor was increased.

From the validation procedure in [34], it was concluded that the attitude of the multirotor leads to differences in ceiling effects between the rotors. For the used design, a distance of $0.25m$ from the ceiling led to a maximum difference in ceiling effect of 2%. Therefore, it was assumed that horizontal flight was only allowed for distance to the ceiling of $z \geq 0.25m$. When using this assumption in the performed outdoor experiment, [34] showed that the designed ceiling effect controller is able to perform autonomous bridge inspections in a safe manner.

4.3. Key Findings: The Influence of Ceiling Effects on Micro Aerial Vehicles

In Section 4.2 it was shown that there are two main approaches for estimating the ceiling effect. The first approach is using thrust and power equations derived from Momentum Theory and Blade Element Theory and the second approach is using variations of the Cheeseman-Bennet model.

The models derived via the two approaches showed promising results in estimating the ceiling effect and also promising initial results in controller design. When it comes to incorporating additional variables to account for multirotor configuration, both approaches do not show a clear path. However, based on the points and conclusions made in the papers that do incorporate these additional variables, it seems that these models are more accurate. This could be the case, because these variables not only account for the different configuration but also for some assumptions that were made, that are not valid in a real life case.

These additional variables need to be estimated with the help of an experimental phase. This will be the case for both approaches and therefore there is not a large difference in the amount of experiments needed before a working model can be obtained.

From the performed research in Section 4.2, it can also be concluded that the ceiling effect indeed increases the thrust and the rotational velocity. Meaning, when flying in proximity with the ceiling the same thrust level can be obtained for a lower input power, which increases the maximum flight time.

An important remark that should be made is, that all the performed experiments, that are described in the articles, are performed with horizontal and relatively smooth ceilings. Hence, to confirm the use of the models for asymmetric surfaces additional research must be performed.

5

Tactile Navigation by Contour Following

In Chapter 3 whisker-based tactile sensing was explained and it was stated that whiskers can be used for distance measuring. The ceiling effect was explained in Chapter 4, which showed that flying close to the ceiling can have advantages, such as a lower power consumption. The use of whiskers for distance measurements and the advantages of the ceiling effect can be combined and used in an exploration task. More precisely a contour following exploration tasks based on a ceiling following approach. To be able to perform such an approach, a specialized contour following controller must be used. Therefore, Section 5.1 discusses multiple contour following controllers.

The distance measurements obtained from the whiskers could be used for mapping the environment. Section 5.2 looks into special algorithms needed for mapping an environment, called Tactile SLAM.

5.1. The Contour Following Approach

Contour following by a robot can be used for many different tasks, such as mine exploration and search and rescue missions.[74] Contour following strategies are often called wall-following (WF) strategies, and these strategies are based on moving along the edge of obstacles, which could be walls, while keeping a constant distance and constant parallel orientation between the mobile robot and the object.

Using controllers based on these strategies would allow a robot to autonomously navigate in an unknown environment. Meaning, that based on these controllers the robot can move independently through the unknown environment without the need of human inputs, which is a big advantage.[33]

The contour following controllers that are discussed in this section are divided in approaches that use conventional (non-)linear controller, Section 5.1.1, and in approaches that use intelligent controllers with fuzzy logic Section 5.1.2.

5.1.1. Contour Following with General Controllers

A lot of contour following controller are based on the WF principle, which in general is based on three main goals. Firstly, the robot should be able to maintain a desired distance to the wall. Secondly, the robot should be able to follow the wall in a parallel matter and therefore its heading angle should be very close to the angle of the wall. Finally, the robot should be able to measure distances to obstacles in its path to be able to account for these.[76] [72]

From these goals it becomes clear that the simple controller should be able to control the distance and the angle between the robot and the wall. From this, control errors can be derived. The distance error between the distance to the wall, d_{wall}, and the desired distance, d_{des}, is shown in Equation 5.1. The orientation error between the wall angle, θ_{wall}, and the heading angle, θ, of the robot can be obtained with Equation 5.2.[76][72]

$$\tilde{d} = d_{des} - d_{wall} \quad (5.1) \qquad \tilde{\theta} = \theta_{wall} - \theta \quad (5.2)$$

However, walls are not always straight and smooth. They can be curved or contain corners. Therefore, distance measurements are not always constant along the sensor array, which means the wall angle varies. Hence, to be able to use the control error equations estimates of the distance towards the wall and the wall angle should be found.

To account for this problem [72] uses its sensor measurements, obtained by a laser sensor, to obtain wall angles between different laser beams. It uses the distance measurements of ten beams to obtain ten wall angles, all calculated with respect to the distance measurement perpendicular to the robots heading angle. A decentralized Kalman Filter obtains an improved wall angle estimate based on these measurements. The Kalman Filter steps are explained in [72]. With this improved wall angle estimate, the improved distance towards the wall can be obtained, which can be used in the control

error equations. Furthermore, using the control errors and a Lyapunov candidate function control laws could be derived for the controller.

However, these simple control laws were not able to account for a loss of wall event or a possible collision event. Therefore, [72] decided to make use of a switching controller consisting of the normal WF mode, an orientation mode, and a rotation mode. The orientation mode was activated in case of a possible collision. The collision is avoided by rotating the robot until a free path is found. When the wall is lost, the rotation mode is activate. The robot will start following a circular path towards the side where it last detected a wall, until it finds the wall.

The block diagram of this switching controller can be found in Figure 5.1. Where the supervisor contains the logic to switch between the different behaviors. Using this controller it was shown that the controller was able to perform a contour following tasks in an unknown environment. Results of a real world experiment are shown in Figure 5.2. It can be seen that the robot was able to follow the wall and able to get out of the trap situation.

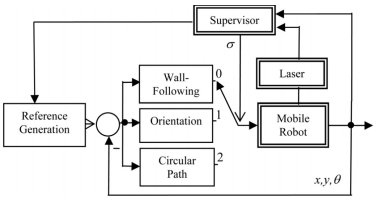

Figure 5.1: Block diagram of the switching controller used in [72].

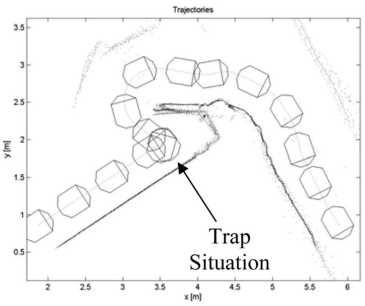

Figure 5.2: Experiment in which the robot should avoid a trap situation.[72]

Instead of using a Kalman Filter to obtain the wall angle estimates, [76] generates a dynamic virtual wall. The wheeled ground robot in [76] obtains distance measurements from its laser sensors. By applying least squares method on the data, a line estimate in the form $y = ax + b$ is obtained, which represents the virtual wall. The slope of the virtual wall, represents the wall angle estimate.

Furthermore, [76] makes use of adaptive velocity, which means no switching controller is needed. However, the adaptive velocity only holds for the linear velocity but not the rotational velocity. For the robot to rotate, a difference in velocity between both wheels is needed. Therefore, [76] uses a PD controller to determine the required difference in velocity, Δv, based on the distance and orientation towards the virtual wall.

An illustration of the used algorithm is shown in Figure 5.3. [76] concluded, that the designed controller can be used for WF and object avoidance in an unknown environment. In Figure 5.4 a simulation result is shown, in which can be seen that the robot is able to follow the walls and avoid obstacles.

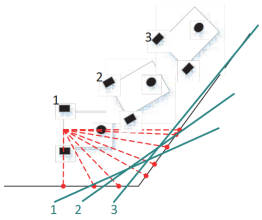

Figure 5.3: Illustration of the working principle of the virtual wall based WF algorithm.[76]

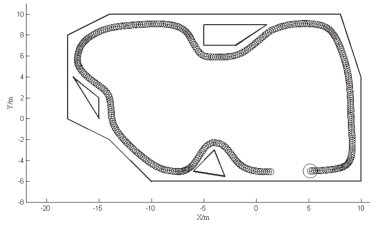

Figure 5.4: Simulation result of the virtual wall based WF controller. [76]

The previously discussed contour following controllers are both based on ground robots with laser sensing. However, [10] proposes a controller design based on tactile contact sensors for a quadrotor. It uses an array of four contact sensors, positioned with a 90 degree angle between each other, together with a velocity control method to perform a contour following navigation task. The contact measured with these contact sensors can be binary, contact or no-contact, or it can be force measurements.

The sensors have two direction vectors, the direction vector following the pointing direction of the

sensor, $\hat{q}_i$, and vector $q_i^{\perp}$, which is the unit vector perpendicular to $\hat{q}_i$ in a counter-clockwise direction relative to the quadrotor.

When an obstacle is encountered the controller should make sure that the quadrotor moves parallel to the obstacle. According to [10] continuous contact can be ensured by using a linear combination of $q_i^{\perp}$ and $\hat{q}_i$. However, it could occur that contact with the obstacle is lost. When this occurs, the quadrotor will fly in the direction it last encountered an obstacle. Using the parallel flight mode and the regain contact mode [10] obtained a velocity-based controller, for movement in x- and y-direction. For movement in z-direction a simple height controller is added.

The discussed controller design can be visualised as a block diagram, which is shown in Figure 5.5. Simulation experiments were performed with the controller and the result for a circular environment is shown in Figure 5.6. From this, and additional experiments, it was concluded reliable contour following could be performed with the proposed controllers.

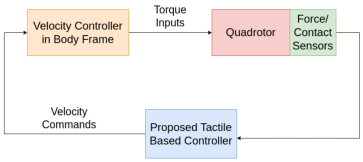

Figure 5.5: Visualisation of the structure of the proposed controller design.[10]

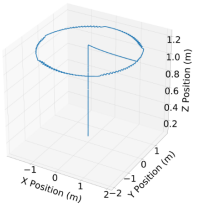

Figure 5.6: Simulation result of the contour following controller in a circular environment. [10]

5.1.2. Contour Following with Fuzzy Controllers

Fuzzy controllers (FC) are intelligent controllers, therefore they could be applied in uncertain and unpredictable situations. According to [74] fuzzy logic is based on a rule-based system, that makes decisions and performs mathematical reasoning with the available data, which could be imprecise and uncertain.

There are two types of fuzzy sets, Type-1 and Type-2. The main difference between the two sets is, the Type-2 sets have more parameters and more degrees of freedom. This allows a Type-2 fuzzy set to handle uncertainties better. For that reason the wheeled ground robot in [74] makes use of Type-2 fuzzy sets in its interval Type-2 FC, IT2FC. This controller makes use of zero-order Takagi-Sugeno type fuzzy rules, IF-THEN rules.

The free parameters of the IF-THEN rule based controller should be designed such that the controller performs the required tasks. The performance of the controller can be evaluated with the help of cost functions.

The inputs for the FC in [74] are the distance and orientation towards the wall. The outputs of the controller are the angular velocities for the wheels. However, to be able to perform the WF task rule bases must be determined, using the two state variables, distance and angle to the wall. These bases use membership functions based on linguistic functions, which will assist the mobile robot in its control tasks. The overview of the used rules in the controller can be found in [74].

With the designed fuzzy IT2FC, [74] performed experiments. In these experiments the path for the robot to travel was obtained by setting a desired goal. An example of such an experiment can be seen in Figure 5.7. From the experiment it was concluded that the robot could successfully reach the desired target by using the IT2FC for WF an obstacle avoidance.

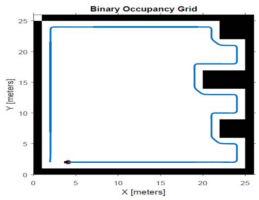

Figure 5.7: Example of a WF and obstacle avoidance experiment using the IT2FC.[74]

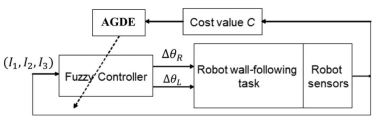

Figure 5.8: Visualisation of the data-driven AGDE based fuzzy controller. [36]

While in [74] the FC is manually designed, it can also be designed with the help of bio-inspired op-

timization algorithms. Two examples of bio-inspired FCs for a WF tasks can be found in [36] and [35]. Where [36] uses an Adaptive Group-based Differential Evolution (AGDE) algorithm to obtain a fuzzy controller for WF control of a hexapod robot and [35] uses a Evolutionary-Group-based Particle-Swarm-Optimization (EGPSO) fuzzy controller for a wheeled ground robot.

Both approaches are based on the same type of zero-order Takagi-Sugeno-Kang fuzzy IF-THEN rules as in [74]. However, the fuzzy sets make use of the Gaussian membership function. All the free variables used in the IF-THEN rules and the fuzzy sets can be combined in a parameter solution vector. In the AGDE algorithm each individual represent a FC with a solution vector and the same holds for each particle in the EGPSO.

In a training stage the evolutionary algorithms will find an optimal solution for the solution vector, which results in the final version of the FC. The methods used by AGDE and EGPSO to obtain the final solution, are described in [36] and [35] respectively. The training is often done in a simulation environment. However, if this training environment does not accurately represent the actual environment the controller will fail in the actual environment. This means, expected shapes of the environment should be known beforehand to be able to properly train the FC's.

A block diagram visualising an evolutionary based FC for the AGDE case can be seen in Figure 5.8. Using this FC approach [36] showed in simulation and real world experiments the effectiveness of the evolutionary fuzzy control approach for a WF task with a hexapod robot. An example of an obtained trajectory in an unknown environment can be seen in Figure 5.9.

Using the EGPSO FC approach, [35] showed that the chosen approach also led to an effective and accurate WF controller. An example of a result obtained by [35] can be seen in Figure 5.10.

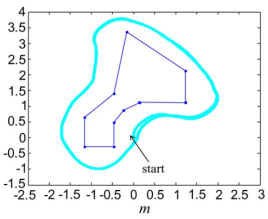

Figure 5.9: Resulting trajectory of the hexapod robot when the AGDE FC in a testing environment.[36]

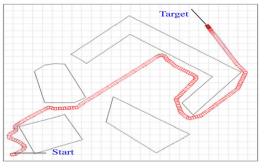

Figure 5.10: Resulting trajectory of the wheeled robot with the EGPSO FC in an environment with convex and concave obstacles.[35]

5.2. Tactile SLAM

When a mobile robot or agent is places in an unknown environment at an unknown location it could be tasked to build a map of this environment and localizing itself within this environment. This describes the simultaneous localization and mapping (SLAM) problem. SLAM uses sensory data obtained by the sensors on the robot to build a map, which is used to determine the robot's location in the map. [22]

There are many different solutions to the SLAM problem. In this section only the Tactile SLAM (tSLAM) solution and different variants of this solution will be discussed. The variants of tSLAM that will be discussed are blob-based mapping, mapping with multi-whisker templates, mapping with hierarchical priors, and Whisker-RatSLAM.

Blob-based Mapping

The basic blob-based mapping approach will link each contact point to a single cell of the grid map of the environment, while assuming no dependency between grid cells. [25] states that using whiskers will lead to a relatively small number of contacts, which will lead to unusable maps. When assuming that there actually is correlation between cells of the grid map, Gaussian likelihood can be implemented in the grid map. Using this approach in combination with a standard particle filter [71], every point of contact will increase the local Gaussian with Δm at that point in particle map m. This increase can be obtained with Equation 5.3. Here, the coordinates of the contact cell are x_c and y_c, σ determines the radius of the resulting blob, and $\Delta[x_c, y_c]$ is the likelihood of occupancy for the current particle map and the contact.

$$\Delta m[x, y] = \Delta[x_c, y_c] \exp\left(-\frac{(x - x_c)^2 + (y - y_c)^2}{2\sigma^2}\right) \tag{5.3}$$

When no contact is made by a whisker the likelihood of occupancy will be lowered for the points along the whisker.[25][54] Besides the maps being updated by whisker readings, the particle maps also get updated by changes in odometry.

In this approach, every particle will develop a map in which each cell contains the chance of a whisker tip being in contact at that cell. From these particle maps the likelihood of the current pose estimate can be determined.

The blob-based mapping approach with a particle filter was used in [25]. Mapping the arena environment, shown as a grid map in Figure 5.11, where the brightness indicates the occupancy, resulted in the maps shown in Figure 5.12. As can be seen the generated maps perform relatively well in showing the global shape of the ground truth. However, [25] stated that due to localisation errors the trials with blob-based mapping sometimes added object outside the arena.

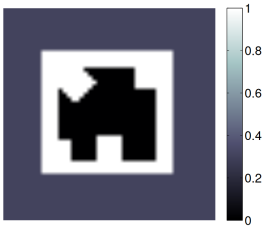

Figure 5.11: Grid map representing the ground truth of the environment.[25]

Figure 5.12: Examples of two grid maps generated in one trial with blob-based mapping.[25]

Mapping with Hierarchical Priors

As mentioned earlier, using whiskers will lead to a relatively small number of contacts with the environment. Laser sensors can easily be used for recognizing and learning complex spatial structures, but whisker sensors can not obtain the required level of detail. This lack of details could be solved by using strong, hierarchical priors about structures. [26] makes use of hierarchical objects for mapping the environment.

[26] showed the application of using strong hierarchical priors in an environment with multiple tables of the same size and with the same texture. A model of a table was generated containing dimensions, texture, and orientation. If a table exists it means that there are four table legs in the environment. Based on the whisker contacts made with the legs of the table, a table was placed in the environment.

It is required to known the type of objects that could be encountered in the environment when such strong hierarchical priors as in [26] are used. However, this is not always known. [25] uses the idea of hierarchical priors but instead of assuming complete object shapes, it is assumed that the environment exists mostly of straight edges. This can be applied in mapping by placing a line of blobs between two multi-whisker contact points if they are on the same surface. The increase in the local Gaussian can be determined by Equation 5.4, where R and θ are the radial coordinates centered on the contact midpoint (x_c, y_c) and θ_c is the estimated surface angle. The σ's represent model sensor noise and can be tuned by hand. In the case of only one contact point the equation for blob-based mapping was used, Equation 5.3.

$$\Delta m[x, y] = \Delta[x_c, y_c] \exp\left(-\frac{R^2}{2\sigma_R^2} - \frac{(\theta - \theta_c)^2}{2\sigma_\theta^2}\right) \tag{5.4}$$

Using this approach [25] obtained more accurate localization and map estimates, than the blob-based mapping approach. Examples of maps generated with individual runs of this method can be seen in Figure 5.13.

Figure 5.13: Examples of two grid maps generated by multi-whisker geometrical hierarchical prior mapping.[25]

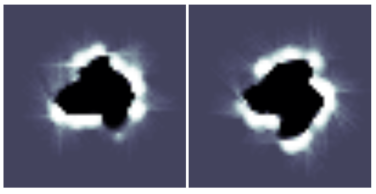

Figure 5.14: Examples of two grid maps generated in one trial with multi-whisker template mapping.[25]

Mapping with Multi-whisker Templates

The use of templates in whisker-based tasks is mainly done for texture classification task, as in [69] and [24]. However, it can also be used in mapping, which is done by [25]. Here, templates are trained based on contact angle classes from time series obtained by the whisker array. The templates were generated by letting the robot drive into a wall at different angles. These templates were then used in the mapping approach to obtain surface orientations by comparing the obtained time-series data with the templates. The template that resulted in the lowest sum of squared errors, obtained via Equation 5.5, was the winner. The templates surface normal was then used in Equation 5.4 to implement a long edge into the particle maps.

$$e(T_i) = \frac{1}{N}\sum_{t=1}^{n}(I(t) - T_i(t))^2 \tag{5.5}$$

[25] showed that this approach improved localization due to more accurate object contour predictions. Examples of the maps created by this approach are shown in Figure 5.14.

Whisker-RatSLAM

Whisker-RatSLAM is based on the RatSLAM algorithm introduced by [46], which makes a 2D topological map called the experience map. In this map the association of local view and odometry are represented as nodes and edges. The initial RatSLAM algorithm was used with visual sensors, but [64] showed that it could also be used in combination with whisker-based tactile sensors.

However, due to the sparse sensory data obtained from whisker contacts, the chance of incorrect localization is relatively high. According to [65], this chance could be decreased by observing landmarks in the environment and implementing them in the experience map. This can be done by switching between the train exploration mode and the object exploration mode. During the train exploration mode the robot pose estimate and the experience map are updated by whiskers sweeping the floor. When an obstacle is encountered by the robot, the object exploration mode is activated, which generates a 6D object exploration map. A visualisation of this switching behavior for a navigation task can be seen in Figure 5.15.

When performing normal RatSLAM simple experience nodes are placed in the terrain exploration map. In this experience node the pose cells, which contain the three degrees of freedom pose of the robot, form the core of the RatSLAM system.[46] The activity in the pose cells is updated by self-motion cues and, in the case of [65], by whisker sensor measurements.

Complex experience nodes are generated when an obstacle is detected. The main difference between the two nodes is that the complex experience nodes contain object exploration maps of an object at that location and the simple experience nodes contain the 3D pose-cell and the feature cells that were active during terrain exploration. [65]

In the original RatSLAM feature cells represent the presence of cues at specific locations, which is similar in Whisker-RatSLAM.[46] In Whisker-RatSLAM a point feature histogram and a slope distribution array are the geometric features that are stored in the feature cells.

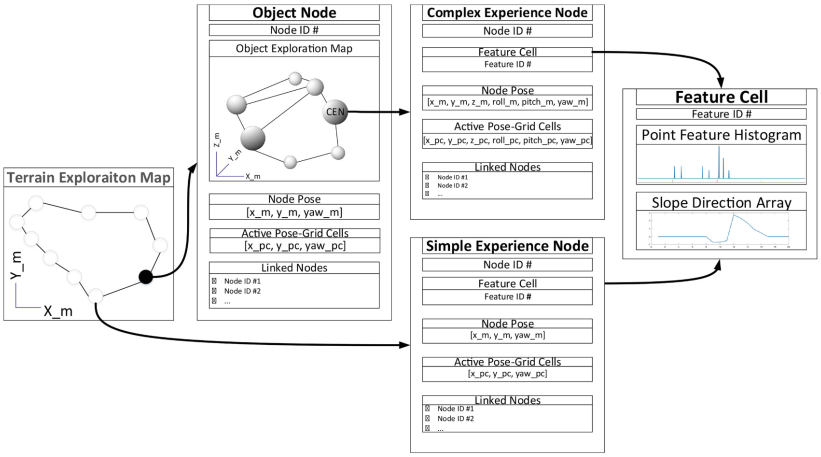

Figure 5.15: Visualisation of the switching behavior combining RatSLAM and Whisker-RatSLAM in a navigation task.[65]

[65] concluded that using the approach displayed in Figure 5.15 would lead to the successful localization of a mobile whisker array in 6D space. Furthermore, the generated object maps can be used to confidently classify object identities. However, the algorithm has low confidence for object identification. This is because the observed features on an object are dependent on the detected surface region by the whiskers. Meaning the obtained features are dependent on the executed trajectory.

5.3. Key Findings: Tactile Navigation by Contour Following

There are controllers that allow mobile robots to perform contour following tasks, as discussed in Section 5.1. These controllers are in general based on two goals, keeping the robot at a constant distance from the wall and keep the robot at the same orientation as the wall. Keeping the robot parallel with the wall, will make it easier to maintain the constant distance towards the wall.

The conventional controllers discussed in Section 5.1.1 are able to perform a WF approach, while also performing obstacle avoidance. Furthermore, the conventional controller are also able to follow walls with variations in shape by obtaining estimates of the global wall angle. This is a big advantage, because it increases the amount of use-cases for the controller. Another important observation was, that contour following can be performed by using tactile contact sensors in combination with a simple controller by a quadrotor.

Section 5.1.2 mentioned the use of fuzzy logic controllers for contour following tasks. These controllers use a rule-based system, allowing them to be applied in uncertain and unpredictable situations. It was shown that using such a rule-based controller promising WF results could be achieved. However, manually designing all the required rules for the FC can be a time-consuming and difficult task. Therefore, FCs are often designed automatically by using evolutionary based algorithms, which make the controller more complex. By training the controller in simulation using the evolutionary algorithms the best optimized FC is found. A disadvantage of this training procedure is that it can be time-consuming and the training environment should accurately represent the actual test environment, otherwise the controller will fail.

When comparing the conventional controller and the FC, it can be concluded that both are able to accurately perform a contour following task. However, even tough FCs could be more accurate in uncertain situations, designing such a controller can be very time consuming. The conventional controllers can relatively easy be designed based on two control errors and they can be applied in complex environments without the need of a training phase, which make the designing phase of the controllers less time consuming. For these reasons, using a general controller approach is deemed to be more favourable for the main research goal mentioned in Chapter 1, which requires a controller that can perform a ceiling following task.

There are also some key observations made related to tactile SLAM, Section 5.2. The first observation is that it possible to perform a mapping task based on sensory data obtained by whisker-based sensors. The best approach was the use of multi-whisker template mapping. However, this method has as a disadvantage that it needs to train templates, which can be a time-consuming task. The mapping with hierarchical priors, which is less time consuming, showed to be only a little bit less accurate and could therefore be a promising approach for mapping.

Furthermore, RatSLAM showed to be useful for not only mapping but also for object identification. This approach would increase the use-cases of tactile SLAM.

6

Conclusion and Recommendations

The goal of this literature study was to identify existing research gaps in previous studies, to find answers to all of the sub-questions that were derived from the main research question, and to find possible future research possibilities. The sub-questions that had to be answered were the following:

1. How can whisker-based tactile sensing be used in navigation tasks?
2. How many whiskers does the whisker array have?
3. What is autonomous decision making?
4. What is contour following and how can it be performed by an autonomous system?
5. What are the desired unknown environments?
6. How does flying in proximity with the ceiling, affect the behaviour of the quadrotor?

The first question can be answered with the help of findings in nature and from current whisker-based robotic applications. It was observed that tactile sensors in nature, such as whiskers, are directly or indirectly used as distance sensors. This allows animals to detect and localize obstacles in the environment. They can use these observations to change their locomotion and exploratory behavior. When a rat encounters an obstacle behavior can change from global to detailed exploration of the obstacle. It uses whisker tapping and brushing behavior to obtain more information about the obstacle. Furthermore, it was observed that rats keep their whiskers in contact with the wall when exploring a new dark environment, they perform a wall-following strategy. This shows that in nature, whiskers are already used in a closed-loop fashion for navigation tasks such as obstacle detection and wall-following.

Whisker-based robotic applications also showed that artificial whiskers can be used to perform accurate localization of tactile stimuli in the environment by using distance measurements. Hence, whisker-based tactile sensors can be used as contact distance sensors which allows them to be used in contact based navigation tasks, such as the wall-following exploration approach and target seeking.

Unfortunately, no specific answer was obtained for the second sub-question. Many different array sizes were found in literature, but no clear reasoning for the choice in array sizes was given. However, trends were seen in literature about the total number of whiskers used and the spacing between the whiskers on the array. For classification tasks a lot of data was needed to perform an accurate classification, which could be achieved by a large number of total whiskers. Furthermore, in such tasks, where accurate and detailed data is required, it was observed that the spacing between the whiskers on the array was relatively small. This leads to more precise sensor readings for a small area.

On the other hand, for whisker-based applications such as obstacle avoidance a larger search space is needed to increase the chance of obstacle detection. Therefore, the whiskers should be more spread out to increase the search space. Depending on the desired accuracy of the environment, the total number of whiskers can vary.

So, while there is no specific answer to this question, important observations were made in the search for this answer. It became clear, that the total number of required whiskers and the required spacing between whiskers on an array are heavily dependent on the desired application of the array.

The third question can be answered with the definition for autonomous systems found in literature. This definition is based on the following principle: an autonomous system is a system which can perform tasks by itself without the need of human commands. Hence, an autonomous decision making system makes its own decision without the influence of external factors, such as human inputs.

The research performed in the field of contour following allows for answering question four. First of all, contour following is based on moving along the contour of an obstacle, which could be a wall, and at the same time keeping a constant distance and parallel orientation between the robot and the

object. This procedure can be performed by an autonomous system with the help of a contour following controller and a sensory array to obtain distance measurements. These controllers are based on the distance error input, the error between the desired distance from the wall and the actual distance from the wall, and the orientation error input, which is is the error between the angle of the wall and the orientation of the robot. The contour following controller will output for example a change in velocity or thrust which leads to a change in the orientation of the robot, which will decrease the control errors. Multiple different controller approaches exist, however for the goal of this project it was concluded that the use of a general (non-)linear controller would be suitable.

It is not exactly known what the desired unknown environments are for this research. However, to have a broad spectrum of use-cases it is important that the final solution of this research can be applied in relatively complex environments. The research into contour following showed that the controller could follow relatively complex environments with convex and concave shapes and obstacles within the environment. While this was based on designing an environment for wall-following, the design choices can be translated into different ceiling designs. However, it is not yet known if these environments are also desired for the ceiling effect.

The final sub-question can be answered with the key findings obtained form the ceiling effect research. When flying close to the ceiling with a quadrotor a greater pressure difference across the rotor disks is generated. It was found in literature, that due to this pressure difference the thrust and the rotor velocities increase. Due to the increase in thrust, the rotor aircraft will be pulled towards the ceiling, which can cause the quadrotor to crash into the ceiling. A specific controller design that takes into account the ceiling effect should be used to prevent dangerous situations. Furthermore, it was found that the ceiling effect allows to achieve the same thrust level with lower power inputs. This could lead to an increase in total flight time.

While performing the literature study in the different field to obtain answers to all the sub-questions, two large research gaps were found. The first research gap is related to whisker-based applications in robotics. It was observed that all the applications shown in literature were based on ground robots, either robotic arms or moving ground robots. This means that whiskers in combination with aerial vehicles are not yet researched and it is unknown how the whiskers will behave on such platforms.

The second gap was derived from the ceiling effect research. In the existing literature, distances to the ceiling were measured with long range distance sensors, but not with tactile sensors, such as whiskers. It is therefore not known if whiskers can be used for measuring distances towards the ceiling and how their behavior will change, while being in proximity with the ceiling.

Furthermore, the experiments related to the ceiling effect are only done for smooth horizontal surfaces. This means that the derived equations to estimate the ceiling effect are so far only valid for smooth horizontal surfaces and might not be applicable for asymmetric surfaces.

The unknowns due to these gaps will be answered at the end of this research project. Because the found gaps can be traced back to the main research question that was established for this project:

How can whisker-based tactile sensing be used to perform autonomous contour following navigation tasks in unknown environments, while flying in proximity with rugged ceilings, with a quadrotor?

Using the answers to the sub-questions, it becomes clear that in theory the goal of the research question could be achieved by using a contour following controller, that can account for the ceiling effect. The required controller inputs required are the distance towards the ceiling and the orientation of the ceiling, which can both be obtained from distance measurements from the whisker-array. However, due to the research gaps it is unknown if in practise the proposed solution will work.

In conclusion, the performed literature research provides insight about all the different aspects of the research question, focusing on whisker-based tactile sensing in nature and in robotics, the ceiling effect principle, and contour following navigation tasks.

This literature research also provides insight in possible future research fields. First of all, this literature study focuses on a whikser-based ceiling contour following navigation task with a quadrotors, but there are many more tactile sensing applications. It would be interesting to analyse if these applications can be performed with a whisker-based quadrotor.

Furthermore, most studies related to whiskers, perform experiments in controlled environments to minimize the effects of induced noise. This means it is unknown how the whisker-based applications would perform in non-perfect environments. This would be a very interesting research topic, because it will give insight about applications of artificial whiskers in the real world.

7 Project Planning

This chapter will describe the phase that comes after the literature review. This next phase aims to fulfill the practical goal of the research, by building a whisker-based drone with the ability to perform a ceiling contour following navigation task. This phase uses the theoretical knowledge that is obtain via the literature review.

To be able to achieve the desired goal, it is important to have a clear overview of the tasks that need to be performed. This practical phase can be divided in six main stages. The overview of the different stages together with their estimated time duration's can be seen in Figure 7.1.

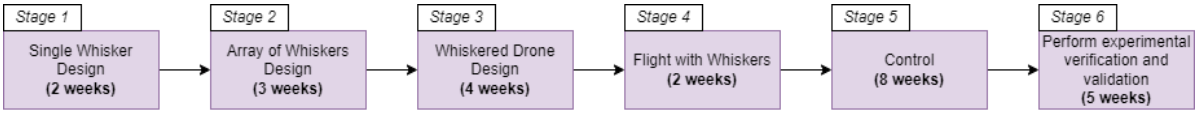

Figure 7.1: Overview of the main stages of the MSc thesis flow and the estimated time to perform the stages.

In every stage there are many different tasks that can be performed, but due to time limitations a selection must be made. An overview of the possible design choices per stage can be found in Figure 7.2. Here, it can be seen that for each of the different whisker-based tactile navigation approaches obtained from literature the same overall flow can be used. The main difference is in the type of controller that needs to be designed. As mentioned, a task selection must be made. The tasks that will be performed are represented by the blocks in Figure 7.2 with a thick green border. The main application goal is tactile contour following.

The first stage will focus on the analysis of the current whisker design that is used in the research group. Static and dynamic testing will be performed to get a complete overview of the behavior of a single whisker. The difference between the static and dynamic testing is that the whisker will move, whisk, in the dynamic testing environment.

The obtained knowledge from the first stage can be used in the design of the whisker array in the second stage. Due to time limitations it was chosen to focus only on a passive whisker array design, specifically with a constant whisker length. The behavior of the designed array will also be analysed in this stage.

The next stage is to design a roof on which the whisker arrays can be placed. It was chosen to go for a roof design, because the distance towards the ceiling must be obtained. In this stage multiple designs will be tested and analysed, to find that design that minimizes the amount of induced noise.

Stage four will focus on perform manual flight tests with the whiskered drone. The goal of this stage is to obtain estimates of the different noises sources. Experiments will be done in hover flight, free flight, and flights close to the ceiling. Furthermore, this stage will also analyse the effect of the ceiling effect on the behavior of the whiskers and to obtain the required parameter estimates to approximate the ceiling effect.

Using the information obtain from the experimental stage in stage four, a drone controller can be designed in stage five. This controller should be able to account for the ceiling effect while it is performing a ceiling contour following navigation task.

Finally, in the last stage the completed design will be tested in multiple unknown environments. The design will be tested in environments with straight ceilings and environments with curved ceilings. This final stage aims to verify and validate the final design. If this final stage is successfully completed a design for whisker-based navigation is obtained. When there is additional time left, it can be decided to look into some of the additional tasks shown in Figure 7.2.

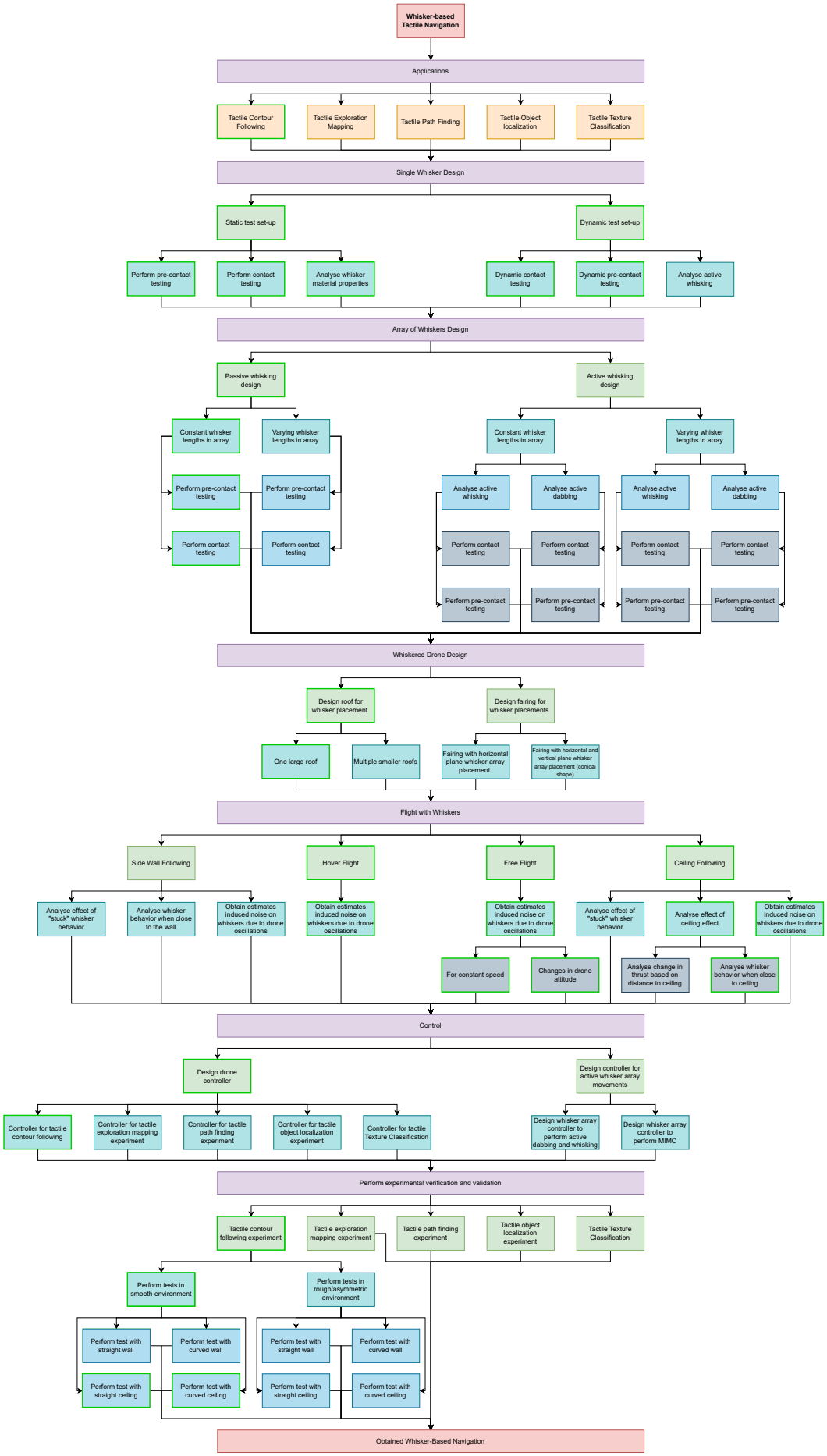

Figure 7.2: Overview of the MSc thesis flow, giving the global overview of the tasks at hand.

References

[1] Ehud Ahissar and Per M Knutsen. “Vibrissal location coding”. In: *Scholarpedia of touch* (2016), pp. 725–735.

[2] Ehud Ahissar and Per Magne Knutsen. “Object localization with whiskers”. In: *Biological cybernetics* 98 (2008), pp. 449–458.

[3] Sean R. Anderson et al. “Adaptive Cancelation of Self-Generated Sensory Signals in a Whisking Robot”. In: *IEEE Transactions on Robotics* 26.6 (2010), pp. 1065–1076. DOI: 10.1109/TRO.2010.2069990.

[4] Tareq Assaf et al. “Visual-tactile sensory map calibration of a biomimetic whiskered robot”. In: *2016 IEEE International Conference on Robotics and Automation (ICRA)*. 2016, pp. 967–972. DOI: 10.1109/ICRA.2016.7487228.

[5] Moses Bangura et al. “Aerodynamics of rotor blades for quadrotors”. In: *arXiv preprint arXiv:1601.00733* (2016).

[6] Friedrich G. Barth. “A Spider’s Tactile Hairs”. In: *Scholarpedia of Touch*. Ed. by Tony Prescott, Ehud Ahissar, and Eugene Izhikevich. Paris: Atlantis Press, 2016, pp. 65–81. ISBN: 978-94-6239-133-8. DOI: 10.2991/978-94-6239-133-8_4. URL: https://doi.org/10.2991/978-94-6239-133-8_4.

[7] BASECAMP. *DJI QAUADCOPTER FLAME WHEEL ARF KIT F450*. July 2023. URL: https://basecamp-shop.com/en/product/dji-quadcopter-flame-wheel-arf-kit-450.

[8] J Alexander Birdwell et al. “Biomechanical models for radial distance determination by the rat vibrissal system”. In: *Journal of neurophysiology* 98.4 (2007), pp. 2439–2455.

[9] Horst Bleckmann and Randy Zelick. “Lateral line system of fish”. In: *Integrative zoology* 4.1 (2009), pp. 13–25.

[10] N. Borkar et al. “Autonomous Navigation of Quadrotors Using Tactile Feedback”. In: *2023 9th International Conference on Automation, Robotics and Applications (ICARA)*. 2023, pp. 70–74. DOI: 10.1109/ICARA56516.2023.10125600.

[11] Michael Brecht, Bruno Preilowski, and Michael M Merzenich. “Functional architecture of the mystacial vibrissae”. In: *Behavioural brain research* 84.1-2 (1997), pp. 81–97.

[12] C Elaine Chapman et al. “Sensory perception during movement in man”. In: *Experimental brain research* 68 (1987), pp. 516–524.

[13] C. Elaine Chapman and François Tremblay. “Tactile Suppression”. In: *Scholarpedia of Touch*. Ed. by Tony Prescott, Ehud Ahissar, and Eugene Izhikevich. Paris: Atlantis Press, 2016, pp. 293–300. ISBN: 978-94-6239-133-8. DOI: 10.2991/978-94-6239-133-8_24. URL: https://doi.org/10.2991/978-94-6239-133-8_24.

[14] IC Cheeseman and WE Bennett. “The effect of the ground on a helicopter rotor in forward flight”. In: (1955).

[15] Stephen A Conyers, Matthew J Rutherford, and Kimon P Valavanis. “An empirical evaluation of ground effect for small-scale rotorcraft”. In: *2018 IEEE International Conference on Robotics and Automation (ICRA)*. IEEE. 2018, pp. 1244–1250.

[16] Stephen A. Conyers, Matthew J. Rutherford, and Kimon P. Valavanis. “An Empirical Evaluation of Ceiling Effect for Small-Scale Rotorcraft”. In: *2018 International Conference on Unmanned Aircraft Systems (ICUAS)*. 2018, pp. 243–249. DOI: 10.1109/ICUAS.2018.8453469.

[17] Anita Cybulska-Klosowicz et al. “A critical speed for gating of tactile detection during voluntary movement”. In: *Experimental brain research* 210 (2011), pp. 291–301.

[18] William Deer and Pauline E. I. Pounds. “Lightweight Whiskers for Contact, Pre-Contact, and Fluid Velocity Sensing”. In: *IEEE Robotics and Automation Letters* 4.2 (2019), pp. 1978–1984. DOI: 10.1109/LRA.2019.2899215.

[19] Dudi Deutsch et al. “Fast feedback in active sensing: touch-induced changes to whisker-object interaction”. In: (2012).

[20] Volker Dürr. “Stereotypic leg searching movements in the stick insect: kinematic analysis, behavioural context and simulation”. In: *Journal of Experimental Biology* 204.9 (2001), pp. 1589–1604.

[21] Volker Dürr. “Stick insect antennae”. In: *Scholarpedia* 9.2 (2014), p. 6829.

[22] Hugh Durrant-Whyte and Tim Bailey. “Simultaneous localization and mapping: part I”. In: *IEEE robotics & automation magazine* 13.2 (2006), pp. 99–110.

[23] WC Eberhardt et al. “A bio-inspired artificial whisker for fluid motion sensing with increased sensitivity and reliability”. In: *SENSORS, 2011 IEEE*. IEEE. 2011, pp. 982–985.

[24] Mathew H Evans et al. “Tactile discrimination using template classifiers: Towards a model of feature extraction in mammalian vibrissal systems”. In: *From Animals to Animats 11: 11th International Conference on Simulation of Adaptive Behavior, SAB 2010, Paris-Clos Lucé, France, August 25-28, 2010. Proceedings 11*. Springer. 2010, pp. 178–187.

[25] Charles Fox et al. “Tactile SLAM with a biomimetic whiskered robot”. In: *2012 IEEE International Conference on Robotics and Automation*. 2012, pp. 4925–4930. DOI: 10.1109/ICRA.2012.6224813.

[26] Charles W Fox and Tony J Prescott. “Mapping with sparse local sensors and strong hierarchical priors”. In: *Towards Autonomous Robotic Systems: 12th Annual Conference, TAROS 2011, Sheffield, UK, August 31–September 2, 2011. Proceedings 12*. Springer. 2011, pp. 183–194.

[27] Charles W Fox et al. “Contact type dependency of texture classification in a whiskered mobile robot”. In: *Autonomous Robots* 26 (2009), pp. 223–239.

[28] Goren Gordon. “Models of tactile perception and development”. In: *Scholarpedia of Touch*. Springer, 2015, pp. 797–808.

[29] Wolf Hanke and Guido Dehnhardt. “Vibrissal Touch in Pinnipeds”. In: *Scholarpedia of Touch*. Ed. by Tony Prescott, Ehud Ahissar, and Eugene Izhikevich. Paris: Atlantis Press, 2016, pp. 125–139. ISBN: 978-94-6239-133-8. DOI: 10.2991/978-94-6239-133-8_9. URL: https://doi.org/10.2991/978-94-6239-133-8_9.

[30] Mitra Hartmann. “Vibrissa Mechanical Properties”. In: *Scholarpedia of Touch*. Ed. by Tony Prescott, Ehud Ahissar, and Eugene Izhikevich. Paris: Atlantis Press, 2016, pp. 591–614. ISBN: 978-94-6239-133-8. DOI: 10.2991/978-94-6239-133-8_45. URL: https://doi.org/10.2991/978-94-6239-133-8_45.

[31] Yi Hsuan Hsiao and Pakpong Chirarattananon. “Ceiling Effects for Hybrid Aerial–Surface Locomotion of Small Rotorcraft”. In: *IEEE/ASME Transactions on Mechatronics* 24.5 (2019), pp. 2316–2327. DOI: 10.1109/TMECH.2019.2929589.

[32] Yi Hsuan Hsiao and Pakpong Chirarattananon. “Ceiling Effects for Surface Locomotion of Small Rotorcraft”. In: *2018 IEEE/RSJ International Conference on Intelligent Robots and Systems (IROS)*. 2018, pp. 6214–6219. DOI: 10.1109/IROS.2018.8593726.

[33] Viktória Ilková and Adrian Ilka. “Legal aspects of autonomous vehicles—an overview”. In: *2017 21st international conference on process control (PC)*. IEEE. 2017, pp. 428–433.

[34] Antonio E. Jimenez-Cano et al. “Contact-Based Bridge Inspection Multirotors: Design, Modeling, and Control Considering the Ceiling Effect”. In: *IEEE Robotics and Automation Letters* 4.4 (2019), pp. 3561–3568. DOI: 10.1109/LRA.2019.2928206.

[35] Chia-Feng Juang and Yu-Cheng Chang. “Evolutionary-Group-Based Particle-Swarm-Optimized Fuzzy Controller With Application to Mobile-Robot Navigation in Unknown Environments”. In: *IEEE Transactions on Fuzzy Systems* 19.2 (2011), pp. 379–392. DOI: 10.1109/TFUZZ.2011.2104364.

[36] Chia-Feng Juang, Ying-Han Chen, and Yue-Hua Jhan. “Wall-Following Control of a Hexapod Robot Using a Data-Driven Fuzzy Controller Learned Through Differential Evolution”. In: *IEEE Transactions on Industrial Electronics* 62.1 (2015), pp. 611–619. DOI: 10.1109/TIE.2014.2319213.

[37] Dacher Keltner. *Hands On Research: The Science of Touch*. Sept. 2010. URL: https://greatergood.berkeley.edu/article/item/hands_on_research.

[38] DaeEun Kim and Ralf Möller. “Biomimetic whiskers for shape recognition”. In: *Robotics and Autonomous Systems* 55.3 (2007), pp. 229–243. ISSN: 0921-8890. DOI: https://doi.org/10.1016/j.robot.2006.08.001. URL: https://www.sciencedirect.com/science/article/pii/S0921889006001400.

[39] Roberta Klatzky and Catherine L Reed. “Haptic exploration”. In: *Scholarpedia of Touch* (2016), pp. 177–183.

[40] Roberta L Klatzky, Susan J Lederman, and Catherine Reed. “There’s more to touch than meets the eye: The salience of object attributes for haptics with and without vision.” In: *Journal of experimental psychology: general* 116.4 (1987), p. 356.

[41] Nathan F. Lepora, Martin Pearson, and Luke Cramphorn. “TacWhiskers: Biomimetic Optical Tactile Whiskered Robots”. In: *2018 IEEE/RSJ International Conference on Intelligent Robots and Systems (IROS)*. 2018, pp. 7628–7634. DOI: 10.1109/IROS.2018.8593653.

[42] M. Lungarella et al. “An artificial whisker sensor for robotics”. In: *IEEE/RSJ International Conference on Intelligent Robots and Systems*. Vol. 3. 2002, 2931–2936 vol.3. DOI: 10.1109/IRDS.2002.1041717.

[43] Marianna Madry et al. “ST-HMP: Unsupervised Spatio-Temporal feature learning for tactile data”. In: *2014 IEEE International Conference on Robotics and Automation (ICRA)*. 2014, pp. 2262–2269. DOI: 10.1109/ICRA.2014.6907172.

[44] Uriel Martinez-Hernandez. “Tactile sensors”. In: *Scholarpedia of Touch* (2016), pp. 783–796.

[45] Matthew J. McHenry and James C. Liao. “The Hydrodynamics of Flow Stimuli”. In: *The Lateral Line System*. Ed. by Sheryl Coombs et al. New York, NY: Springer New York, 2014, pp. 73–98. ISBN: 978-1-4614-8851-4. DOI: 10.1007/2506_2013_13. URL: https://doi.org/10.1007/2506_2013_13.

[46] Michael J Milford and Gordon F Wyeth. “Mapping a suburb with a single camera using a biologically inspired SLAM system”. In: *IEEE Transactions on Robotics* 24.5 (2008), pp. 1038–1053.

[47] Ben Mitchinson. “Tactile attention in the vibrissal system”. In: *Scholarpedia of touch* (2015), pp. 771–779.

[48] Ben Mitchinson et al. “Active vibrissal sensing in rodents and marsupials”. In: *Philosophical Transactions of the Royal Society B: Biological Sciences* 366.1581 (2011), pp. 3037–3048.

[49] Jan Andries Neethling. *Arachnid sensory structures*. Mar. 2021. URL: https://nationalmuseumpublications.co.za/arachnid-sensory-structures/.

[50] Takuzumi Nishio et al. “Stable Control in Climbing and Descending Flight under Upper Walls using Ceiling Effect Model based on Aerodynamics”. In: *2020 IEEE International Conference on Robotics and Automation (ICRA)*. 2020, pp. 172–178. DOI: 10.1109/ICRA40945.2020.9197137.

[51] Martin J Pearson et al. “Biomimetic vibrissal sensing for robots”. In: *Philosophical Transactions of the Royal Society B: Biological Sciences* 366.1581 (2011), pp. 3085–3096.

[52] Martin J Pearson et al. “Scratchbot: Active tactile sensing in a whiskered mobile robot”. In: *From Animals to Animats 11: 11th International Conference on Simulation of Adaptive Behavior, SAB 2010, Paris-Clos Lucé, France, August 25-28, 2010. Proceedings 11*. Springer. 2010, pp. 93–103.

[53] Martin J Pearson et al. “Whiskerbot: a robotic active touch system modeled on the rat whisker sensory system”. In: *Adaptive Behavior* 15.3 (2007), pp. 223–240.

[54] Martin J. Pearson et al. “Simultaneous localisation and mapping on a multi-degree of freedom biomimetic whiskered robot”. In: *2013 IEEE International Conference on Robotics and Automation*. 2013, pp. 586–592. DOI: 10.1109/ICRA.2013.6630633.

[55] Tony J Prescott and Volker Dürr. “Introduction: The world of touch”. In: *Scholarpedia of touch*. Springer, 2015, pp. 1–28.

[56] Tony J Prescott, Ben Mitchinson, and Robyn Anne Grant. “Vibrissal behavior and function”. In: *Scholarpedia* 6.10 (2011), p. 6642.

[57] Tony J Prescott et al. “Whisking with robots”. In: *IEEE robotics & automation magazine* 16.3 (2009), pp. 42–50.

[58] Eric Ralls. *Nature vs. nature at odds in aggression of male mice*. July 2023. URL: https://www.earth.com/news/aggression-male-mice/.

[59] G Carleton Ray et al. “Pacific walrus: benthic bioturbator of Beringia”. In: *Journal of Experimental Marine Biology and Ecology* 330.1 (2006), pp. 403–419.

[60] Roger Reep and Diana K Sarko. “Tactile hair in Manatees”. In: *Scholarpedia* 4.4 (2009), p. 6831.

[61] David Rosen. *Long-term studies quantify the prey requirements of pinnipeds, and help predict the effects of nutritional stress.* 2021. URL: https://mmru.ubc.ca/2022/01/long-term-studies-quantify-the-prey-requirements-of-pinnipeds-and-help-predict-the-effects-of-nutritional-stress/.

[62] Claudia Roth-Alpermann and Michael Brecht. “Vibrissal Touch in the Etruscan Shrew”. In: *Scholarpedia of Touch*. Ed. by Tony Prescott, Ehud Ahissar, and Eugene Izhikevich. Paris: Atlantis Press, 2016, pp. 117–123. ISBN: 978-94-6239-133-8. DOI: 10.2991/978-94-6239-133-8_8. URL: https://doi.org/10.2991/978-94-6239-133-8_8.

[63] Prasanna Kumar Routray et al. “Towards Multidimensional Textural Perception and Classification Through Whisker”. In: *2022 IEEE International Symposium on Robotic and Sensors Environments (ROSE)*. 2022, pp. 1–7. DOI: 10.1109/ROSE56499.2022.9977409.

[64] Mohammed Salman and Martin J Pearson. “Advancing whisker based navigation through the implementation of bio-inspired whisking strategies”. In: *2016 IEEE International Conference on Robotics and Biomimetics (ROBIO)*. IEEE. 2016, pp. 767–773.

[65] Mohammed Salman and Martin J. Pearson. “Whisker-RatSLAM Applied to 6D Object Identification and Spatial Localisation”. In: *Biomimetic and Biohybrid Systems*. Ed. by Vasiliki Vouloutsi et al. Cham: Springer International Publishing, 2018, pp. 403–414. ISBN: 978-3-319-95972-6.

[66] P. J. Sanchez-Cuevas, G. Heredia, and A. Ollero. “Multirotor UAS for bridge inspection by contact using the ceiling effect”. In: *2017 International Conference on Unmanned Aircraft Systems (ICUAS)*. 2017, pp. 767–774. DOI: 10.1109/ICUAS.2017.7991412.

[67] Matthias Schöpfer et al. “Identifying relevant tactile features for object identification”. In: *Towards Service Robots for Everyday Environments: Recent Advances in Designing Service Robots for Complex Tasks in Everyday Environments* (2012), pp. 417–430.

[68] Anthony Smith. *Explorers of the Amazon*. University of Chicago Press, 1994.

[69] J. Charles Sullivan et al. “Tactile Discrimination Using Active Whisker Sensors”. In: *IEEE Sensors Journal* 12.2 (2012), pp. 350–362. DOI: 10.1109/JSEN.2011.2148114.

[70] Yaroslav Tenzer, Leif P. Jentoft, and Robert D. Howe. “The Feel of MEMS Barometers: Inexpensive and Easily Customized Tactile Array Sensors”. In: *IEEE Robotics & Automation Magazine* 21.3 (2014), pp. 89–95. DOI: 10.1109/MRA.2014.2310152.

[71] Sebastian Thrun. “Probabilistic algorithms in robotics”. In: *Ai Magazine* 21.4 (2000), pp. 93–93.

[72] Juan Marcos Toibero, Flavio Roberti, and Ricardo Carelli. “Stable contour-following control of wheeled mobile robots”. In: *Robotica* 27.1 (2009), pp. 1–12.

[73] Marco Tranzatto et al. “CERBERUS in the DARPA Subterranean Challenge”. In: *Science Robotics* 7.66 (2022), eabp9742.

[74] N Poornima Varma, V Aivek, and V Ravikumar Pandi. “Intelligent wall following control of differential drive mobile robot along with target tracking and obstacle avoidance”. In: *2017 International Conference on Intelligent Computing, Instrumentation and Control Technologies (ICICICT)*. 2017, pp. 85–91. DOI: 10.1109/ICICICT1.2017.8342539.

[75] Xinkuang Wang, Shanshan Du, and Yong Liu. “Research on ceiling effect of quadrotor”. In: *2017 IEEE 7th Annual International Conference on CYBER Technology in Automation, Control, and Intelligent Systems (CYBER)*. IEEE. 2017, pp. 846–851.

[76] Xin Wei et al. “A wall-following algorithm based on dynamic virtual walls for mobile robots navigation”. In: *2017 IEEE International Conference on Real-time Computing and Robotics (RCAR)*. 2017, pp. 46–51. DOI: 10.1109/RCAR.2017.8311834.

[77] Christopher M Williams and Eric M Kramer. “The advantages of a tapered whisker”. In: *PLoS one* 5.1 (2010), e8806.

[78] Stephan R Williams, Jafar Shenasa, and C Elaine Chapman. “Time course and magnitude of movement-related gating of tactile detection in humans. I. Importance of stimulus location”. In: *Journal of neurophysiology* 79.2 (1998), pp. 947–963.

[79] Chenxi Xiao et al. “Active multiobject exploration and recognition via tactile whiskers”. In: *IEEE Transactions on Robotics* 38.6 (2022), pp. 3479–3497.

References

[1] Charles Fox et al. “Tactile SLAM with a biomimetic whiskered robot”. In: *2012 IEEE International Conference on Robotics and Automation*. 2012, pp. 4925–4930. DOI: 10.1109/ICRA.2012.6224813.

[2] Charles W Fox et al. “Contact type dependency of texture classification in a whiskered mobile robot”. In: *Autonomous Robots* 26 (2009), pp. 223–239.

[3] Martin J Pearson et al. “Scratchbot: Active tactile sensing in a whiskered mobile robot”. In: *From Animals to Animats 11: 11th International Conference on Simulation of Adaptive Behavior, SAB 2010, Paris-Clos Lucé, France, August 25-28, 2010. Proceedings 11*. Springer. 2010, pp. 93–103.

[4] Tony J Prescott, Ben Mitchinson, and Robyn Anne Grant. “Vibrissal behavior and function”. In: *Scholarpedia* 6.10 (2011), p. 6642.

[5] Marco Tranzatto et al. “CERBERUS in the DARPA Subterranean Challenge”. In: *Science Robotics* 7.66 (2022), eabp9742.